Negative microfilm
received from university

62-2746

HUNTING, Alfred Curtis, 1928–
AN INTERFEROMETRIC STUDY OF THE INTERACTION OF PLANE SHOCK WAVES WITH MONOTONIC CHANNEL–AREA CONSTRICTIONS IN THE 2" x 7" SHOCK TUBE.

University of Michigan, Ph.D., 1962
Physics, general

University Microfilms, Inc., Ann Arbor, Michigan

AN INTERFEROMETRIC STUDY OF THE INTERACTION OF PLANE SHOCK WAVES WITH MONOTONIC CHANNEL-AREA CONSTRICTIONS IN THE 2" x 7" SHOCK TUBE

by
Alfred Curtis Hunting

A dissertation submitted in partial fulfillment
of the requirements for the degree of
Doctor of Philosophy in the
University of Michigan
1961

Doctoral Committee:

Professor Otto Laporte, Chairman
Associate Professor Peter A. Franken
Associate Professor Karl T. Hecht
Associate Professor James A. Nicholls
Associate Professor C. Wilbur Peters

ACKNOWLEDGEMENTS

The author wishes to thank Professor Otto Laporte for proposing the subject of this thesis and for supervising the research that went into it. A very considerable debt of gratitude is owed to the many former members of the Shock Tube Project whose efforts over the course of many years contributed to the construction of much of the equipment used in this research; thanks are particularly due Dr. Eugene B. Turner, who designed and constructed our Mach-Zehnder interferometer. The author also expresses his very great appreciation to Virgil Barbat and to Jackson Steffes for their devoted and invaluable assistance and support during the course of research for and the preparation of this thesis.

The generous financial support of this research activity by the Office of Naval Research, under its contract NONR-1224-18-0, is gratefully acknowledged.

Of a different but certainly no less important nature is the debt the author owes his wife, Shirley Wolff Hunting, for her long-continued patience and encouragement during the entire course of this research.

TABLE OF CONTENTS

	Page
LIST OF TABLES	iv
LIST OF FIGURES	v
CHAPTER I. INTRODUCTION	1
1. Introduction	1
2. Laporte's Theory of the Shock - Convergence Interaction	3
3. Survey of Related Literature	9
CHAPTER II. DESCRIPTION OF EXPERIMENTAL EQUIPMENT	18
1. Shock Tube Hardware	18
2. Electronics and Timing Optics	25
3. The Mach-Zehnder Interferometer System	29
4. Models for the Shock Tube	42
5. Equipment for Reading Interferograms	47
CHAPTER III. EXPERIMENTAL PROCEDURES	51
1. Introduction	51
2. Acquisition and Treatment of the x-t Data	57
3. Obtaining the Interferograms	62
4. The Fringe - Shift Measuring Process	65
5. Roll - Over	71
6. Reduction of the Fringe - Shift Data	79
CHAPTER IV. CORRELATION OF THEORY WITH THE EXPERIMENTAL RESULTS	83
1. Precision of the Values of the Measured Fringe Shifts	83
2. Propagation of the Precision of Measurement	85
3. The Theories of Laporte and of Chisnell: Outline and Numerical Calculations	91
4. Discussion of the Results of the Experiment	102
CHAPTER V. CONCLUSIONS AND RECOMMENDATIONS	116
1. Conclusions and Summary	116
2. Recommendations for Further Research	117
REFERENCES	125

LIST OF TABLES

Table		Page
1.	Calculated values for the coefficients of the propagation of imprecision.	58
2.	Values of the strengths y_c and y_{rt} of the channel and tip-reflected shocks as calculated from the theories of Laporte and Chisnell.	93
3.	Measured values of the shock strengths y_c, y_{rc}, $y_c(y_{rc})$ for the 2-unit 2:1 model at the various constricted - channel locations x.	106
4.	Measured values of the shock strengths y_c, y_{rc}, $y_c(y_{rc})$ for the 5-unit 2:1 model at the various constricted - channel locations x.	107
5.	Measured values of the shock strengths y_c, y_{rc}, $y_c(y_{rc})$ for the 5-unit 5:1 model at the various constricted - channel locations x.	108
6.	Qualitative indication of the relative amount of scatter in the sets of data points.	111

LIST OF FIGURES

Figure		Page
1.	Schematic wave diagrams for the solutions "in the large."	4
2.	Distance-time (i.e. x - t) diagrams for the interaction of an incident shock S_1 and a channel-area constriction, in the cases both of unchoked and choked flow through the constrictions.	5
3.	Schematic diagram of the shock tube and of the models used in this experiment.	19
4.	View of a typical burst shock tube diaphragm that is ten mils thick and is scribed seven mils deep.	23
5.	Block diagram of the electronic circuitry used in this experiment.	26
6.	Schematic diagram of the Mach-Zehnder interferometer with its associated optical system.	30
7.	A quartet of interferograms taken for a single shot of the shock tube.	32
8a.	View of the spark source end of the Mach-Zehnder interferometer system.	34
8b.	View of the camera end of the Mach-Zehnder interferometer system.	35
9.	Views of the wedge models used in this experiment.	43
10.	View of a wedge model in place at the shock tube test section.	44
11.	View of the fringe-shift measuring equipment.	49
12.	Schlieren photographs showing the progressive formation of the tip-reflected shock from the individual wedge-tip wavelets.	53
13.	A graphic demonstration of the occurrence of roll over.	74
14.	Graph of channel shock strength measurements for the 2-unit 2:1 model.	103

LIST OF FIGURES (Concluded)

Figure		Page
15.	Graph of channel shock strength measurements for the 5-unit 2:1 model.	104
16.	Graph of channel shock strength measurements for the 5-unit 5:1 model.	105
17.	Sketch of the regime of ambiguity in the $\mathcal{R}, y_o$ plane.	

CHAPTER I

INTRODUCTION

1. INTRODUCTION

The interaction of plane aerodynamic shock waves in a uniform channel cross sectional area is a subject that has attracted steadily increasing attention in recent years. Much of the early work was concerned with relatively complex physical situations, such as the interaction of shocks with grids, ports and other abrupt and often convergent - divergent changes in channel area, but progress in this field was somewhat limited until relatively recently when attention was directed to shock interactions with the elementary forms of channel area change.

This present work is an experimental study of the interaction of shocks with a particular form of area change. The 2" x 7" shock tube and associated Mach-Zehnder interferometer system in the University of Michigan Physics Department were used in an effort to compare some calculated values for this interaction, derived from a theory by Laporte, with interferometrically determined values for the wave strengths arising from this interaction.

In Chapter I, there is first an introduction to the general nature of the channel configuration used for this study and to the nature of the flow patterns in the various regions of interest in the shock tube. Next there is a fairly detailed outline of Laporte's theoretical analysis of the shock-convergence interaction. In addition there is a survey of the related literature, including some work which, while it does not bear directly on the particular experimental conditions of this research,

does point out some of the only - recently - appreciated properties of the basic equations on which the theoretical analysis of present interest is based.

Chapter II is a detailed description of the experimental apparatus and the configurations of the models used in this experiment. Particular emphasis is placed here on bringing up to date those descriptions of the state of the shock tube and its associated equipment that were contained in previous reports from this project and also on describing in detail the features of our particular Mach-Zehnder interferometer, which have not been discussed in any of the earlier project reports.

In Chapter III, we report on the various experimental procedures used in obtaining interferograms and in determining values of the shock strengths from them. This chapter also includes a discussion of a phenomenon which complicates the measuring of large-magnitude fringe shifts across flow discontinuities. Only recently was this phenomenon, termed "roll over" by Curtis[24], first described in terms appropriate for application to interferometric measurements of shock waves, so the description given of it here is suitably detailed.

In Chapter IV, which is concerned with correlating theory with the experimental results, we first consider the nature and magnitude of the experimental factors that limit the precision with which the resultant shock strengths can be measured by the techniques we have used. This is followed by a section treating some additional details of Laporte's analysis; this leads up to a discussion of the problem of reducing this analysis to an efficient calculating program. This program is described, and the resulting calculated values, along with previous calcu-

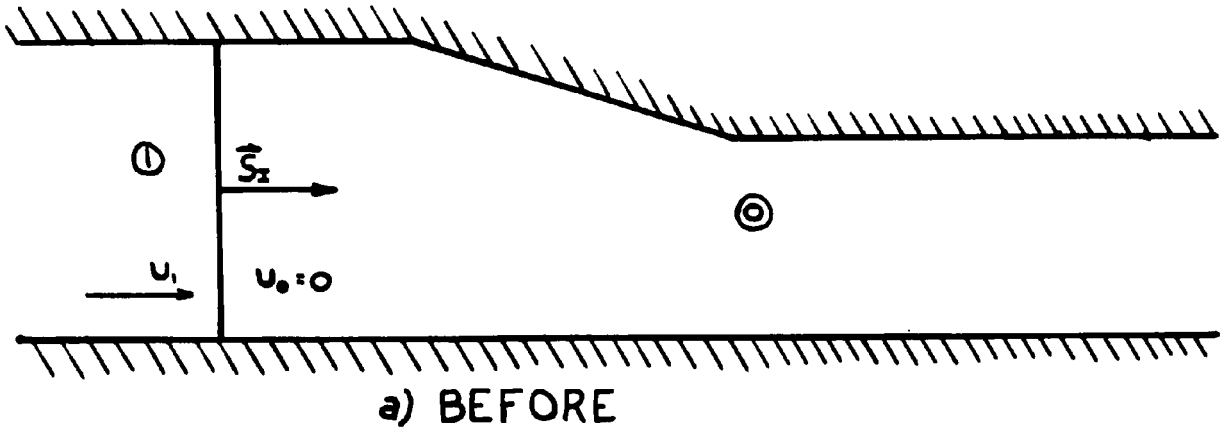
lations by Laporte and also some calculated values based on another less exact theory, are displayed. The last section of this chapter includes the results of the experimental measurements of shock strengths arising from the shock-convergence interaction, also some observations on the correlation of these results with theory, and finally an attempt to account for some unexpected "regularities" in the experimental results.

The last chapter deals with the extent to which the theory was confirmed by this experiment, and offers the conclusions that can be drawn from this research. It is concluded with a series of recommendations both for improvements in the experimental procedures used here, and also for additional related experimental research that, it is felt, would be of value in this area.

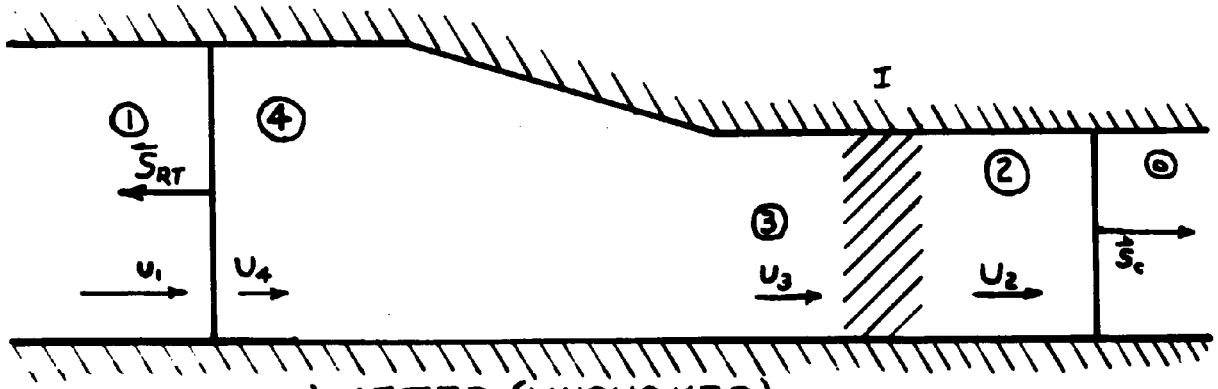
2. LAPORTE'S THEORY OF THE SHOCK - CONVERGENCE INTERACTION

Several years ago, Laporte[1] considered the interaction of a plane shock wave of low to moderate strength with a particular class of models for the conventional shock tube. In the course of this study, attention was focused on one of the component parts of this interaction, i.e. the interaction of a plane shock with a simple gradual monotonic change in the cross sectional area of the shock tube - a continuous change connecting a channel of uniform cross section to another channel of smaller uniform cross section. The configuration of concern here, in its elemental form, is shown in Fig. 1. The corresponding time-history of the locations of the various shocks is indicated by the x-t plot of Fig. 2b for the unchoked case.

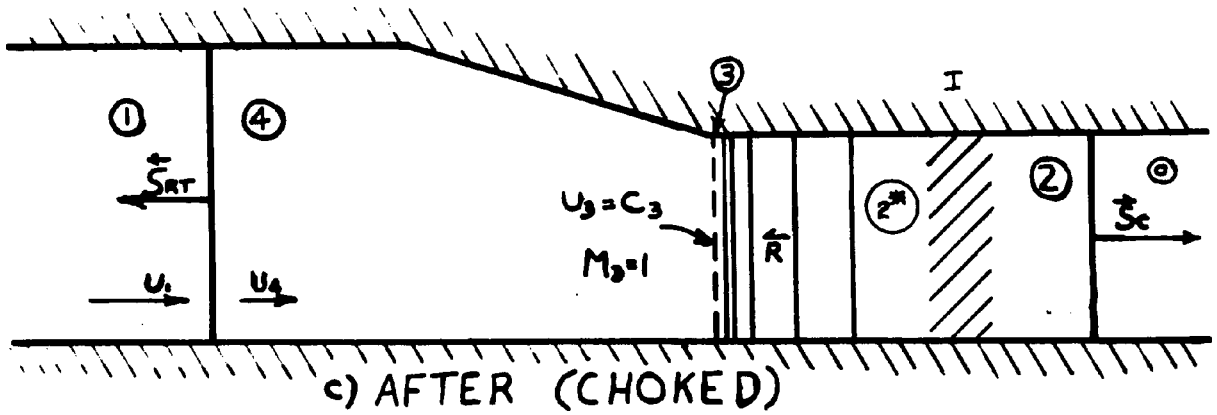
The theories for the various simple wave interactions would lead one to expect (the most qualitative observations of the flow bear



a) BEFORE



b) AFTER (UNCHOKED)



c) AFTER (CHOKED)

Figure 1. Schematic wave diagrams for the solutions "in the large", showing the locations of the waves and flow regions before and after the interaction, for both the unchoked- and choked- flow cases.

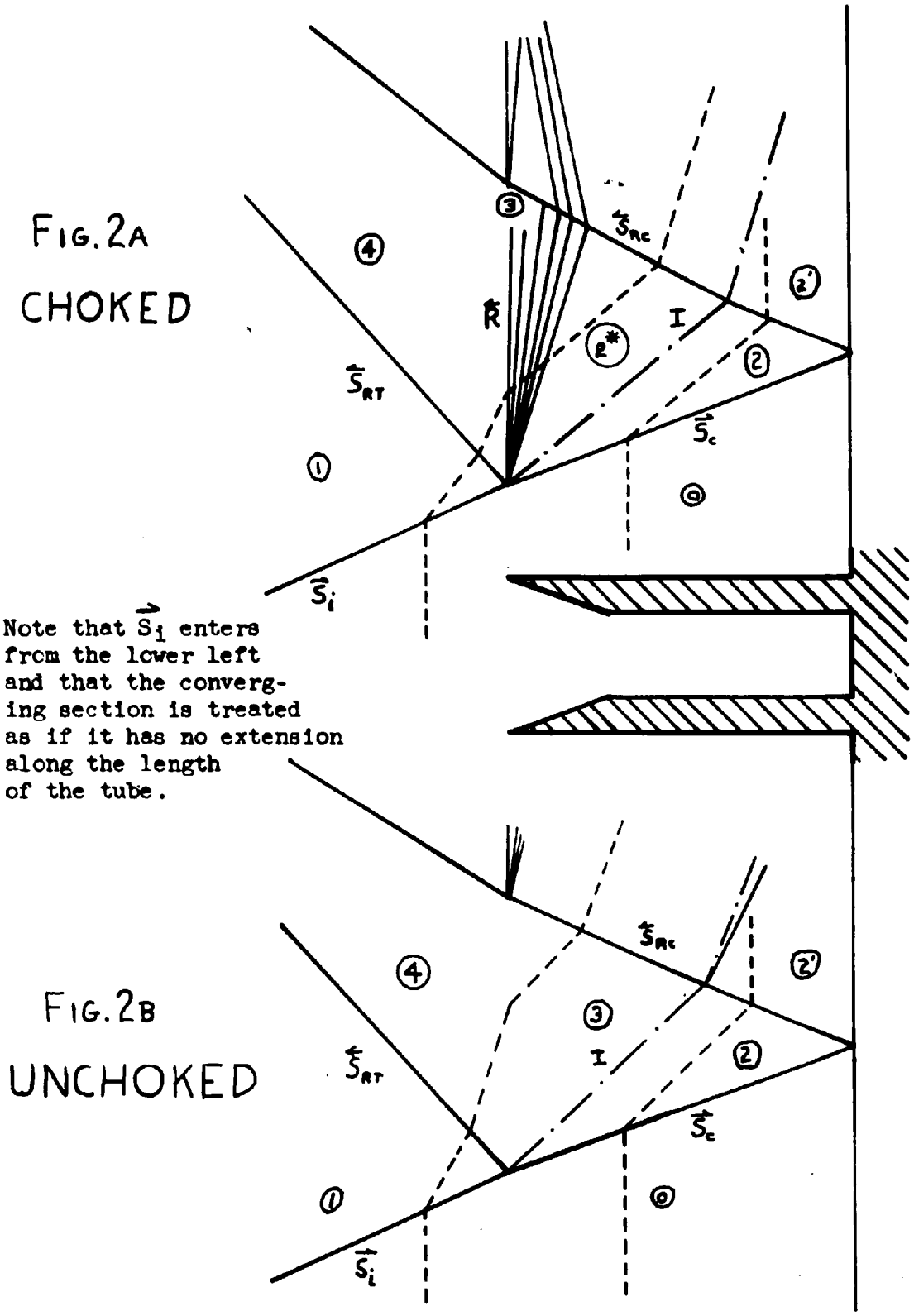


Figure 2. Distance - time (i.e. x-t) diagrams for the interaction of an incident shock $\vec{S}_i$ and a channel - area constriction, in the cases both of choked and unchoked flow through the constrictions.

this out) that the following flow pattern would occur. A portion of the incident shock $\vec{S}_i$ penetrates through the converging section into the narrower channel and eventually forms a plane shock S_c of greater shock strength. A portion of $\vec{S}_i$ is reflected from the converging section, and especially from the leading edge of the convergence. Eventually, in the case of low and medium shock strengths, the reflected wave forms an upstream-facing plane shock $\overleftarrow{S}_{rt}$ that more or less gradually moves upstream from the converging section. Between these two extremities of the region of interaction there are typically a number of complex wave patterns, both deriving from the interaction of the flow (that follows after $\vec{S}_i$) with the convergence and also left behind as remnants of the formation processes of $\vec{S}_c$ and $\overleftarrow{S}_{rt}$.

Problems of this general nature had been of concern to a number of earlier workers in this field, but with few exceptions they had either fixed their attention on the local details of the shock-convergence interaction or had been concerned with composite geometries, usually of the convergent-divergent type. The essential simplification of this problem, which opened the way to later generalizations and extensions, was the hypothesis of the solution "in the large". That is to say, if the change in channel area is continuous and suitably gradual, the local details of the interaction with the convergence can be neglected insofar as they affect the strengths of the transmitted and the reflected shocks when these are observed sufficiently far away from the converging section. Thus, confronted in reality by a number of interacting weak waves in the vicinity of the area change, one assumes a much simpler wave diagram that is presumed to be

essentially equivalent to the actual physical situation.

In the simplest case, this wave diagram, Fig. 2a, consists of plane shocks $\vec{S}_c$ and $\overleftarrow{S}_{rt}$, and of an interface I in the narrower channel. This interface marks the boundary between, on the one side, gas that was originally in the constricted channel and was then singly compressed and accelerated by $\vec{S}_c$ and, on the other side, gas that was initially in the main channel, was passed over by $\vec{S}_i$ and $\overleftarrow{S}_{rt}$ and then flowed through the converging section into the constricted channel. It is further implicit in the wave diagram that the gas flow behind $\overleftarrow{S}_{rt}$, with net flow velocity $\vec{u}_+$, passes smoothly and without turbulence through the converging section, and that the entire region from $\overleftarrow{S}_{rt}$ to the interface in the narrower channel is <u>isentropically</u> connected. An interface is not a wave being propagated with respect to a gas flow but is a boundary (with no mass flow across it) between contiguous portions of the flow that have different values of temperature, density and entropy. Pressure and flow velocity, on the other hand, are continuous across the interface. It is just these conditions that are used to "patch" the flow solution for the conditions in region 3 to the solution for the conditions in region 2. The conditions in region 2 are related to those in region 0 by the specification of the channel shock $\vec{S}_c$.

This form of solution holds so long as the Mach number (i.e. the local flow speed in laboratory coordinates divided by the local sound speed) of the flow, which is less than 1 behind $\overleftarrow{S}_{rt}$ can remain less than 1 throughout the converging section. Now suppose that the ratio of the cross sectional area of the main channel to that of the

constricted channel (i.e. the area ratio $\mathcal{R}$) is held constant while the strength y_o of the incident shock $\vec{S}_1$ is gradually increased. Then the Mach number M_4, which increases monotonically with y_o, eventually attains such a value M_{crit} (< 1) that the effect of the convergence is just sufficient to make the outflow be sonic, i.e. to raise the flow Mach number M_3 at the outlet of the converging section to the value 1. It is a basic principle[20] of gas dynamics that a steady-state gas flow in a variable-area channel cannot be changed from a subsonic to a supersonic flow state or vice versa save by the occurrence of at least a local minimum in the channel area, i.e. by the occurrence of a throat. Since we have in this experiment only half a throat, i.e. a monotonic constriction, then $M_4 < 1 \Rightarrow M_3 \leq 1$. As y_o is gradually increased still further, M_4 must remain fixed at the value M_{crit}, but the channel-shock strength y_c continues to increase monotonically with the incident shock strength y_o. Clearly the flow speed $\vec{u}_3$ at the outlet of the convergence, limited in its increase by the condition $M_3 = 1$, will no longer be directly connectable to the steadily increasing value of $\vec{u}_2$. Thus another element is added to the wave diagram — an upstream-facing rarefaction wave $\overleftarrow{\mathcal{R}}$ with its head fixed at the end of the convergence — anchored, so to speak, against being swept downstream with the flow. This is shown in Fig. 1c; the corresponding x-t plot is shown in Fig. 2b. The effect of $\overleftarrow{\mathcal{R}}$ is to overcome the deficiency in $\vec{u}_3$ and also to reduce p_3 so that the velocity- and pressure-matching conditions at I can continue to be met. M_4 remains fixed as y_o is further increased; the flow through the area change is in this case conventionally referred to as "choked", because the mass flow per unit area passes through a maximum when M_3 has just reached the value 1.

To be sure, not all the features of the theory that have been touched upon here were introduced for the first time by Laporte, but as far as we know, his report was the first to include all these features in a single theory. We shall try in the next section to relate this particular theory to other earlier and subsequent works on the same general subject.

3. SURVEY OF RELATED LITERATURE

As noted previously, most of the early work on the interaction of plane shocks with simple convergent channel-area changes was either concerned with the details of the flow variations in the immediate vicinity of the converging section, or else was done with models of more complex geometry, such as a convergent-divergent geometry. Of this latter class, probably the most noteworthy of the early works was that of Dosanjh[2], who studied the passage of plane shocks through a fairly thick plate perforated by a large number of close-spaced holes. In most of his work, the perforated plate was parallel to the incident shock. His shadowgraphs showed the transmitted and reflected shocks, both quite rapidly formed from the multitude of wavelets. Because of the discontinuous nature of the area changes he was studying, the "interface" in his case was the leading edge of a highly turbulent region. Since he observed that the velocities of the transmitted and reflected shocks remained essentially constant once the waves were fully formed, it can be said that in a sense he was studying the flow situation "in the large", as described below. However, having observed the relatively constant shock speeds, he could not take the essential next step of hypothesizing a simplified wave diagram

because with his abrupt-area-change model and the highly turbulent flow that it induced, he could not simply connect the flow regions on the two sides of the perforated plate. It should also be noted that he observed an almost standing shock, located just downstream of the plate and facing upstream, that was equivalent to the standing shock in the diverging part of a converging-diverging nozzle[23].

So far as is known, Kahane et. al.[3] were the first actually to shift their attention to the solution "in the large", that is, to suggest that at a time long enough after the interaction of the shock with the area change, all the secondary waves arising from the interaction will have died away or have caught up with the main shocks or, in the choked-flow case, have amalgamated to form the standing rarefaction wave. The complex pattern of weak waves in the vicinity of the convergence can then be approximated by simpler wave diagrams that are essentially similar to those described in the previous section. The assumption of simple isentropic flow through the converging section, the interposition of an interface following after the transmitted shock (to allow for the non-isentropic nature of the shocks), the introduction of with its head anchored at the outlet of the converging section - these features of the shock-convergence interaction were included in a single theory apparently for the first time in this paper.

One of the differences between Kahane's and Laporte's theories is that Kahane treated the shocks for the most part as isentropic compression waves, although he asserted that an analytical refinement allowed him to treat the incident shock wave separately

as if it were a shock during during the time when it was in the converging section. This isentropic approximation made possible a direct graphical solution for the strengths of the transmitted and reflected finite-compression waves. This Kahane achieved by plotting the ratio of the flow Mach number at the outlet of the converging section to the flow Mach number at the inlet, with as the parameter, then superposing on this a graph of the same flow Mach number ratio using as the parameter the ratio P_4/Q_2, where $P_4 = P_1$ is the left-facing-wave Riemann invariant[21] appropriate for $\overleftarrow{S}_{rt}$ (which was treated as a finite compression wave) and where $Q_0 = Q_2 = Q_3$ is the corresponding right-facing-wave invariant for $\vec{S}_c$ and for the entire region within the constricted channel. Even though the interface I was indicated on Kahane's wave diagrams, his use of the isentropic approximation implied that his numerical calculations were in error at least to the extent of the magnitude of I.

Another difference between Kahane's work and that of Laporte is the following. Kahane's formulation of his problem would lead one to expect the wave strengths themselves to be the principal objects of interest. However, Kahane's experimental work was exclusively concerned with the time histories of the densities near the inlet and the outlet of the converging section (and of the diverging section, since he studied both kinds of area change); the strengths of the main waves generated by the interaction were not dealt with at all. In a certain sense this permitted him to achieve better results, since the flow in the immediate vicinity of the outlet of the converging section

became stabilized quite quickly; thus none of the difficulties caused by the incomplete catch-up of the trailing waves were met with in this work. Another interesting limitation in this work was that, while the notions of choked flow and standing rarefactions were introduced into the theoretical treatment, the strongest shocks used in our experiments ($y_o = 5$, $\mu = 6$, $\mathcal{R} = 2$) were just at the lower edge of the choked-flow regime. A last interesting, though minor, point of contrast, associated with the neglect of the main shocks produced by the interaction, was Kahane's display of all his results as density ratios rather than as pressure ratios.

Following the publication of Laporte's work, Chisnell[4] treated the general problem of the interaction of a shock and an infinitesimal area change that connects two tubes of constant cross section. From this he obtained a differential equation $\frac{dA}{dy} = f(y,\mathcal{R})$, which he integrated to achieve a closed-form function $f(y)$, such that $Af(y)$ is a constant across a finite area change. Involved in this derivation were the assumptions that the interaction, in the converging channel, of the reflected wavelets with the main shock could be neglected and that the average shock strength over the area of the shock would remain essentially constant in time, once the shock emerged from the converging section. The relation of this latter assumption to the notion of the solution "in the large" is evident. It is also of interest to note that this solution is equivalent to the technique of considering a given continuous area change as a series of constant-area tubes connected by area discontinuities, then letting the individual discontinuities become infinitesimal. Chisnell's work also included the

specialization of his general solution to the cases of cylindrical and spherical flow, and also a comparison of the resulting solutions with earlier work on that subject.

Soon thereafter, Bird[5] reported on a series of schlieren wave-speed measurements dealing with the effect of the shape of the converging section on the degree of strengthening of the transmitted shock. In particular, for a fixed area ratio and a fixed incident shock strength (such that the flow through the convergence was very definitely choked) the shape of the convergence was varied from a single area discontinuity to a smooth gradually converging section with a 15° half-angle and with rounded shoulders at the inlet and the outlet. The resulting values for the shock strengths "in the large", derived from the shock speeds, were measured with a claimed precision of 1%. They were found to approach, in the case of the smoothest and most gradual of the converging sections, within about 10% of the theoretical value for the transmitted shock strength as calculated from Chisnell's theory. It should be noted parenthetically that it was difficult to understand, on the basis of the examples of typical wave-speed pictures included in this paper, how Bird could measure his shock speeds to a precision of 1/2 % in order to assure his claimed 1% precision in his shock strength values.

The particular distinctions between this work and ours include the fact that Bird's experimental values of the shock strengths were derived from the shock speeds — the dependence here being a dynamical one — while our experimental values were derived from the discontinuity across the shock of one of the state parameters of the

gas, in this case the discontinuity in density. Furthermore, Bird's work was done exclusively with a single incident shock strength and a single area ratio; he did not study the transition from the unchoked to the choked flow regime.

Bird was evidently the first to become aware of the fact that in the regime of relatively strong shock waves incident on constrictions of appropriately small area ratio (i.e. relatively shallow convergences) there is a domain of values of the incident shock strength y_o and the area ratio $\mathcal{R}$, in which two quite different steady-flow wave diagrams are both capable of fulfilling all the quasi-steady boundary conditions for a single pair of values y_o and $\mathcal{R}$. However, it remained for Oppenheim[6] to spell out the details of this "regime of ambiguity" and to attempt to resolve the ambiguity. In essence the situation is as follows.

Assume that the choked-flow solution holds for a particular choice of values of $\mathcal{R}$ and y_o. In this case, the tip-reflected shock $\overleftarrow{S}_{rt}$ serves to reduce the Mach number of the flow into the convergence to just that value $M_{crit} < 1$ for which the effect of the convergence will be to bring the flow to the sonic state $M_3 = 1$ at the outlet of the convergence. As y_o, and thus the flow Mach number M_1 behind $\vec{S}_i$, is gradually increased,[22] well into the regime of $M_1 > 1$, the point will eventually be reached if $\mathcal{R}$ is less than a certain limiting value beyond which M_1 can no longer be reduced to the value M_{crit} by the action of $\overleftarrow{S}_{rt}$. At this point the wave diagram changes from one with S_{rt} standing at the converging section inlet to one with no reflected shock, in which the flow throughout the convergence is supersonic. For

fixed and y_o variable, we shall call this transition point the upper bound for the occurrence of $\overleftarrow{S}_{rt}$ (see Fig. 17).

Now, on the other hand, let us begin with this latter condition of the flow — with no $\overleftarrow{S}_{rt}$ and with entirely supersonic flow in the convergence. Recall[20] that the action of a monotonic constriction on supersonic incoming flow is to reduce the Mach number. As y_o, and thus the value of M_1, is gradually decreased, the point will eventually be reached past which M_1 would be so low that the effect of the constriction of fixed area ratio $\mathcal{R}$ would be to reduce the outlet flow Mach number to less than 1. Hence, the flow solution must change at this point to one with an upstream-travelling shock $\overleftarrow{S}_{rt}$ and with subsonic flow in the convergence. This transition, again for fixed $\mathcal{R}$, is the lower bound for the absence of $\overleftarrow{S}_{rt}$.

The ambiguity arises from the fact that for fixed $\mathcal{R}$, the upper bound for the occurrence of $\overleftarrow{S}_{rt}$ is at a larger value of y_o than the lower bound for the absence of $\overleftarrow{S}_{rt}$. Thus between the two bounds is a regime — the regime of ambiguity — wherein both solutions fulfill all the usual flow conditions. Oppenheim actually went even further and postulated yet a third form of solution — one with a shock $\overleftarrow{S}$ standing part way into the convergence — which was also supposed to be an allowable solution in the interior of the ambiguous regime. By an appeal to Prigogine's[7] "principle of minimum entropy production", Oppenheim determined that "nature's choice" for the solution in the ambiguous regime was the standing shock, the location of which was presumably to be displaced upstream as y_o was decreased through this regime, so that at the lower boundary of the regime, the standing shock

would be at the inlet and would carry over directly to the $\overleftarrow{S}_{rt}$ solution.

It remained for Rudinger[8] to attack this ambiguity from the generic point of view. He considered the starting processes for the flow in the converging section; for values of y_o and $\mathcal{R}$ in the ambiguous regime he carried through detailed solutions by the method of characteristics. From this he concluded that in the regime of ambiguity, a reflected shock could not be formed, so long as the convergence was monotonic. In addition he called belated attention to an earlier work of Kantrowitz[9] that indicated that a standing shock within a convergent change in channel area would be unstable, and thus need not be considered as a possible steady-state solution in the "ambiguous" regime — a regime that might better be characterized as one governed by the transient starting flow.

In Oppenheim's calculations for the three possible wave solutions for a particular set of values y_o and $\mathcal{R}$ within the ambiguous regime, the entropy change across the transmitted shock was indeed the least in the case of the shock standing within the convergence. If, however, that solution is ruled out as unstable, it is interesting to note that the case with the next higher entropy change — the one that includes a $\overleftarrow{S}_{rt}$ — is just the one that Rudinger found cannot be achieved. As Rudinger pointed out, it is scarcely appropriate to attempt to apply Prigogine's extremum principle (which, it is claimed, is useful, at the most, in the case of neighboring possible solutions) to a case with discrete, noncontiguous solutions.

It should further be pointed out that the ranges of area ratio

and of incident shock strengths used in our work were far removed from the regime of "ambiguity". This is brought out in more detail in the discussion of Laporte's theory in Chapter IV.

From this survey of the recent related literature, it is evident that on the one hand, the subject of shock-convergence interactions is an active area of interest, while on the other hand, the body of experimental data concerning this interaction is still quite limited. It was felt appropriate, therefore, that we explore the potentialities of the Mach - Zehnder interferometer as an experimental tool for determining the strengths of the transmitted shocks produced by these interactions.

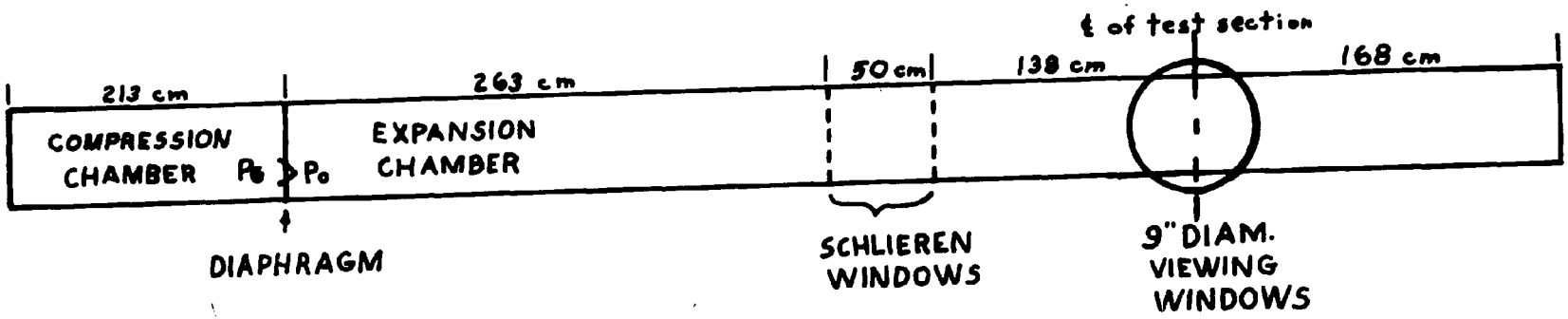
CHAPTER II

DESCRIPTION OF EXPERIMENTAL EQUIPMENT

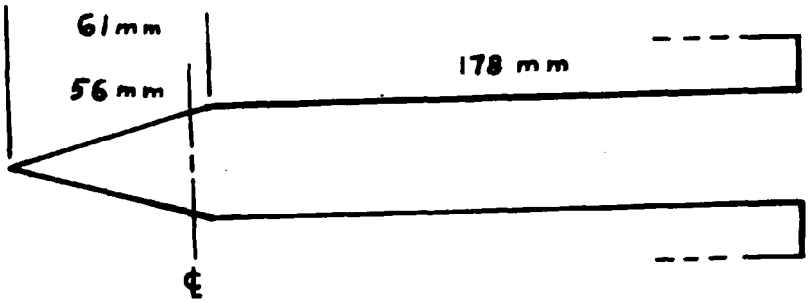
1. SHOCK TUBE HARDWARE

The basic design of the original shock tube (with internal cross-section of 2" by 7") of the University of Michigan Shock Tube Project is essentially unchanged from the description of it given by Geiger[10]. The dimensions and locations of the various parts of it are shown in Fig. 3. The distance between the diaphragm and the test section is nearly twice the length of the compensating chamber - a common rule of thumb in shock tube design. This ratio is quite satisfactory so far as the duration of the hot-flow following the primary shock is concerned, for all except the lowest value of shock strength we used. In this latter case, as will be noted in more detail in the discussion of the results, the head of the reflected refraction wave, which at first faces backward (i.e. upstream), is reflected from the end of the compression chamber and travels forward through the primary expansion wave, then through the contact surface or interface (between the hot and the cold flow). It arrives at the test section appreciably ahead of the interface. To be sure, this behavior does not affect the region of experimental interest in the present study, but it does indeed perturb the conditions in the region into which the tip-reflected shock travels.

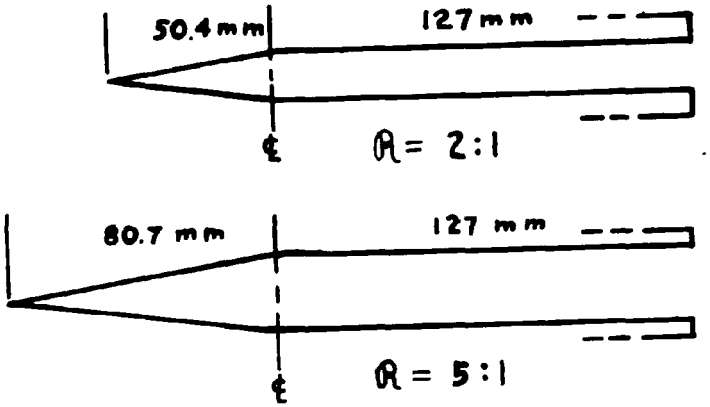
A number of additional sections, of varying lengths up to 28", have been added to the expansion chamber since 1950; the essentially different design of these sections was intended to allow simpler construction and assembly, to permit leak-tight joints to be achieved more readily and to contribute to the long-term stability of the critical internal



SCHEMATIC OF 2"×7" SHOCK TUBE



SCHEMATIC OF 2-UNIT 2:1 MODEL



SCHEMATICS OF 5-UNIT MODEL

Figure 3. Schematic diagram of the shock tube and of the models used in this experiment.

dimensions. Each section consists of 4 pieces of 1" thick tool-and-jig aluminum plate, suitably shaped and grooved to ± 1/2 mil tolerance, provided with end-face O-ring grooves, then bolted together to provide an internal rectangular cross-section of 7.000" x 2.012". The joints were sealed by coating the faces of the joints with non-hardening Permagasket No. 2, then quickly assembling the joints while this gasketing material was still tacky. This simple technique produced joints that were far more than adequately vacuum-tight for our purposes.

A test section of unusual design was also added to the expansion chamber. The test section was shaped from a single forged block of tool-and-jig aluminum by a sequence of successively finer machining operations alternated with annealings to relieve machining strains. This mode of construction was planned and started before the Permagasket joint-sealing technique was developed; this technique might well have made possible a less Herculean approach to an appropriately vacuum-tight test section.

As is pointed out in the section on the precision of the fringe-shift-measuring process, one of the critical factors determining the precision of measurement for the shock strengths was the initial pressure p_o in the expansion chamber. For a given shock strength $y_o \equiv p_1/p_o$, the initial compression chamber pressure p_6 is uniquely related to p_o by the Taub equation[11] $z \equiv \frac{p_6}{p_o} = z(y)$; z is monotonic in y and increases more than linearly with y. Hence the maximum available value for p_6 was a limiting factor in the precision of the interferometric measuring process. Here $p_{6\,max}$ was limited to about 3 atm abs by the strength and the leak rate of some of the older sections of the shock tube that

had been made part of the compression chamber. Since the precision of measuring fringe shifts was only proportional to p_o and thus less than proportional to p_6, a large increase in that precision would have involved strengthening these limiting sections very considerably, if not completely replacing them; this was not deemed worthwhile when all the other factors limiting the fringe-shift-measuring precision were taken into account. Nonetheless, reconstruction of the compression chamber to withstand at least twice as much pressure would be high on the list of recommendations for refining, improving and extending the present experimental program of measurements.

Geiger described the use of red zip tape (a modified form of cellophane) as the basic diaphragm material. More recently, sheets of cellulose acetate of various thicknesses have been used as diaphragms. Both types of material are well suited for use as diaphragm material insofar as they are fairly brittle and they tear readily when once punctured, but they are undesirable insofar as their very brittleness allows small fragments to be broken off in the rupturing process and hurled projectile-like down the expansion chamber by the high speed flow behind the shock. On the infrequent but not negligible occasions when these fragments were carried as far as the test section, they evidently were able to do considerable damage to the hardened razor-sharp small-angle wedge tips of models such as those used in these experiments; under these circumstances the wedge tips gradually became nicked and chipped. In addition, a fragmenting diaphragm material makes necessary the blowing out of the accumulation of fragments left scattered down the tube after each shot; this conflicts directly with the

need to have the wedge models for this experiment span the test section from floor to ceiling. Thus much advantage was found in using thin aluminum sheets as diaphragms. On 10-mil sheets of half-hard aluminum, the diagonals of a 2" x 7" rectangle were scribed by a rotating cutter on a vertical mill. The depth of scribing was variously 5 or 7 mils. For the 5-mil scribing, the minimum pressure differential $\Delta p = p_6 - p_o$ across the diaphragm for reliably clean tearing along all the scribe lines was about 900 mm Hg.; the maximum available Δp, approximately 3 atm., was normally insufficient to cause self-bursting. For the 10-mil diaphragms scribed 7 mils deep, $(\Delta p)_{min.}$ was about 600 mm , Δp(self-burst) was between 1000 and 1500 mm. Considerable care evidently had to be used in setting up the diaphragm-clamping jig used in scribing these diaphragms, in order for the scribing-depth tolerance to be held to $\pm$ 1/2 mil over the entire length of the scribe lines - a necessary specification if even minimal reproducability of $(\Delta p)_{min.}$ was to be assured. In all our experience with these diaphragms, only a very few times under unusual circumstances did any portions of the tips of the narrower petals of the breaking diaphragms snap off during tearing; these few pieces, being denser than corresponding acetate fragments, never reached the wedge tips. Fig. 4 shows a typical burst diaphragm.

In order for a model that fills the entire cross section of the test section to be in place while the expansion chamber was being pumped out - a feature not envisioned in the original design of the shock tube, a flush-sealing valve similar to the one described by Turner[12] was mounted in the side wall of the expansion chamber half-way between the diaphragm section and the test section. The expansion chamber was



Figure 4. View of a typical burst shock tube diaphragm that is ten mils thick and is scribed seven mils deep.

considered to be adequately evacuated, prior to being filled with the test gas to a pressure p_o, when its terminal pressure was reduced to 100-150 microns; an overall leak rate of 50 microns/min. was considered acceptable.

At certain of the joints between successive expansion-chamber sections, notably between the last of the older, welded-steel sections and the first of the newer aluminum-plate sections, there were irreducible unconformities of as much as a few mils. These were smoothed with Cold Solder (a steel-filled solvent-type epoxy) and apparently did not give rise to any noticeable flow perturbations or to any unduly rapid growth of the wall boundary layer.

2. ELECTRONICS AND TIMING OPTICS

The basic layout of the electronic circuitry for the 2" x 7" shock tube, as shown in Fig. 5, was essentially similar to the one reported by Geiger. Some of the modifications since that time were noted in Cole,[13] but will be described again for the sake of completeness, since that report was not widely distributed.

As in Geiger, the shock speed was determined by measuring the time of transit of the shock between two schlieren light screens separated by a measured baseline 500 ± 1 mm long. The pulses from the light-screen photomultipliers were amplified, passed through a discriminator, and shaped to serve as input trigger pulses to start and stop the velocity-time gate. The design of the gate and the associated master 1 Mc clock pulse generator was derived principally from a commercial circuit - the Potter chronograph. The gate design featured a double-triode shunt-type gate, with positive before-and-after lockouts on the start and stop pulse input circuits. The 1 Mc crystal-controlled oscillator was of conventional tuned-plate tuned-grid design, and was regularly checked by being heterodyned 5:1 with the 5 Mc transmission of WWV. The gated 1 Mc output pulses were counted by the velocity-time scaler, which was either a straight binary type scaler of the Geiger vintage, or it was a 1 Mc decade scaler (copied from the Baird-Atomic 1 Mc plug-in decade scaler) followed by lower-speed commercial plug-in decades. In the case of the old binary scaler, it was found that, given the available amplitude of the gated 1 Mc pulses, the gate-opening transient caused a minmum of 3 to 4 pulses to be lost at the start of the count. The gate-closing transient in turn caused 1 to 2 pulses to be added. A routine correction for these effects was made in the recorded

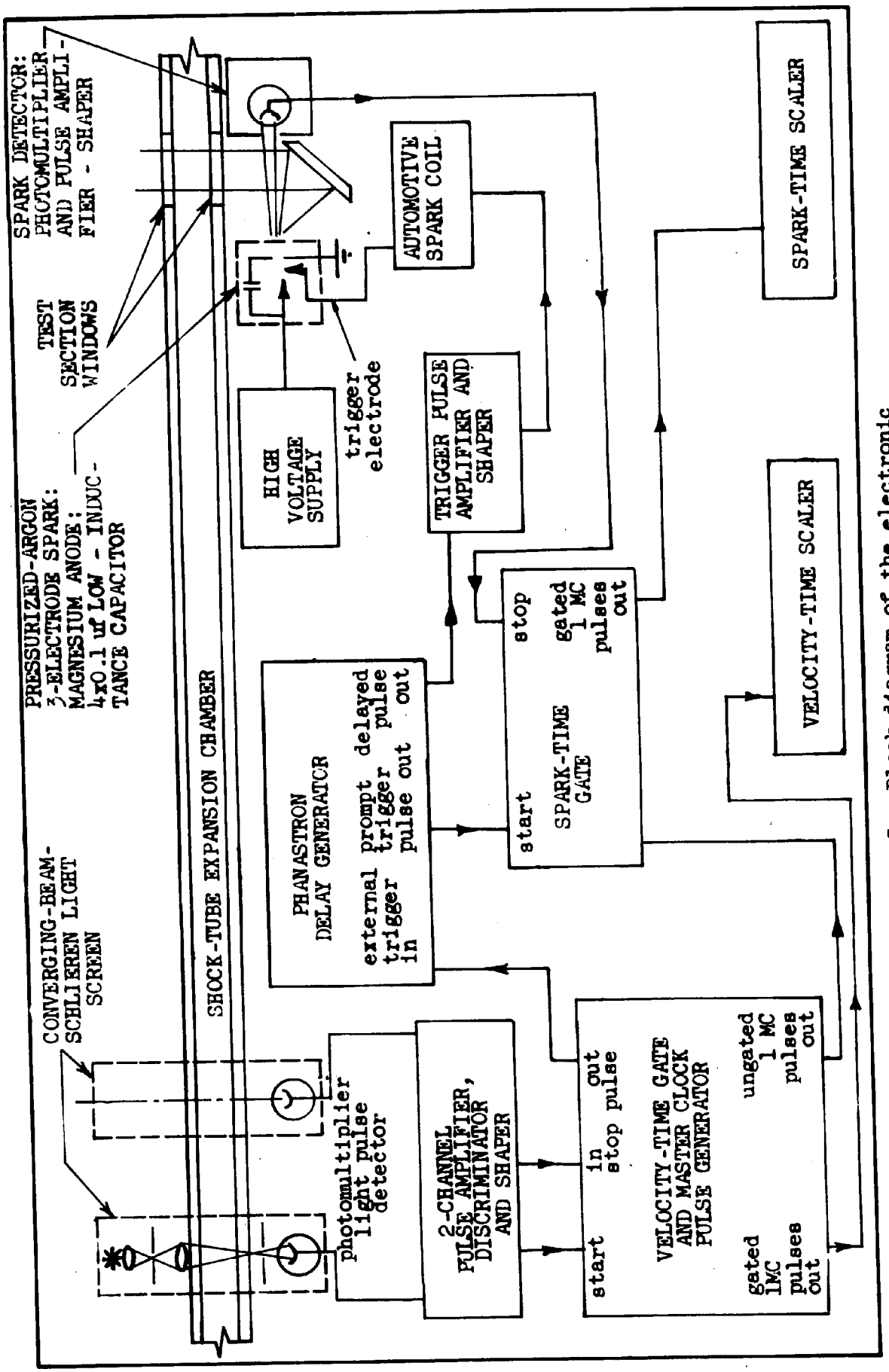


Figure 5. Block diagram of the electronic circuitry used in this experiment.

values of velocity time T_v, but the uncertainties in the actual net number of counts lost added an uncertainty of $\pm$ 1 to 2 usec to the recorded values. On the occasions when the 1 Mc decade scaler was available, no such uncertainty was imposed on the T_v values.

A pulse taken from the stop-pulse-channel lockout circuit was used to initiate the delay interval that synchronized the photographic spark with the phenomena of interest in the test section. In the phantastron delay generator[14] this pulse was shaped and then used to start the grid run-down cycle which is characteristic of the phantastron circuit[15]. At the same time, a prompt trigger pulse was sent out to start the spark-delay-time-measuring gate and scaler. At the end of the run-down portion of the cycle a delayed pulse was sent out to a trigger-pulse amplifier-shaper. The reproducibility of the delay interval thus generated was found to be within 1 usec for delays of the order of a few msec, within 4 - 5 usec for the upper end of the delay range — 30 - 40 msec. The amplified pulse was passed through the primary of an auto spark coil; the output of the secondary was directly connected to the third or tickler electrode of a three-electrode spark source using argon at 100 psig. There are various notes[16] in the literature on micro-second spark sources advising against the use of spark coils as high-turns-ratio pulse transformers, but we have found them reasonably satisfactory; the interval between the sending out of the delayed pulse from the delay generator and the firing of the spark was 15 - 25 usec, the jitter was about 5 usec. Because of this jitter, the spark-delay-time gate was stopped, not by the "delayed-pulse-out", but by the output of a photomultiplier-amplifier-shaper circuit. The light input to this photo-

multiplier was restricted by a long collimating tube that was aimed at the transparent plastic insulator of the spark. As in the case of the velocity-time gate and scaler, the use of an old-style binary scaler for measuring the values of T_{spark} added an uncertainty of 1 - 2 usec, similarly caused by the unreproducibility of the net loss of counts caused by the starting and stopping transients.

The use of a single master 1 Mc clock pulse source for both T_v and T_{spark} served to insure that in the event of a small deviation from the 1 Mc rate, the effect of it on T_v and T_{spark} would be proportional to their lengths. Thus suppose we had determined, say, that for a prescribed value of T_v, the phenomena in the test section would be at a desired location at a particular value of T_{spark}. Then if the 1 Mc pulse rate were to deviate slightly, we would be able to correct the measured value of T_v to its desired value and find that the situation at the test section would be the same for the same value of T_{spark}.

For this to be strictly true, all wave and flow velocities would have to be strictly proportional to the velocity of the primary shock, which is not the case; but for the principal object of interest in this study—the incident shock traveling in the constricted channel — this condition is nearly enough met to justify the refinement. Note also that this arrangement serves to correct only the x-t locations of the waves of interest for variations in the 1 Mc rate; maintaining T_v constant in the presence of a 1 Mc rate deviation causes the value of the incident shock strength y_o to be changed, so the strength of the channel shock, as determined from the fringe shifts, is appropriate to a value of y_o slightly different from that indicated by T_v. Gener-

ally, however, the deviation in the 1 Mc rate, due to changes in ambient temperature, component ageing, etc., was found by successive calibrations with WWV to be limited to much less than 1 part in 10^3, so whatever error was introduced by this small deviation was relatively small compared to the other uncertainties in the measurements, and was not substantially affected by the arrangement described here. If the shock strength is to be determined from the x - t data, then, to be sure, we are concerned with the fractional imprecision of the difference between two fairly large and nearly equal values of T_{spark}. Even if the 1 Mc rate was off but was constant during a single sequence of shots, each value of Δt would be off only by the fractional deviation of the rate, i.e. by $< 10^{-3}$.

3. THE MACH-ZEHNDER INTERFEROMETER SYSTEM

The detailed design of the Mach-Zehnder interferometer system was the work of Dr. E.B. Turner in 1952-53, but since it has not previously been described in a Shock Tube Project report, its main features will be noted here. The interferometer, as shown schematically in Fig. 6, is of the conventional 30° - 60° Kinder design, which provides that an 8" diameter working beam can be obtained with 9" diameter interferometer elements, and that the fringe pattern can be moved or changed by means of the motor-controlled adjustable mirror No. 4 without the focusing of the fringes in the image plane being changed. The light-source and the camera arms are perpendicular to the plane in which the interferometer elements are situated. The axes of the main parabolic mirrors are tilted slightly from the plane of the elements, in order that an on-axis parallel beam can be formed from the light beam coming from the

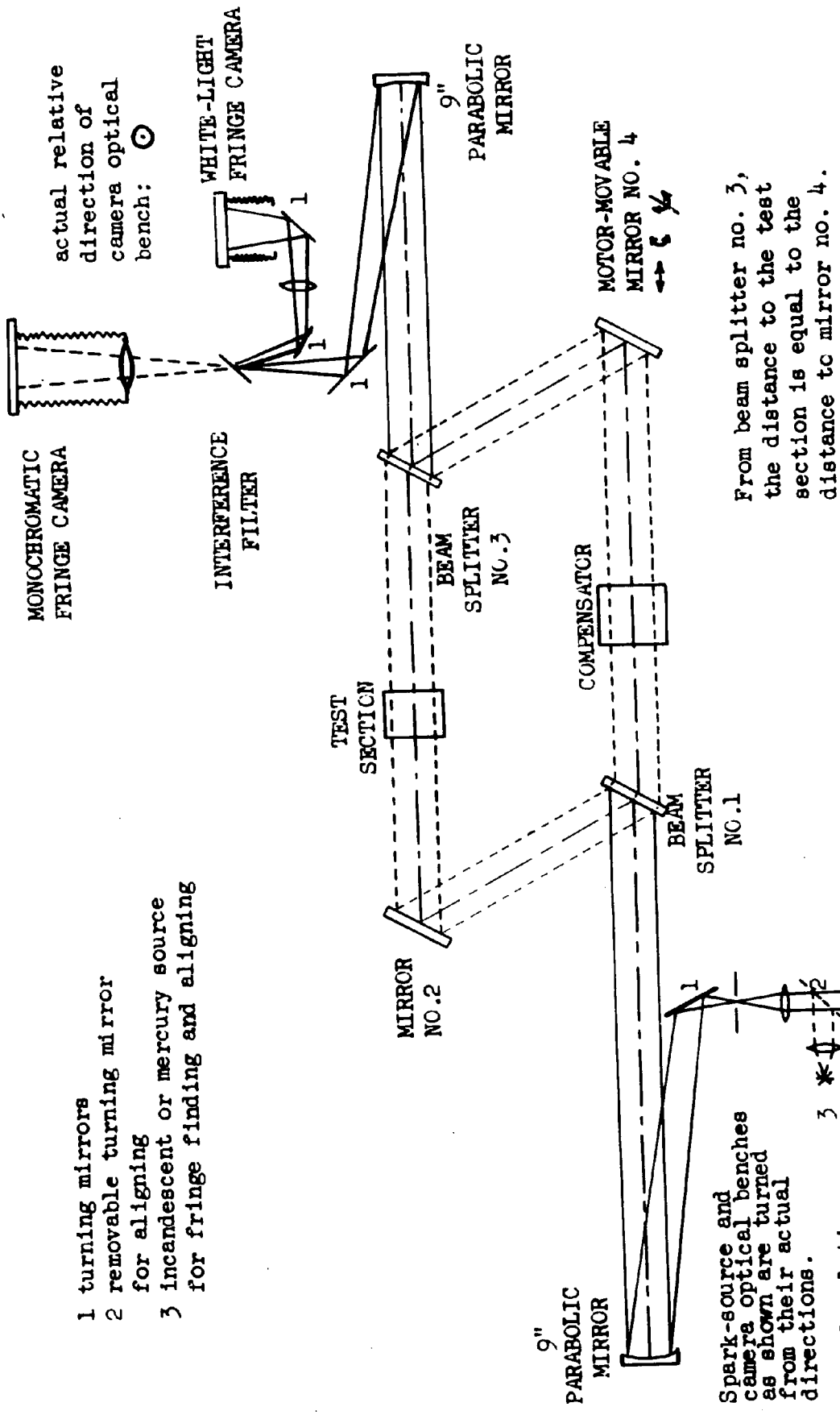


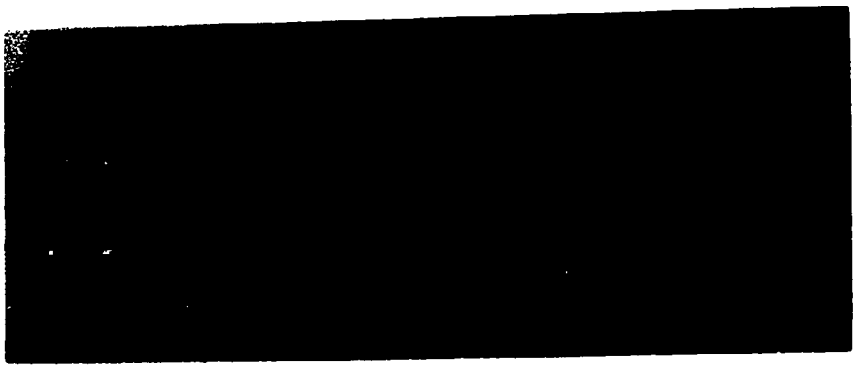
Figure 6. Schematic diagram of the Mach-Zehnder interferometer with its associated optical system.

first turning mirror, which is just at the edge of the main parallel beam, and similarly in order that the outlet beam from the interferometer can be diverted by the second turning mirror to the cameras. This conventional Z-symmetry, used with the tilted on-axis parabolic mirrors, minimizes the coma defect if the angles of mirror tilt are the same.[37] Note that the Mach-Zehnder interferometer system is readily convertible to a schlieren system, by blocking off the reference or compensating-chamber beam and replacing the interference filter with a knife edge.

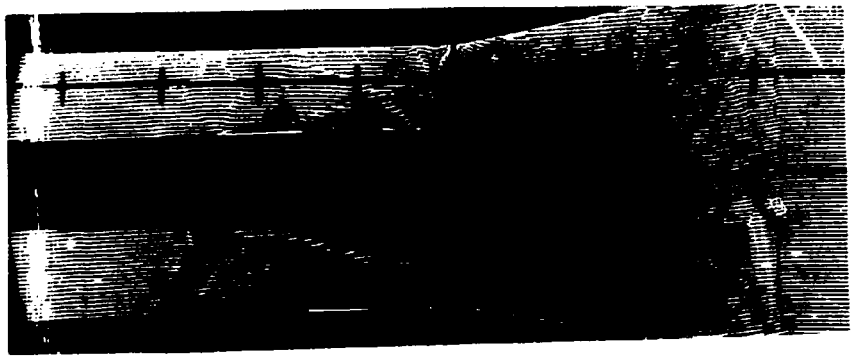
The 9" diameter interferometer elements are a matched set obtained from the Naval Gun Factory. Using the interferometer elements alone, i.e. without windows in the test section or the compensating chamber, one can obtain fringes of better quality than can be recorded by the film we regularly used. Accompanying the interferometer elements was a matched quartet of optical-quality wind tunnel windows for test section and compensating chamber; each window was flat and smooth to $\lambda/20$. Introducing them into the test-section and compensating-chamber beams had a scarcely detectable effect on the visual quality of the fringes. For exploratory runs, or for use when the Mach-Zehnder system has been converted to a schlieren system, we have found that windows of selected and matched plate glass have proved useable. For routine shooting for which the quality of the fringes is of importance but for which one would be disinclined to risk the optical—quality tunnel windows, a reasonably priced set of intermediate-quality windows was obtained from the Buchele Optical Co. of Toledo, Ohio. These windows were made flat to 3 - 4 λ, smooth to $\lambda/20$, matched as to wedge defect. The quality of fringes obtained with this set of windows is indicated in Fig. 7, a



a) monochromatic fringes; no-flow



b) white light fringes; no-flow



c) monochromatic fringes; flow



d) white light; flow

Figure 7. A quartet of interferograms taken for a single shot of the shock tube. Note [redacted] channel shock, tip-reflected shock, and the criss-crossing trailing wave pattern in the pair of flow pictures.

typical quartet of fringe pictures constituting the record of a single "shot" of the shock tube. The quality was such that the interferometer system was considered not to be a limiting factor in the precision of measurement of the fringe shifts. It is quite possible, though, that if the photographic aspects of producing interferograms were substantially improved by using fine-grain techniques and by reprinting the interferograms to increase the contrast of the fringes greatly, these intermediate-quality windows might be a limiting factor.

The various elements of the light-source end of the Mach-Zehnder system are shown in Fig. 8a. The three-electrode, pressurized argon spark was of conventional design, with four non-inductive C.1 μf, 8 kv capacitors arranged coaxially, with the third or tickler electrode brought in from the top, and with lucite as the high-voltage insulating material. The anode was a rounded-end rod of magnesium; the light from the spark, including a continuum toward the red produced by the initial discharge in the high-pressure argon and a series of magnesium emission lines that was chiefly in the green and blue, emerged through an axial hole in the cathode. The spark light was collimated by a pair of plano-convex collimating lenses, that were separated by a short distance. This made it possible for an auxiliary continuous light source to be introduced conveniently into the optical system for alignment purposes by simply inserting a turning mirror between the two condensing lenses for the spark. A third identical condensing lens was used in conjunction with the auxiliary source . This continuous source was either a mercury lamp used in conjunc-

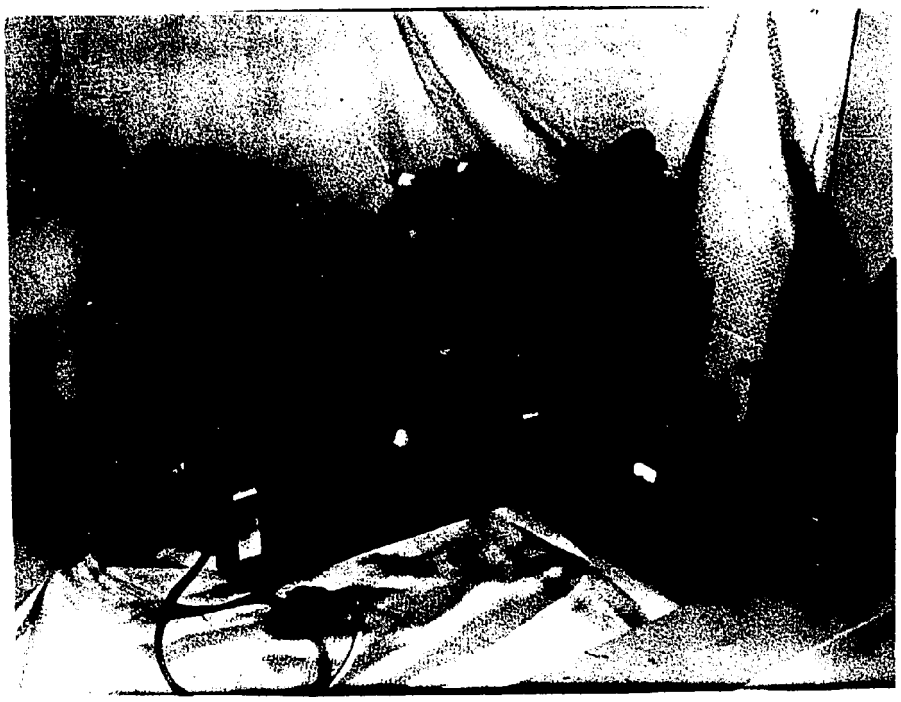


Figure 8a. View of the spark source end of the Mach-Zehnder interferometer system. Note the spark source with coaxially arrayed capacitors, the condensing lens pair, the steady incandescent or mercury-discharge lamp for fringe aligning, the mask and the turning mirror.

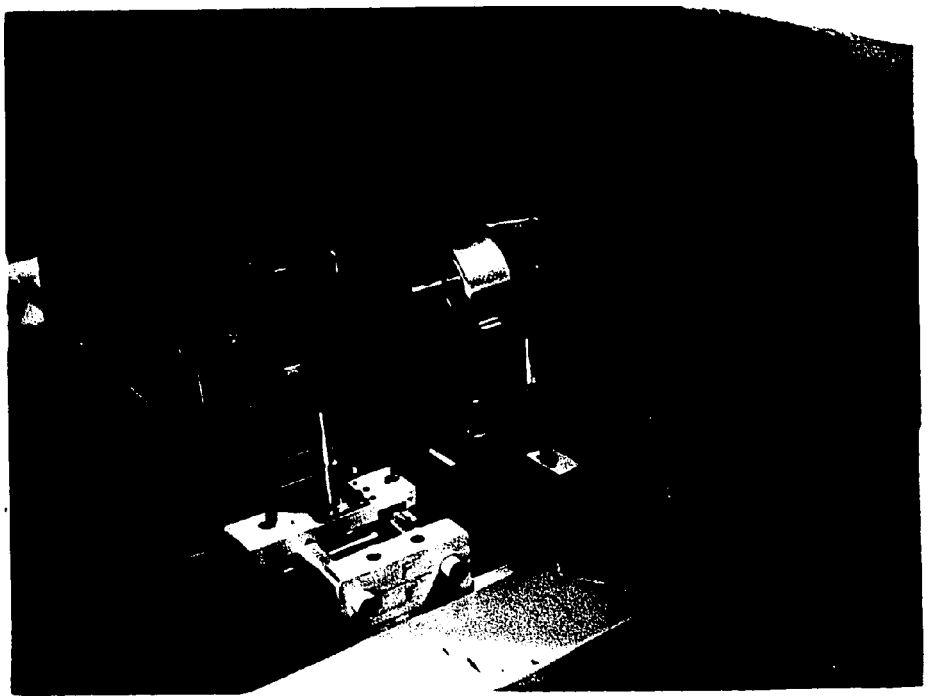


Figure 8b. View of the camera end of the Mach-Zehnder interferometer system. Note the turning mirror, the interference filter and the monochromatic and white light cameras.

tion with a transmission filter for the mercury green line, or a ribbon-filament incandescent lamp.

The various optical elements at the camera end of the Mach-Zehnder system are shown in Fig. 8b. At the image point of the spark source there was a multiple-layer interference filter that transmitted only the magnesium emission line of interest, in this case the very strong green magnesium triplet 5167-5173-5184 ($4\ ^3S \rightarrow 3\ ^3P^o$). The filter was a Baird-Atomic narrow-pass-band filter with a transmission ratio specified to be at least 60% at the center of the pass band and also with additional side-wing-suppressing filters. The filter was tilted slightly with respect to the incident beam, in order to divert into the white-light camera that part of the spark light that was reflected by the filter. This tilt caused the pass-band to be slightly broadened, but since the argon continuum was very weak in the green, this was no problem. The light of the magnesium triplet was transmitted directly to the monochromatic camera.

The lenses of the two cameras were identical; thus in order that the two image planes could be parallel, as shown in Fig.6, it was necessary to remove the lens from the white-light camera and mount it between the two optical benches so that the distances from the spark image to the camera lenses were the same in both cases. This arrangement proved to be a great convenience in adjusting the fringes and in making the images the same size. The two images were substantially smaller than full-size: the reduction ratio was usually about 0.45. This made it possible to display the entire 8" diameter beam on a 4" x 5" sheet of film, but also contributed to limiting the precision of the fringe-shift-

measuring process.

It was determined that a very strong magnesium emission line in the deep blue was adding its monochromatic fringe pattern to the white-light fringe pattern, thereby decreasing the contrast and the sharpness of the zero-order fringes and also obscuring the first minima. A Wratten K2 filter, with a cut-off in the bluish-green, was interposed in the white light beam and markedly improved the appearance of the white light fringes.

Interposed in the test beam of the interferometer at the exit window of the test section was a pair of crossed fiducial lines, the vertical one a tightly stretched nylon thread, the horizontal one a steel wire stretched tight at each end by short lengths of nylon thread. Short pieces of wire were laid crosswise along this steel wire at 20 mm intervals and attached by epoxy. The vertical thread served as a fiducial line defining the center of the test section. The horizontal line and its markers served as a direct measuring scale, by means of which the model and the waves of interest could be located in the interferograms. The horizontal line also served as a fiducial line; in flow pictures taken at long times after the passage of $\vec{S}_1$, the image of the test-section ceiling was displaced and obscured by the boundary-layer density gradients near the ceiling and was also obscured by the very close spacing of the monochromatic fringes there, caused by the density excess in the boundary layer; in these cases we were able to determine the actual location of the ceiling by measuring from the horizontal line.

The interferometer elements were housed in, and their gimbal mounts were supported by, an interferometer box made of 1/4" welded steel plate, with access holes cut out of the sides, and with entrance and exit holes

for the beam cut out of the ends. The box was mounted on pneumatic rubber tires for vibration isolation. Included in the original design of the interferometer was an arrangement for aligning the planes of each of the four elements parallel to one another at the intended orientation of 60° with respect to the horizontal axis of the Mach-Zehnder elements. This was accomplished by establishing an optical base line, consisting of a very well collimated light beam from a point-of-light source. This was precisely oriented with respect to the interferometer box. Then, in turn, the plane of each element was to be made parallel to this optical baseline and at the same time perpendicular to the plane of centers of the elements. Here use was made of a pentaprism, which has the property of refracting a beam of light by exactly 90°, regardless of its axial orientation (within broad limits). The use of such a device in the alignment of Mach-Zehnder interferometer is described by Ladenburg[17]. Such a pentaprism was mounted accurately on a heavy brass rod, then this rod was mounted, via a ball bearing coupling, on a support which could be positioned quite precisely with respect to any of 4 machined co-planar reference surfaces laid out along the length of the optical base line. The elements were then, one by one, made parallel to the base line (and perpendicular to the plane of the reference surfaces) by simple autocollimating: the beam of parallel light was passed through the pentaprism to the Mach-Zehnder element, was reflected back through the pentaprism to the back side of the pin-hole source-disk. The micrometer adjustments on the double-gimbal-ring mounts for the mirrors were altered until the reflected image of the source was superimposed back onto itself.

This entire procedure suffered from its relative inconvenience, in as much as the pentaprism and mount had to be moved and bolted down to

four separate locations in turn, and also evidently from either the bending of the solid supporting rod of 3/4" diameter brass or from excessive play in the bearings. Instead, the technique of "near and far" light sources* was found to be much more direct and efficient.

We first roughly aligned the mirrors, either by use of the pentaprism or more easily by using a protractor to set each of the mirrors to an inclination of 60° with respect to the horizontal reference direction of the interferometer box; we also as closely as possible set the distance between beam splitter No. 1 and the motor-movable mirror No. 4 equal to the distance between mirror No. 2 and beam splitter No. 3. Next we placed a small source at the regular source-location. A telescope facing upbeam was placed on the mirror arm at the beam exit of the Mach-Zehnder box, and focused on the images of the source. In general there would be two main images, corresponding to the 2 paths of the light beam through the interferometer - the lower or compensating chamber path and the upper or test section path. It was arbitrarily decided to adjust, say, mirror No. 2 in order to bring these two images of the far source to superposition. Then the far source was masked off and a "near" source, consisting conveniently of a flash light masked to emit only a pinhole of light, was mounted facing downbeam directly at the beam-entrance hole of the Mach-Zehnder box. Again, in general, two main images of this source would be visible through the telescope; these were superposed by adjusting the motor-adjustable mirror No. 4. This done, it was found that the images of the far light source had become separated and could be superimposed again by adjusting mirror No. 2. Thus by alternating between the near and the far sources and successively superposing

*This technique was, it would appear, first reported by Lamla[18]; the best recent reference known to the author is by Wood[19].

the respective image pairs by use of the appropriate mirrors, we found that the sequence rapidly converged to the point where both pairs of images were superposed with the same setting of the mirrors.

At this point the far and near sources were replaced by a filtered mercury source at the regular source-location, and fringes were looked for in the beam emerging from the exit of the Mach-Zehnder box. The virtual source of the fringes was usually far distant from the test section; their possible spacing would range from very narrow to very wide; when the elements were being aligned initially, it was usually the case that the adjustable mirror needed to be translated up-or-down-beam by a distance that should not be greater than the uncertainty in the process of equalizing the distances between the pairs of elements.

The fringe pattern could then be thought of as arising from the interference between two superposed virtual planar sources that intersected at a small angle and that were located somewhere along the line of the emerging beam. The sketch on p.72 shows these planar sources in cross section. To move the fringes to the test section, the orientation of mirror No. 2 was slowly varied about its horizontal axis; at the same time the fringes were kept in view by adjustment of mirror No. 4. At this point the fringes were still being viewed by looking upbeam near the exit window of the Mach-Zehnder box, ahead of the second parabolic mirror; we could determine whether the virtual source of the fringes was being moved closer to the test section by observing the parallax of the fringe pattern with respect to the test section.

The cameras had previously been focused on the test section by placing the image planes midway between the focal planes of the outside surfaces of the entrance and the exit windows of the test section.

Then, the regular interference filter having been replaced by the line filter appropriate to the mercury source, monochromatic fringes from the mercury source became visible on the ground glass focusing screen of the monochromatic camera. This monochromatic pattern was then translated in the direction of increasingly sharp, bright fringes to such a point that the white-light pattern of the mercury source was visible when the line filter was removed from the beam.

At this point it was likely that the two virtual beams forming the fringe pattern were slightly skewed with respect to each other, i.e. the equivalent planar sources were slightly tilted laterally as well as vertically with respect to each other. This could be detected by noting the apparent rotation of the straight-line fringe pattern as one changed one's point of observation from the image plane of the camera to the original point of viewing the fringes near the beam-exit hole. For this to be eliminated, mirror No. 2 was adjusted about its "vertical" axis until the fringe pattern had the same orientation at both points of observation; during this adjustment, the fringes were kept in view by simultaneous adjustment of mirror No. 4. This last was usually a delicate adjustment, since the "twist" of the fringe pattern was found to be very sensitive to the skewness of the two beams.

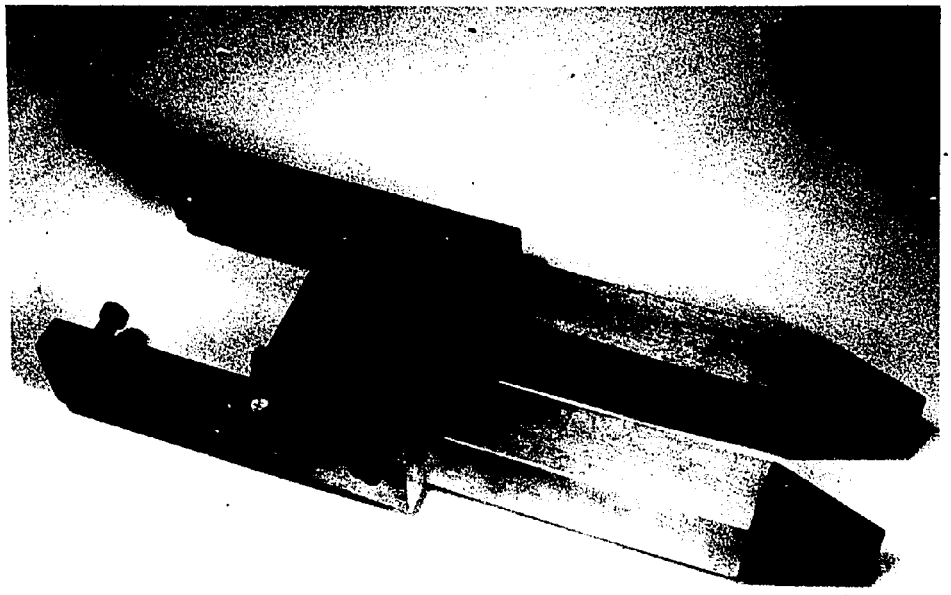
Once the optimally sharp fringe pattern was obtained in this fashion, the mercury source could be replaced by the incandescent ribbon-filament lamp, and the mercury line filter replaced by the magnesium line filter. The fringes could then be given their final alignment using only the motor-movable mirror No. 4, since the Kinder-type mount made it possible for fringes properly focused at the test section to be adjusted, without defocusing, by means of the movable mirror alone.

With the Buchele medium-quality windows in the test section, it was found that in the beam there was a peripheral ring 1" wide, in which the fringe pattern was tilted slightly with respect to the main pattern inside the ring, but this regular "defect" in the windows in no way impaired the usefulness of the fringe pattern.

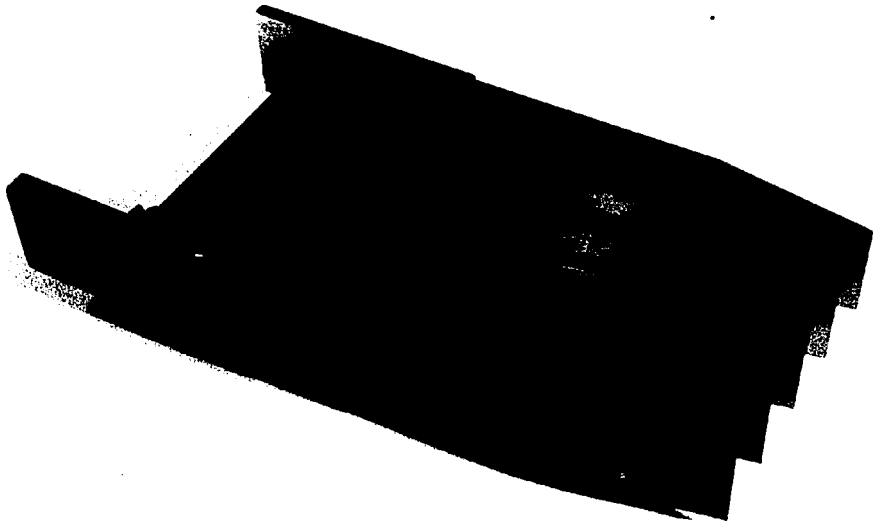
After both the monochromatic and the white-light cameras had initially been focused at the midpoint between the foci of the outsides of the entrance and the exit windows of the test section, then despite the nominal equivalence of the two camera lenses, the image plane of one of the cameras usually needed slight adjustment to equalize the sizes of the two images exactly. This equalizing was brought about in order to make the monochromatic and white light interferograms of a given shot as exactly superposable as possible (see next chapter).

4. MODELS FOR THE SHOCK TUBE

As shown in Figs. 9 and 10, the models used in this experiment each consisted of a stack of wedge-tipped channel separators, usually called wedges, alternated with spacer blocks whose height defined the height of the constricted area channels. The models consisted of two or of five units instead of a single unit, as would appear to be the logical choice for these shock-convergence interaction studies, because the multiplicity of origins for the wavelets that amalgamated to form the tip-reflected shock was very desirable for the purposes of another study of a related interaction that was being conducted simultaneously. The spacers and the main bodies of the wedges were made from tool-and-jig quality aluminum; the tips were of steel, first rough-cut, then case hardened by carburizing, then drawn back to about Rock-



a) View of the two-unit model with area ratio of 2:1.



b) View of the five-unit model with area ratio of 5:1. (This model can be adapted to an area ratio of 2:1.)

Figure 9. Views of the wedge models used in this experiment.

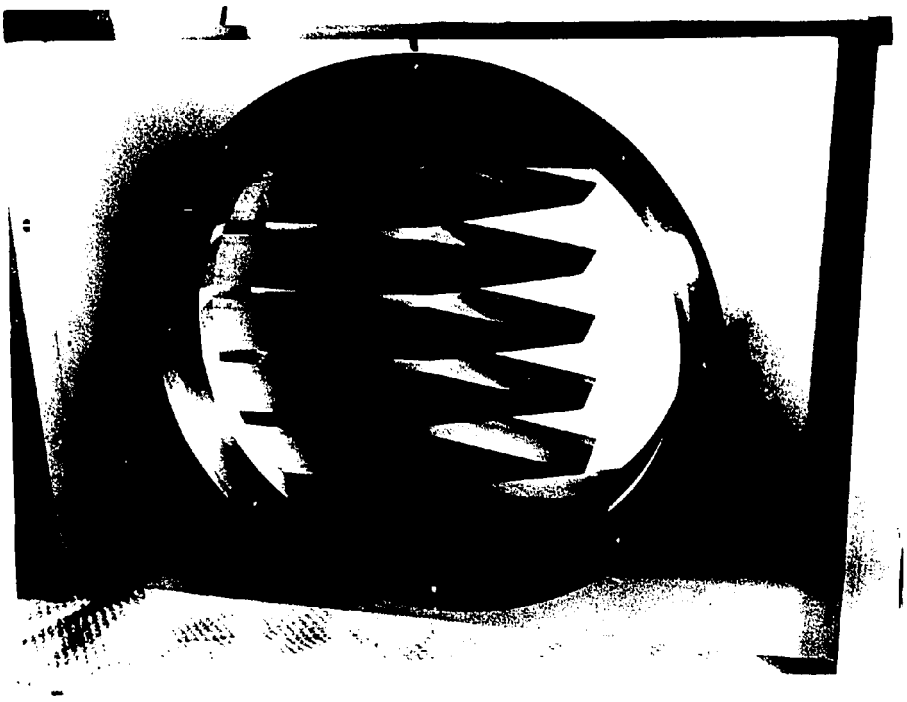


Figure 10. View of a wedge model in place at the shock tube test section. (The test section windows have been removed.)

well C65 and given the finish grinding. Because the effect of the carburizing was most pronounced near the small-angle tips of the wedges, the razor edge tips were somewhat brittle in spite of the partial annealing and had to be treated with some care. Fortunately, because of the use of aluminum diaphragms, the tips did not need to withstand the impacts of large diaphragm fragments, as would have been the case with plastic diaphragm materials like acetate. The tips were aligned with respect to the wedge bodies by two aligning pins each and attached by bolts running the length of the wedge bodies.

The two newer 5-unit models, with wedge tip half-angles of 10° and area ratios of 2:1 and 5:1, were designed to make use of the same basic interchangeable parts. Only the wedge tips were changed, and for the 5:1 version of the model, extender plates were attached to either side of each wedge body to reduce the area of the individual channels to 1/5 of the area of the main channel. These extender plates were aligned flush with the edges of the wedge bodies and with the front surfaces of the spacer blocks by use of two very shallow aligning disks; the plates were attached by the sparing use of Duco cement at the corners of the plates, so that they could readily be removed when the 2:1 configuration was needed again.

The components of the 5-unit stack of wedge bodies and spacer plates, common to the 2:1 and 5:1 configurations, were aligned with respect to each other by two aligning holes (with corresponding dowel rods) laid out on a diagonal of the horizontal rectangular cross section of the spacer blocks, so as to provide a long base line for good angular orientation. The aligned components of the stack were clamped together by two bolts with recessed heads and nuts. The vertical sides of the stack

assembly were then surface-ground to achieve the specified tolerance on the flatness and parallelness of the two sides and on the 2.000" thickness of the model.

Models for the shock tube are usually positioned in and clamped to the shock tube by external bolts that pass through holes drilled in the ceiling or floor of the shock tube and then into the model. Because it was necessary to have the various models in so many different locations at and downstream from the test section, it was not feasible to provide the great number of mounting holes in the floor of the shock tube that would have been needed, so a scheme of self-clamping of the models was necessary.

The top and bottom spacer blocks were extended 3" beyond the back end of the other spacer blocks and the wedge bodies, in order to provide bearing surfaces for clamping the model internally to the shock tube ceiling and floor. A rod with one end threaded was passed through the top plate and screwed into a tapped hole in the bottom plate. A recessed bearing plate was provided on the upper side of the top plate, so that when the rod was then partially unscrewed out of the bottom plate, the top end of the rod would press the bearing plate against the ceiling of the shock tube and press the bottom plate to the floor. With the model in place either at or downstream of the test section, hooked-end meter sticks were inserted upstream from the end of the expansion chamber, the stick ends were hooked onto a toothed wheel that had been locked onto the threaded end of the rod, and the clamping torque was exerted on the rod by pushing and pulling appropriately on the meterstick "wrenches". In order for the model to be clamped in place firmly enough to resist its being displaced downstream by the shock and by the

remaining differential pressure on the model after the shot, the top and bottom bearing surfaces were coated with very thin layers of Pro-Chem (an air-curing liquid neoprene); in the layer of Pro-Chem on the upper clamping surface, very fine emery powder was embedded to give further resistance to displacement of the model by the shock.

When a model was used at the test section, the sides of the model were covered with Scotch No. 11 cloth tape, about 4 mils thick, in order that the narrow gaps between the model and the windows would be filled (and thus not contribute to the slight gas leakage around the sides of the model) and primarily in order to cushion the windows from direct contact with the model, especially with the wedge tips. The sides of the models could not, of course, be taped when the model was downstream from the test section, but no adverse effect of the very narrow gaps around the sides and top of the models could be detected in the interferograms.

5. EQUIPMENT FOR READING INTERFEROGRAMS

As described in the next chapter, a set of four interference-fringe pictures (see Fig. 7) was obtained for each shock tube shot; this consisted of white-light and monochromatic fringe pictures both of the initial or no-flow state and of the instantaneous state of interest in the test section during the shot. Note that the very contrasty appearance of the monochromatic interferograms in Fig. 7 does not give a true indication of the actual contrastiness of the original films. The measurements derived from each set were obtained by superposing the flow and no-flow monochromatic interferograms. The fringe shift between corresponding fringes in various regions of interest in the two pictures

was determined by counting the number of cycles of opposition and superposition of the fringe patterns as the flow picture was translated with respect to the no-flow picture.

This translation was carried out in a film comparator as shown in Fig. 11. This consisted of an upper window and frame, an identical lower window mounted in a base plate, and a microscope-type mechanical stage connecting the two parts. The two monochromatic interferograms from a particular run were carefully aligned by using the edges of the shadows of the model, of the ceiling and of the reference wires. They were then clamped together between the two windows in the comparator. Each film was held fixed with respect to the window next to it by a "frame" of Pro-Chem, which gripped the film sufficiently to overcome the tendency of the two films to stick together. The mechanical stage made it possible to move the upper window in two directions with respect to the lower window, although usually only one direction of translation was used in measuring fringe shifts. Since the vernier scale on the slide could be read only to 0.1mm, it was found appropriate to mount a micrometer head on the base plate so that the motion of the movable part of the stage in the direction of principal interest could be read to within 0.5 mil. Direct superposition of the flow and no-flow monochromatic interferograms was made possible by the fact, as verified by numerous checks into this matter, that no detectable difference could be found between the image sizes of these two interferograms in any one set; thus we could assume that at any point in the flow picture that was free of local density gradients, the fringe spacing would be the same as at the corresponding point in the no-flow picture. This made possible the direct linear

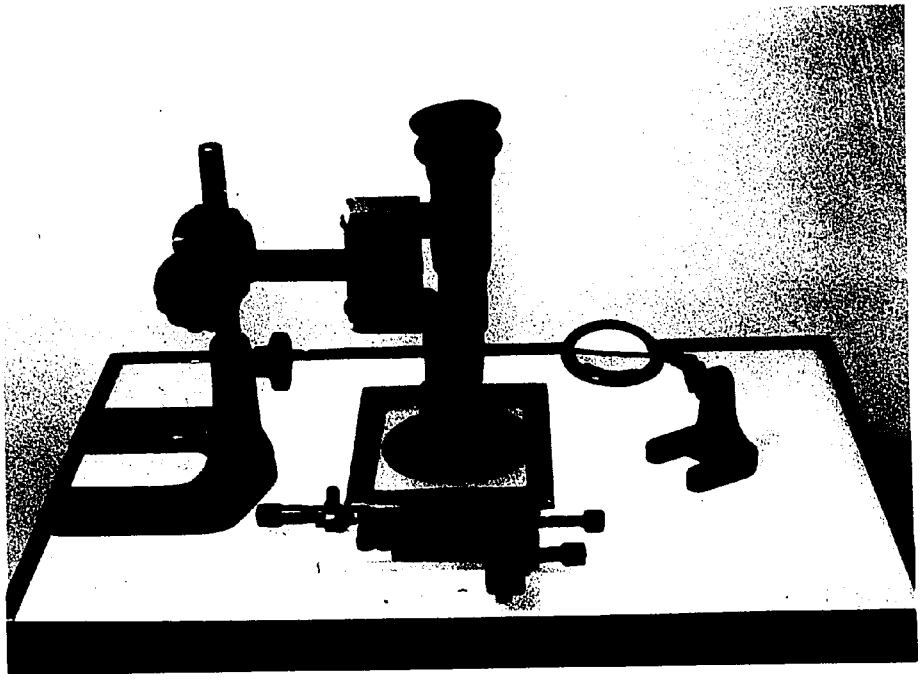


Figure 11. View of the fringe-shift measuring equipment. Note the viewing microscope, magnifying glass for use in fringe marking, and the film comparator with microscope stage mechanism - all on a portable light table.

interpolation of the location of wire-shadow superposition between successive locations of optimum fringe opposition. A microscope of 10 to 20 power was used to view the optimum opposition of the fringe patterns and the superposition of the wire shadows sufficiently closely that the viewing process was not a limiting factor in the reproducibility of the three distance values used in determining each fractional fringe shift. Indeed, too great a microscope magnification for a given monochromatic fringe pattern density and contrastiness seemed to make the fringe setting process less reproducible. In addition, some experimenting was done in varying the brightness of the light transmitted through the superposed interferograms by interposing neutral density filters between the light table surface and the comparator; this was done in an effort to keep the fringe shift readings as reproducible as possible under varying conditions of fringe spacing and photo image density.

The physical non-coplanarity of the two superposed emulsions, amounting to the thickness of a sheet of film - about 8 mils, had no evident effect in producing a parallax uncertainty in the determination of the fringe shifts. The amount of displacement of the visual image of one emulsion with respect to the other as one's eye was moved from side to side in the visual field at the eyepiece was quite small; thus even a modest effort to keep the eye centered on the eyepiece was more than adequate to eliminate parallactic displacement as a factor in the reproducibility of fringe shift readings.

CHAPTER III

EXPERIMENTAL PROCEDURES

1. INTRODUCTION

The x - t diagram for the interaction of a shock with an area convergence, as shown in Fig. 2, and the corresponding schematic diagram of the resulting wave configuration " in the large", as shown in Fig. 1b, both show the principal waves arising from the interaction: the shock wave $\vec{S}_c$ penetrating into the constricted channel, and the upstream-facing shock $\overleftarrow{S}_{rt}$ formed from the individual wedge-tip wavelets. The strength of the wave $\vec{S}_c$ is $y_c \equiv \frac{p_2}{p_0}$; for the wave $\overleftarrow{S}_{rt}$, it is $y_{rt} \equiv \frac{p_4}{p_1}$. It is the long-established custom at the Shock Tube Project to consider the wave strength y as the basic parameter of a shock, and to consider all the other parameter ratios associated with the shock as functions of y. Thus our attention was focused on the problem of determining the various shock strengths from the interferograms and also on the comparison of the measured values of the shock strengths with some theoretical predictions for the strengths of the shocks arising from the interaction.

Of these two waves, $\vec{S}_c$ was of much greater interest, and indeed was the only one that was actually measured and used for comparison with the theoretical predictions. The reasons for this were essentially as follows: $\vec{S}_c$ traveled into gas at rest, which was free of boundary layer, while $\overleftarrow{S}_{rt}$ moved upstream into gas that was already substantially accelerated and that was also accompanied by a steadily thickening wall boundary layer. In addition to the local effect of the boundary layer on $\overleftarrow{S}_{rt}$ advancing into it, the time-and space-integrated effect of

the boundary layer throughout the shock tube flow was to alter the flow Mach number and the flow speed of the free-stream gas into which $\overleftarrow{S}_t$ was advancing. In many of the sequences much time was needed for S_{rt} to be at all well formed from the tip wavelets; this gave the boundary layer time to alter the value of y_{rt} substantially. Fig. 12 shows some of the stages in the formation of a plane shock $\overleftarrow{S}_{rt}$ from the wavelets. Furthermore, y_{rt} was a relatively weak function of y_o, so it was far less sensitive an indicator of the interaction than was y_c; this more than offset the greater precision of measurement due to ρ_1 being larger than ρ_o.

To be sure, the precision of measurement of the strength y_c of $\overrightarrow{S}_c$ was limited for strong shocks, as will be explained in more detail later, by the low value of the pressure p_o ahead of the incident shock, whereas this factor would have been less important in limiting the precision of measurement of y_{rt}. However, it was just in the regime of strong shocks that the boundary layer has a more perturbing effect on the measured values of y_{rt}. Thus it was felt that y_c was the appropriate parameter of the interaction that we should measure.

The experimental program consisted of taking sequences of interferogram sets for values of the shock strength y_o of the incident waves $\overrightarrow{S}_i$ ranging from 2 to 12 in argon and for both the area ratios 2:1 and 5:1. In addition the 2:1 area ratio was studied in conjunction with wedge tips both of 20° and of 10° wedge half-angle. Each sequence consisted of a number of sets of interferograms with $\overrightarrow{S}_c$ at successive positions along the constricted channel, and one or two sets showing the end-channel-reflected wave $\overleftarrow{S}_{rc}$ shortly after reflection. The

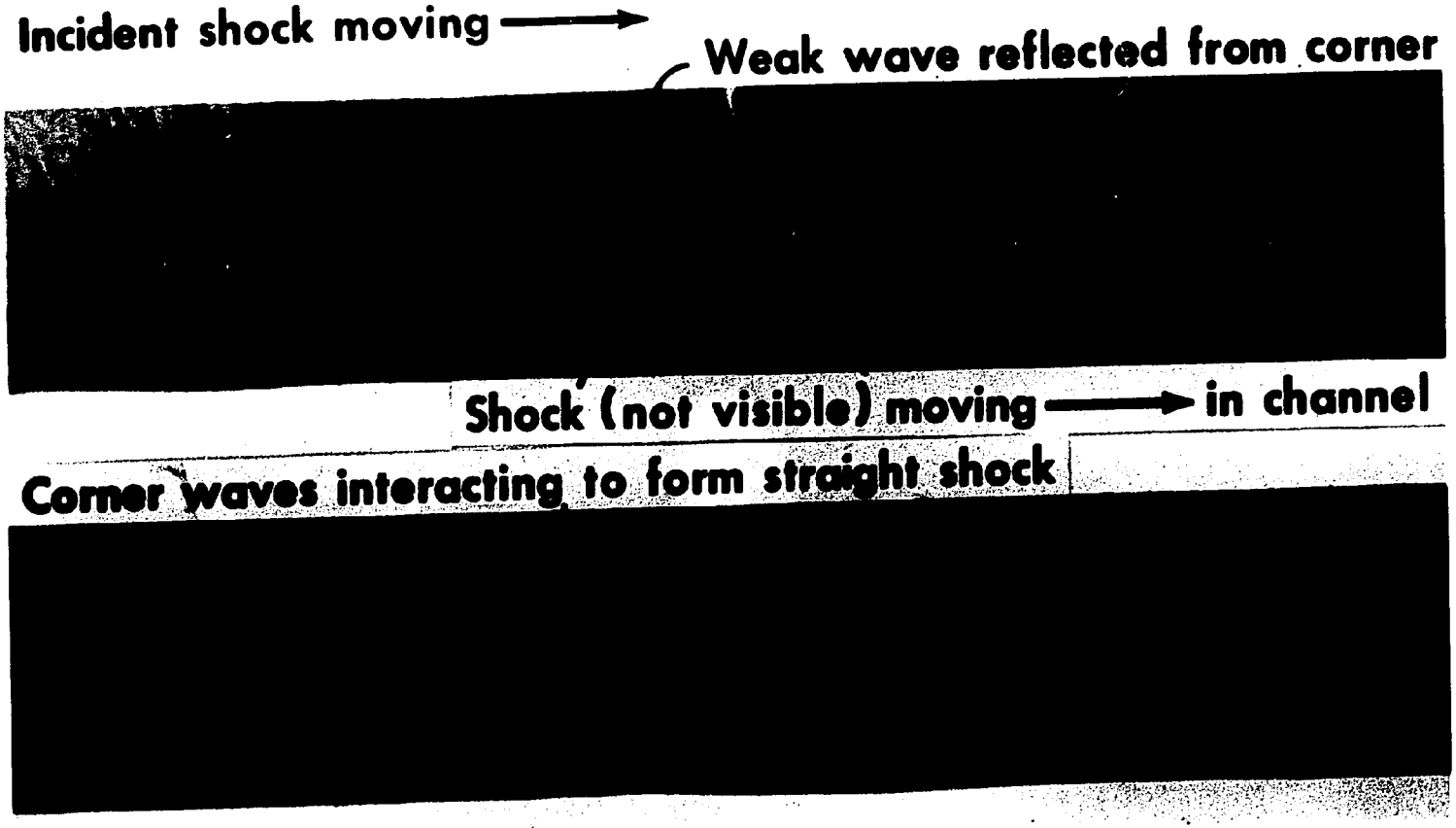


Figure 12. Schlieren photographs showing the progressive formation of the tip - reflected shock from the individual wedge-tip wavelets. Note also the development of strong trailing waves just downstream from the outlet of the convergence.

purposes in taking pictures at several locations in the channel were: to determine to what extent the precision of the interferometrically measured values of y_c would allow the process of formation and stabilization of $\vec{S}_c$ to be observed; also to provide a modicum of x-t data for $\vec{S}_c$, so that it could be determined whether the speed of $\vec{S}_c$ could be measured precisely enough to give a significant comparison with the interferometric measurments.

The pictures of $\overleftarrow{S}_{rc}$ that were taken shortly after reflection at the end of the narrow channel were to provide an additional check on the value of y_c at an effectively later time than y_c could be measured directly; note here that just as y_{rc} is usually taken to be $y_{rc}(y_c)$, the converse is at times appropriate, i.e. $y_c = y_c(y_{rc})$. The forms of these relations are given in the section on reduction of the fringe shift measurements.

When we made use of interferometric measurements of y_{rc} in determining the corresponding values of y_c, we were assuming, of course, the validity of the relation $y_{rc} = y_{rc}(y_c)$; there was no particular reason to question the appropriateness of the assumptions involved in the derivation of this relation, but, on the other hand, no one, to the best of our knowledge, has ever extensively examined normal shock reflection in the shock tube in the low to medium shock strength range that we studied. This is discussed somewhat further in the section on recommendations for further experimental work. In addition, it was appropriate to require that $\overleftarrow{S}_{rc}$ be observed shortly after leaving the end of the channel. It should be noted here, though it is spelled out in more detail later in this chapter, that for the 5-unit 2:1 model,

a special technique was needed in order for us to obtain usable interferograms of $\overleftarrow{S}_{rc}$, while for the 5-unit 5:1 model, it was not possible, with the techniques and the models we had available, for us to obtain reliable interferograms of $\overleftarrow{S}_{rc}$.

The expansion chamber gas, and thus the working gas for all the flow regions of interest here, was chosen to be argon because of Shock-Tube-Project tradition, because it is monatomic and has an essentially fixed value of γ for a broader range of shock strengths than other common shock tube gases, because it makes possible stronger shocks $\vec{S}_i$ for given limitations of p_o and compression chamber pressure p_6, and also in large part because Laporte's calculations were made for a monatomic gas. It was at first planned that a series of sequences would also be obtained for a gas with a very low value of γ, i.e. SF_6, with a value of γ of 1.1 (or by Shock Tube Project custom, with a value of $\mu \left(\equiv \frac{\gamma+1}{\gamma-1}\right)$ of 22 at room temperature). However, it appears that μ for SF_6 is quite a strong function of temperature even for the relatively small temperature jumps associated with values of y_o of from 2 to 12; thus a Laporte-type calculation for the interaction with the constriction would, for SF_6, have had to include real-gas effects - a task that was out of the question for us. In addition, SF_6 is a much more optically refractive gas than argon; thus even a relatively small amount of turbulence in the boundary layer had the effect of making the fringes so irregular in appearance that fringe shifts could not be measured. This effect was particularly significant for pictures taken at relatively long times after the passage of $\vec{S}_i$. (Such pictures were needed for a separate but related study to be reported in a subsequent publication.)

The first set of interferogram sequences was taken using a 2-unit model with wedge-tip half-angles of 20° and with an area ratio of 2:1; the main series of sequences were taken using the 5-unit model with wedge-tip half-angles of 10° and with area ratio of 2:1 and of 5:1. The two values of wedge angle and of constricted channel height for a single area ratio were used in an effort to see if wedge angle or channel size had an appreciable effect on the formation process for $\vec{S}_c$ or on the final stabilized values of y_c.

Note that in Fig.7c, a typical monochromatic interferogram of the constricted-channel flow, there is, following after $\vec{S}_c$, a series of criss-cross waves generated by the interaction of the flow with the converging section and especially with the tip and the shoulder of the wedge. These waves were collectively referred to as trailing waves. To the extent that these waves were strong enough that they differed significantly from isentropic waves, the connection between $\vec{S}_c$ and $\overleftarrow{S}_{rt}$ could not properly be regarded as isentropic - a condition assumed in Laporte's analysis of the shock - wedge model interaction.

For the flow conditions to correspond reasonably with theory, the trailing waves should be weak from their beginning or they should have largely caught up and amalgamated with $\vec{S}_c$ and have left behind, at most, only a few weak waves that would be essentially isentropic. In general, the more significant values of y_c were to be obtained at the end of the constricted channel. It is for this reason, primarily, that values of $y_c = y_c(y_{rc})$ were in a few cases the more precise measures of y_c. Tending to work against the relative precision and significance of the values $y_c(y_{rc})$ were the following factors:

the relative imprecision (see Chap. IV, Sec. 1) for $y_c(y_{rc})$ was greater than for y_c (see Table 1). This is reasonable since y_{rc} is a weak function of y_c ($y_{rc} \to \mu+2$ as $y_c \to \infty$); this offsets the gain arising from ρ_2 being greater than ρ_o. In addition, in certain cases the trailing wave patterns evidently did not become effective in perturbing the local values of y until the shock was either near the end of the channel or had already been reflected from it.

It is seen then, that attention was directed to the details of the flow-constriction interaction chiefly insofar as the resulting trailing wave trains caused deviations from the assumed nature of the channel flow.

2. ACQUISITION AND TREATMENT OF THE X-T DATA

The vertical reference line for horizontal distance measurements was the vertical nylon thread referred to in the section on the Mach-Zehnder interferometer. The thread was stretched vertically across the exit-window frame at the test section. The depth of focus of the cameras was such that the thread was in reasonably good focus when the center of focus of the cameras was half way between the two test-section windows.

On each of the two basic models a particular location was chosen to be the center line for measuring the locations of the shocks with respect to the model. These center lines were chosen to be at or near the vertical line of the shoulders of the wedge tips; when this arbitrarily chosen line was aligned with the reference line of the test section, the coordinate systems of the model and of the test section coincided. With respect to each coordinate system, positions downstream

y_o	y_c (Laporte)	x_c	N(vac,0)	y_{rc} (Laporte)	$\frac{\delta_c}{\varepsilon}$	$\frac{\delta_{rc}}{\varepsilon}$	$\frac{\delta_{c(rc)}}{\delta_{rc}}$	$\frac{\delta_{c(rc)}}{\varepsilon}$
				2:1				
2	2.30	1.62	15.0	2.03	.109	.0955	1.40	.134
4	4.84	2.30	9.2	3.18	.165	.120	2.05	.246
6	7.35	2.68	5.6	3.80	.296	.181	2.66	.481
8	9.86	2.94	3.5	4.20	.525	.278	3.26	.906
10	12.4	3.09	2.6	4.48	.786	.366	3.87	1.42
12	14.9	3.21	1.9	4.68	1.19	.491	4.50	2.21
				5:1				
2	2.60	1.73	15.0	2.22	.105	.0885	1.44	.127
4	5.59	2.43	9.2	3.39	.168	.116	2.22	.258
8	11.4	3.02	3.5	4.38	.560	.274	3.64	.998
12	17.4	3.30	1.9	4.84	1.31	.486	5.06	2.46

$$\frac{\delta_c}{\varepsilon} = \frac{(\mu + y_c)^2\sqrt{2}}{N(vac,0)(\mu^2 - 1)y_c}$$

$$\frac{\delta_{c(rc)}}{\delta_{rc}} = \frac{(\mu + y_c)((\mu + 2)y_c - 1)}{y_c(\mu + 1)^2}$$

$$\frac{\delta_{rc}}{\varepsilon} = \frac{2\sqrt{2}}{N(vac,0)\mu(\mu - 1)} \frac{y_c+(\mu-1)/2}{y_c + 1/\mu}\left[(\mu^2-\mu+1)(1/y_{rc}^2+1)-(\mu^2-4\mu+1)/y_{rc}\right]^{1/2}$$

Table 1. Calculated values of the coefficients of the propagation of imprecision $\frac{\delta_c}{\varepsilon}$, $\frac{\delta_{rc}}{\varepsilon}$, $\frac{\delta_{c(rc)}}{\varepsilon}$

of the center line were considered positive, those upstream were negative.

From the spark-time gate and scaler, we obtained the time interval T_{spark} in microseconds between the moment $\vec{S}_i$ passed the second light screen and the moment the photo spark fired. If the centerlines of the model and the test section coincided, the T'_{spark} relative to the test section equalled T_{spark}, which was the measure of spark - delay time in the coordinates of the model. For many of the picture sets, the model was displaced from this position of alignment, either upstream so that $\vec{S}_c$ and $\overleftarrow{S}_{rc}$ could be observed near the end of the channel, or downstream, principally for the purposes of the separate but related study previously referred to. When, for example, the center line of the model was upstream of the test section center line, $\vec{S}_i$ actually arrived at the model center line sooner than if the center lines had coincided, and T'_{spark} was shorter than if the shock were at the same location with respect to the model and if the model had not been displaced upstream. T'_{spark} was shorter by the time interval it took $\vec{S}_i$ to travel the distance of the model displacement. It was desired that values of spark time be transformed to the model coordinate system, so that a consistent x-t plot could be obtained from data obtained using a number of model locations; thus in this case T'_{spark} needed to be increased in value.

Because the attenuation of $\vec{S}_i$ was not great, it was reasonable to assume, for the purposes of this correction, that the shock velocity V_s of $\vec{S}_i$ near the model was the same as in the light-screen interval, where the interval L of 500 mm was traversed in the time T_v. Thus if

Δx was the displacement of the model center line and was >0 or <0 as the displacement was down or upstream from the test section center line, then $\frac{\Delta x}{L} T_v$ was the time for $\vec{S}_i$ to travel from the test section center line to the model center line (and was <0 for the example above). So

$$T_{spark} \equiv T'_{spark} \text{(from the spark-time scaler)} - \frac{\Delta x}{L} T_v .$$

In similar fashion, the locations x' of the shocks with respect to the test section, as measured with the aid of the distance markers, were referred to the model coordinate system by the form

x (model) = x' (test section) - Δx (<u>from</u> test section to <u>model</u>).

In many cases Δx could not be directly measured at the test section, so it was inferred from the distance of the end of the model from the end of the shock tube.

From the set of four interferograms that were obtained for each shot, the locations x' of the shocks of interest were measured on the flow pictures, usually to within $\pm$ 1/2 mm in the test-section scale units. For each day's series of shots, the ambient temperature θ_{amb} (in °K) was recorded, since the sound speed c_o was a function of the temperature. Then from T_v, used in conjunction with θ_{amb}, the actual values of y_o are obtained for monitoring purposes. The formulae used in this calculation were as follows:

c_o(standard) for argon = 0.3215 mm/usec at 25°C

$$\frac{c_o(\text{amb})}{c_o(\text{standard})} = \left(\frac{\theta_{amb}}{\theta_{standard}} \right)^{1/2} \qquad V_s = \frac{L}{T_v} = \frac{500 \text{ mm}}{T_v(\text{usec})}$$

$$y_o = \frac{\mu + 1}{\mu} \left(\frac{V_s}{c_o(\text{amb})} \right)^2 - \frac{1}{\mu} = \frac{5}{4} \left(\frac{1555}{T_v} \right)^2 \frac{298}{\theta_{amb}} - \frac{1}{4}$$

It turned out, however, that adjusting the nominal value of y_o for the small variations in y_o from shot to shot was not actually warranted. To be sure, for pictures with $\vec{S}_c$ only part way down the constricted channel, the effective values of T_{spark} could have been relatively simply adjusted in a directly proportional fashion. This would have made allowance for the fact that, for example, a slightly stronger shock would have traveled farther downstream during a given T_{spark} interval than would a shock of the nominal strength y_o, and thus its location should properly have been associated with a slightly longer value of T_{spark}. Thus T_{spark} would have been adjusted by the ratio $\frac{T_v}{T_{v\,(nominal)}}$, where both T_v and $T_{v(nominal)}$ would have been adjusted to a common temperature, say 25°C. Actually, however, the order of magnitude of this correction was relatively small for most of the ordinary shot-to-shot variations in T_v. Furthermore, once the channel shock begins to change in strength from its initial value y_o, and certainly by the time $\vec{S}_c$ has been reflected to form $\overleftarrow{S}_{rc}$, it was clear that a strictly proportional adjustment of T_{spark} was no longer quite appropriate: in fact, the form that the correction should have taken was complicated by the relationships between y_o and y_c and also between y_c and y_{rc}. It became evident, at all events, that the magnitude of the other imprecisions in the x - t data would have overshadowed any adjustments of this order of magnitude.

3. OBTAINING THE INTERFEROGRAMS

The procedure for taking a "shot" with the shock tube was as follows. The delay generator was adjusted so that the spark would occur when the shocks of interest were at their desired locations in the test section. All the resetable circuits were reset and checked for readiness. The entire tube, both the compression and expansion chambers, was pumped out to less than 1 mm of dibutyl phthallate (a low-vapor-pressure manometer oil, of such a density that 12.94 mm DBP = 1 mm mercury). Part of the H_2 (the usual driver gas) was put into the compression chamber, so the diaphragm would neither be burst by overpressure nor impaled on the prod. The expansion chamber and also the interferometer compensating chamber were filled to the desired expansion chamber pressure p_o. The spark was flashed to provide the no-flow white-light and monochromatic interferograms. The remainder of the driver gas was added, to bring the driver pressure to p_2. For all except the low y_o sequences this was 1900 mm, i.e. near the maximum operating value of p_2, which was fixed by the leak rate of a number of relatively weak joints in the compression chamber. Film packs were opened in the camera for the flow interferograms, the diaphragm prod was released, the measured values of T_v and T'_{spark} were recorded, and the four interferograms on Kodak Royal Pan 4" x 5" sheet film were developed for 5 minutes in Kodak D19.

The resulting white-light interferograms were, of course, appropriately dark and contrasty; the monochromatic fringe pictures were much less dark and less contrasty in appearance, but were nonetheless quite readable. Occasionally the condition of the argon spark source, and especially the anode tip, deteriorated and the brightness of the

monochromatic pictures fell off quite a bit before occasion was taken to refurbish the spark. Various photo materials and development procedures were tried in an attempt to obtain substantially darker monochromatic interferograms, but nothing of any particular advantage was found that could have been applied conveniently to our system. As noted in more detail in the conclusions, it has appeared in retrospect that the darkness of the monochromatic fringes and the graininess of the photo material used were among the limiting factors in the precision of the fringe shift measurements.

The basic data that were to be obtained in this experiment were fringe shifts across shocks $\vec{S}_i$ and $\vec{S}_c$ moving into still gas at pressure p_o or, at most, across shocks $\overleftarrow{S}_{rc}$ that had not yet moved very far back from the end of the channel and were moving into gas at a pressure p_2. To be sure, in the case of interferograms of $\overleftarrow{S}_{rc}$ with the 5-unit 2:1 model, it was often the case that the fringes would have had to be very close-spaced in order to fit enough fringes into one of the narrow channels so that the central fringe locations for the 0-state (for the no-flow picture) and the 2- and 2'-states could all be seen in the same channel. But narrowing the fringes so much would have meant that 1) the process of identifying corresponding white-light fringes across the fringe jump would become very difficult and 2) the fraction-of-a-fringe precision of measuring the fringe shift would become much worse because of the finite resolution of the photographic emulsions.

In this case a technique was worked out that involved repeating each $\overleftarrow{S}_{rc}$ shot in the sequence. For the first shot, the fringes in the channel were adjusted so that the central-fringes of the 0- and the 2-

regions were visible in the channel; for the repeated shot, the fringe spacing was changed so that the central fringe for the 0-state was left unmoved and the central fringe for the 2'-region was visible in a neighboring channel. Thus for the same shot conditions and the same T_{spark}, the fringe shifts 0-2 and 0-2' could be measured on separate but presumably nearly identical pairs of interferograms.

In the case of the sequences with the 5-unit 5:1 model the fringe pattern, as in the 5-unit 2:1 case, would have had to be broadened sufficiently so that the central fringe for the 0-region would be visible in the original channel while the central fringe for the 2'-region would be visible in the neighboring channel. It was found that with this broad a fringe spacing, the zero order and the first minima of the white-light fringe pattern could not be fitted into the narrow neighboring channel. In the absense of a sufficient part of the white light fringe pattern for purposes of comparison, the task of positively identifying a corresponding white-light fringe would have become much more difficult, if not impossible. Thus measurements of $\overleftarrow{S}_{rc}$ with the 5-unit 5:1 model were not feasible within the limits of our technique and of our model design, which was made necessary by the requirements of a separate but related experiment that was being conducted using the same model.

For some fringe picture sets, additional fringe-shift measurements were made from the 0-state to various regions along the channel behind $\vec{S}_c$, both in the constriction itself and behind the tip-reflected shock $\overleftarrow{S}_{rt}$ at various stages in its formation as a plane shock. The changes in the pressure along the channel behind $\vec{S}_c$ were of interest in indica-

ting the degree of completion of the interaction of the trailing waves with $\vec{S}_c$, but neither these variations nor the variations in the constriction itself were of interest as basic data values.

4. THE FRINGE-SHIFT MEASURING PROCESS

The purpose in obtaining a no-flow monochromatic interferogram for each shot was principally to use it as a fringe calibration or reference, with respect to which the shift of the fringe pattern could be measured in the various regions of interest in the flow monochromatic interferogram. This use of the no-flow fringe pattern involved the assumption that there had been no displacement of the fringe pattern associated with the 0-region from the time the no-flow picture was taken to the instant of the flow interferogram.

In flow pictures in which $\vec{S}_c$ was only part way down the constricted channel, the region ahead of $\vec{S}_c$ was of course still in the 0 - state; thus the fringe pattern in this region could be compared with the corresponding part of the fringe pattern in the associated no-flow interferogram. When this was done, it was found that in some cases there were small shifts of the 0 - region fringe pattern from the time of the no-flow to the time of the flow picture. These shifts were erratic, i.e. not consistent in their appearance even in a single sequence of shots. In fact, these observed fringe "slippages" from the no-flow to the flow pictures were well distributed between being positive and negative, and they were not substantially larger than the precision with which the fringe shifts were presumed to be measured. Wherever such a slippage was observed, it was allowed for in the fringe shift measurements, but in shots in which the 0 - region was no

longer visible in the picture, it was necessary to assume the absence of such slippage.

Note, however, that in all cases where this assumption had to be made, the pressures ahead of the shock waves of interest were uniformly higher by at least the ratio y_o than the initial pressure p_o. As is shown in the discussion on the precision of the fringe shift measurements, the higher the pressure ahead of a shock whose strength was to be determined by fringe-shift measurement, the less the fractional error, other things being equal, that was introduced by uncertainties or even small errors in the actual fringe shift represented by the region ahead of the shock. Thus it was just those shocks, the fringe shift measurements for which unavoidably involved the presumption of no fringe-slippage, which were the ones whose measured strengths were less uncertain for a given additive uncertainty in the actual value of the fringe shift from the vacuum to the O - state.

We considered the slowness of the leak rate into the expansion chamber and also the very slow rate of "natural" displacement of the fringe pattern arising from displacement of the Mach-Zehnder elements by vibrations passing through the pneumatic tires into the interferometer; as a result we were led to suspect that the fringe slippage was much more probably due to a precursor vibration traveling down the tube walls and, say, causing the test section windows to twist or vibrate in such a way that a small apparent fringe shift of rapidly changing character was superposed on the flow-picture fringe pattern.

If it was granted, nonetheless, that the no-flow monochromatic fringe pattern could be used as a reference for measuring shifts of the

fringes in the flow picture, then the procedure was as follows. A particular white light fringe, say, a light fringe near the central maximum of the pattern on the no-flow white-light picture was marked (with a number of light pencil marks); the same light white-light fringe was identified and marked in the various regions of interest in the flow white-light picture; then with the flow monochromatic picture exactly superposed over the flow white-light picture, the monochromatic fringe corresponding to the marked white-light fringe in the various parts of the picture was similarly marked. Thus the white-light flow picture was used to make it possible to track a particular monochromatic fringe across discontinuous fringe jumps that in some cases were as large as 20 to 25 fringes in magnitude.

In similar fashion the marked fringe on the no-flow white-light picture was carried over to the no-flow monochromatic picture by superposition. The two monochromatic pictures were then, presumably, ready to be superposed, flow on top of no-flow, in the film comparator apparatus described previously. Note that the marked white-light no-flow fringe was by choice taken at or near the central maximum of the white-light fringe pattern, in order that there could be no question about the superposablility of the corresponding white-light and monochromatic patterns. The question of superposability of the fringe patterns is treated in the discussion on the "second-order" roll-over that is to be included in a forthcoming report.

Proper aligning of the two monochromatic pictures particularly involved their rotational alignment with respect to each other, so that the various corresponding channel boundaries were parallel to each other;

it also involved the alignment along the horizontal direction of the test section, so that, say, the various wedge tips in the two pictures were all superposed. Alignment in the vertical direction was inappropriate, since it was in that direction that the pictures were to be displaced with respect to each other in the fringe-shift counting process.

For the fringe shift from the 0 - state to some particular region in the flow picture to be measured, the upper or flow picture was moved in the film comparator so that the marked fringe in the region of interest in the flow picture was approximately superposed with the marked fringe in the same region of the no-flow picture. Then the flow picture was slowly translated in the direction toward superposition of the horizontal reference lines of the model images,etc. In the course of this translation, count was kept of the units of fringe shift that were traversed. Each unit consisted of a cycle of coincidence of the marked light fringe on the flow picture successively with a dark and a light fringe on the no-flow picture. As the condition of superposition of the flow and no-flow horizontal reference lines was approached, then the last previous coincidence of the marked light fringe on the flow picture with a dark fringe on the no-flow picture was chosen as a location to be measured. At this point the flow picture was carefully adjusted in the comparator to the condition (referred to as optimum fringe opposition) of optimally central coincidence of the superposed light flow-picture fringes and dark no-flow-picture fringes, with emphasis given to optimizing the opposition particularly for the marked flow-picture fringe. This fine adjustment was of course observed through the microscope that was part of the comparator system.

It was usually observed that when the condition of optimum opposition was achieved, a pair of much-fainter symmetrical light "fringes" appeared between the no-flow dark fringe of interest and the two dark fringes on the flow picture that bracketed the marked light fringe of the flow picture. This could readily be understood by considering the superposition of two identical wave patterns that were exactly out of phase, each wave pattern having a value of intensity varying as, say, the square of the sine of the distance. The symmetry of the intensities of these half-spaced fringes was usually the most sensitive indicator of optimum fringe opposition. It was largely because of this sensitivity that the location of optimum fringe opposition could be determined substantially more precisely and more reproducibly than the optimum superposition of light fringe with light fringe (which, correspondingly, would be referred to as optimum apposition). A factor that appeared to make the advantages of opposition over apposition more marked was the relatively low intensity of the monochromatic fringes.

When this optimum adjustment had been achieved, the location of the movable window frame was determined by turning in the micrometer head until its measuring flat was just in contact with a corresponding rounded reference surface on the window frame, then reading the distance to the window frame to the nearest 0.5 mil. The optimum opposition of the marked light fringe on the flow picture with the no-flow dark fringe that was next after the condition of reference-line superposition was similarly obtained by fine adjustment, and its location was measured.

Next the optimum superposition of the reference lines was sought. This was a somewhat more difficult setting, since the shallow angle at which the fringe patterns crossed the shadows of the horizontal reference wires tended to make location of the edges of those shadows somewhat uncertain. Usually the best objects on which to fix one's attention were the wedge tips and also the ends of the distance markers attached to the horizontal reference line. In those pictures in which $\vec{S}_c$ had traveled at least part way down the channel, the beginnings of wall boundary layer caused a slight refractive uncertainty in the location of the horizontal boundaries of the constricted channels; this, coupled with the effects arising from the small angle of incidence at which the fringe pattern crossed these horizontal boundaries, sometimes brought it about that these top and bottom boundaries of the constricted channel were not useful in the process of adjusting to superposition of the images of the test section. When the condition of optimum superposition was achieved, the location of the window frame was again measured in similar fashion.

The three locations thus measured corresponded to shifts of, say, $j - 1/2$ fringes and $j + 1/2$ fringes, and to the unknown fringe shift, where the integral value j was obtained directly by counting units of fringe shift from the initial superposition of the marked fringes. A linear interpolation of the unknown fringe shift location between the locations of the $j - 1/2$ and $j + 1/2$ fringe shift values gave the fractional fringe shift, which was then to be added to $j - 1/2$ to give the interpolated value of the total fringe shift from the 0 - state (represented by the no-flow) to the j - th region. Just such counts of

integral fringe shifts and similar triples of readings for the fractional fringe shifts were obtained for regions ahead of and behind the shock waves of interest for each of the shots in the various sequences. The resulting values of the fringe shifts were the principal data taken for this experimental study.

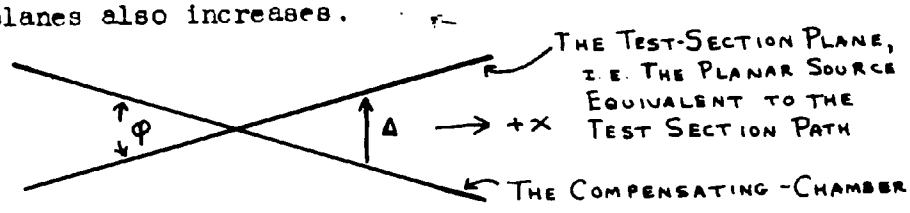
5. ROLL OVER

The technique described above for identifying a particular monochromatic fringe across a discontinuity in the fringe pattern was a classical technique used in every interferometric study of shock waves. Yet this technique, as it stood, was in need of a substantial correction that, to the best of our knowledge, was not explicitly displayed in a form appropriate for application to shock wave interferometry until the appearance of the report by Curtis[24] in 1958. On the one hand it seemed curious that this particular application had not been made much earlier, since, according to Candler,[25] essentially the same phenomenom was observed as early as 1915 by Adams,[26] in connection with interferometric measurements of the concentrations of solute in aqueous solutions. On the other hand, it was very strange indeed that none of the earlier workers in this field ever turned up the sizable errors in shock strength measurement that neglect of this correction would lead to. So far as we know, this was the first application of Curtis' correction to an interferometric study of shock waves.

In an ideal Mach-Zehnder interferometer that is fully compensated, the two optical paths through the instrument - the paths through the test section and through the compensating chamber - are truly identical; this implies that each dispersive element in one path is exactly matched

by an identical element in the other path. Thus the gas (if any) in the test section and the compression chamber must be the same and must be at the same density. This is just the condition that holds for the no-flow interferograms. As soon as the gas density in the test section is changed, as it must be, since the function of the interferometer in this research was to measure abrupt uncompensated changes in gas density, then the two paths are no longer fully compensated and the effects of dispersion must be taken into account.

So far as producing a fringe pattern is concerned, an ideal interferometer can in its entirety be considered to be two planes representing equivalent coherent plane sources generated by the action of the first and second ideal beam splitters. The spacing of the resulting fringe pattern is dependent on the included angle of intersection φ between the two planes when they are combined by the second splitter to form the interference fringes. Thus, if the x-direction is in the plane of the test section image and is taken to be normal to the line of intersection of the equivalent source planes, then as x increases, the difference Δ in the optical path lengths between equivalent points on the two planes also increases.



The increment in x corresponding to an increase of a wave length λ in the length Δ is just the fringe spacing at that point. The central or zero-path-length fringe is at the line of intersection of the two planes.

Now if there is an uncompensated increment in the gas density ρ in the test section, which has a thickness L parallel to the beam, this can

be exactly represented for a particular wavelength of light by an equivalent displacement of the test-section source plane in the direction of Δ by an amount $KL\,\delta\rho$, where K is the Gladstone - Dale constant for the expansion chamber gas (and is defined by the relation $n - 1 = K\frac{\rho}{\rho_s}$), $\delta\rho$ is the change in the test-section density, n is the optical index of refraction for the gas, ρ_s is some standard gas density at which $K = n - 1$. If the gas is dispersive, this implies both that $K = K(\lambda)$, so the distance that the equivalent test-section plane is displaced for a given $\delta\rho$ as a function of λ and, in addition, that the location x_o of the intersection of the fixed and the displaced planes is also a function of λ for fixed $\delta\rho$. Thus, in the case of a white-light continuum, the location of the central fringe will vary considerably for the various wavelength components in the white-light spectral distribution.

Recall now that for, say, a flat-topped white-light spectral distribution with sharp upper and lower cut-off wavelengths, the fringe-pattern intensity distribution that is derived from the Fourier transform of the spectral distribution is analogous to the Fraunhofer diffraction pattern generated by two wide slits; it consists of a close-spaced fringe pattern modulated by an envelope that has a central or zero-order maximum, symmetrical first minima, weaker first-order maxima, etc. This is essentially the appearance of the white light interferograms shown in Fig. 7b or in Fig. 13.

It can readily be appreciated that the variation in location of the central maximum with wavelength [because of $K = K(\lambda)$] can and indeed does lead to a difference between the displacement of the close-spaced white-

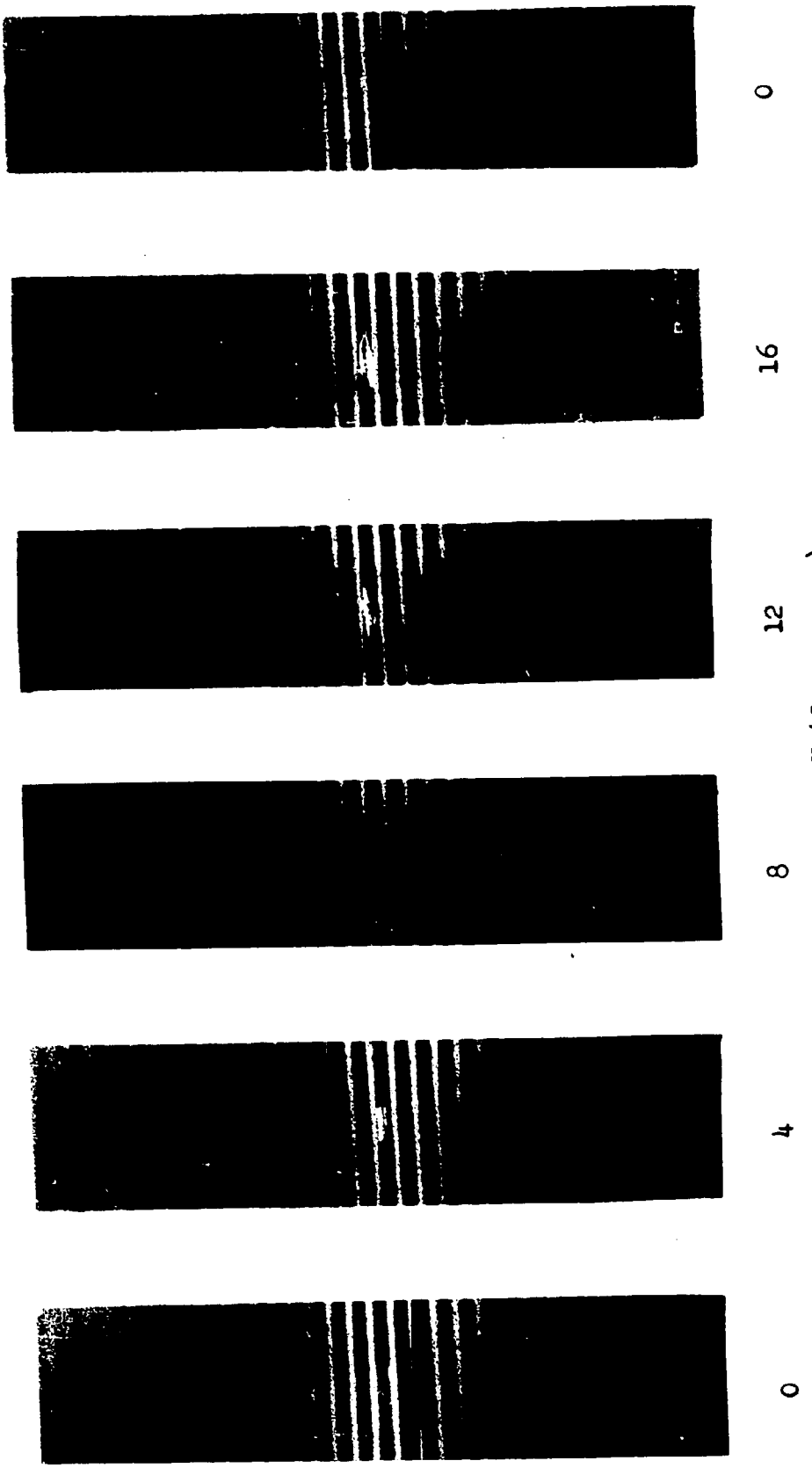


Figure 13. A graphic demonstration of the occurrence of roll-over — the displacement of the fringe-density envelope with respect to white light fringes. The marked fringe that is carried through the sequence is displaced with respect to its fringe-density envelope by approximately one fringe between the pictures ΔN = 0 and ΔN =16.

light fringe pattern and of the modulating envelope of that pattern, as ρ is gradually changed from the condition of complete compensation. It can further be appreciated that for sufficiently large values of $\delta\rho$, the difference in the displacements could be large enough to have moved the modulating envelope by an entire fringe interval with respect to the white-light fringe pattern. In the case that this large a change in density occurs across a single shock wave, then since it is the fringe-intensity modulating envelope which is used in identifying corresponding white-light fringes on the two sides of the shock, the result is that the magnitude of the fringe shift indicated by this technique is indeed in error by an entire unit fringe shift. Furthermore, there is no direct indication on the flow and no-flow white-light interferograms that this is actually the case.

The magnitude of the density change $\delta\rho$ that is associated with such a unit-fringe-shift displacement of the envelope with respect to the white-light fringe pattern is expressed in terms of the number of units of monochromatic fringe shift that corresponds to this value of $\delta\rho$. This number of fringe shift units is the roll over interval, so named by Curtis because it can be imagined that the white-light fringe pattern "rolls over" by a complete cycle with respect to the envelope; it is of the order of 15 to 20 monochromatic fringes in the cases both of argon and of nitrogen. The exact value depends on K_2 - the coefficient of the first λ-dependent term in the expansion of K in powers of λ, and also on the wavelength of the monochromatic light being used and the effective center wavelength of the white-light spectral distribution; it is, however, independent of the test section width and

of the total gas density in the test section.

The occurrence of roll over can be demonstrated directly, as shown in Fig. 13, by taking a series of no-flow white-light and monochromatic interferograms as one increases the uncompensated gas density in the test section stepwise from 0 in steps small with respect to δ_f (roll over), i.e. in steps of $\frac{\delta_f(\text{roll over})}{4}$ or less. Starting with the $\Delta N = 0$ (i.e. $\delta_f = 0$) picture, we mark, say, the light fringe at the center of the zero order group, then in the next white-light picture in the series, we compare the white-light fringes to the marked fringe in the first picture and mark that fringe that appears to correspond most closely to it in relative intensity in the zero order group. We continue this process until the total value of δ_f is of the order of 15 to 20 fringe shift units. We note that the marked fringe has gradually been displaced from the center of the zero order group; at the half roll over point, there should ideally be two central fringes of equal intensity. Then we juxtapose the first and last white-light fringe patterns, for $\Delta N = 0$ and $\Delta N = 16$, and observe that the fringe on the last picture that corresponds most closely with the marked fringe on the first picture is indeed one removed from the marked fringe that was identified by carrying the first marked fringe through the series in the fashion just described.

All ordinary gases, like most other optical media, display normal dispersion in the visible portion of the spectrum, a fact that is associated with the occurrence of strong absorption in the ultraviolet. Thus $\frac{dn}{d\lambda} = \frac{dK}{d\lambda} < 0$. For all such media, the relative displacement of the envelope is in the same direction as the steady displacement of the

fringes by changing the gas density; thus if, for example, we did not take into account the occurring of a full unit of roll over, the corresponding apparent monochromatic fringe shift would be one unit too large. (Note that this corrects a misstatement in Curtis, p. 12.)

Note that the demonstration of roll over can be made even more graphic and the problem of carrying through a particular fringe made easier if a technique of masking alternate lateral halves of the beam in the interferometer is employed, in order to obtain "artificial fringe discontinuities". Thus at any particular density, the second side of one pair of interferograms would be exposed, then the masking would be switched and the first side of the next pair of interferograms would be exposed. In this way the fringe identification across a 1/4 to 1/3 of a unit of roll over could be achieved at the center of an interferogram, and across a thin straight line, rather than at the juxtaposed edges of successive pictures.

This demonstration of roll over points to a technique - the only one we could devise - that allowed us to "work around" the occurrence of roll over with a considerable degree of confidence. It was often not enough to say that whenever a fringe shift ΔN of 15 to 20 occurred across a discontinuity in an interferogram, the occurrence of a unit of roll over should be assumed, and that for shifts of much more than half of a roll-over interval the tell-tale signs associated with more than half a unit of roll over should be watched for. Sometimes the size of the region, the fringe jump to which was sought, was not large enough to give an impression of the relative white-light fringe intensities that was clear enough to make one confident in presuming the

occurrence of a unit of roll over. Likewise, in cases where turtulent wall boundary layer was adding its random contribution to the appearance of the fringes in a region of interest, as was particularly the case in interferograms taken for the separated but related study, that also made use of fringe shift measurements across shocks, the relative fringe intensities could not be determined clearly enough, at least visually, to permit the unaided presumption of the occurrence of roll over.

In these cases particularly, and indeed in all cases where it proved feasible, wherever the occurrence of at least a major fraction of a unit of roll over was suspected, the white-light fringe pattern on the low density side was juxtaposed to another white-light pattern of similar fringe spacing, that corresponded to a fringe shift larger by 1/4 to 1/3 of a roll over interval. This white-light pattern could be either on the same interferogram or on another one, for example, in the same sequence. The fringe on the intermediate fringe pattern that corresponded to the original marked fringe was then marked, and this intermediate pattern was then compared with yet another intermediate pattern corresponding to a yet somewhat larger fringe shift, just as in the case of the series for the static calibration of roll over. This process was continued until the high-density side of the original fringe jump was reached, and a marked fringe obtained on the high density side in the original interferogram which could confidently be regarded as corresponding directly to the marked fringe on the low density side. To be sure, in many cases where broad clear fringe fields were available on both sides of a sharp discontinuity that was

either small with respect to half a roll over interval or relatively close to a full roll over interval, the added assurance of the occurrence of roll over that this intermediate-fringe-transfer technique provided was not really needed.

6. REDUCTION OF THE FRINGE SHIFT DATA

The relationship between the pressures and the densities on either side of a plane shock wave is called the Rankine-Hugoniot relation; it is an immediate consequence of the three basic conservation equations for the flow through the shocks[22]. Let ρ_{i-1} and ρ_i be the gas densities on the low and high density sides of a shock, let $x_i \equiv \frac{\rho_i}{\rho_{i-1}}$; similarly let p_{i-1} and p_i be the corresponding gas pressures, and $y_i \equiv \frac{p_i}{p_{i-1}}$, in line with the previous usage for y. Let γ be the adiabatic exponent of the gas, and $\mu \equiv \frac{\gamma+1}{\gamma-1} = f + 1$, where f is the effective number of degrees of freedom of this perfect gas. Then the Rankine-Hugoniot relation for this perfect gas takes the form $x_i = \frac{\mu y_i + 1}{\mu + y_i}$. This can be inverted to yield $y_i = \frac{\mu x_i - 1}{\mu - x_i}$. From either of these forms the outstanding characteristic of this relation is evident: as $y_i \longrightarrow \infty$, $x_i \longrightarrow \mu = 4$ for a monatomic gas. More will be made of this behavior in the discussion on the precision of measurement.

The relationship between fringe jump and density ratio can readily be derived as follows. Imagine a test section and a compensating chamber, both optically identical, each completely evacuated. Let a particular fringe pattern be associated with this condition. Then as the gas density in the test section is increased from zero, the optical path length through the test section is increased by $L(n(\rho) - 1)$, and the associated number of unit fringe shifts is $\frac{L}{\lambda}[n(\rho)-1]$, where $n(\rho) =$

index of refraction of the gas, L = test section width, λ = wavelength of monochromatic light. The Gladstone-Dale relation, as referred to previously, for gases under "ordinary" conditions is of the form $n - 1 = \frac{K\rho}{\rho_s}$; this form also constitutes a definition of the Gladstone-Dale constant K. Here ρ_s is some standard density at which K is just the excess of n over the value 1. If the density is increased to ρ_{i-1} and then to ρ_i, the corresponding values of the total fringe shift from vacuum conditions to the states i-1 and i are

$$N(vac, i-1) \equiv N_{i-1} = \frac{KL}{\lambda} \frac{\rho_{i-1}}{\rho_s}$$

and $$N(vac, i) \equiv N_i = \frac{KL}{\lambda} \frac{\rho_i}{\rho_s}$$

Thus $$\frac{N(vac, i)}{N(vac, i-1)} \equiv \frac{N_i}{N_{i-1}} = \frac{\rho_i}{\rho_{i-1}} \equiv x_i$$

Thus the expression for the strength y of a shock wave, in terms of the measured values of the fringe shifts from the vacuum state to either side of the shock wave is

$$y_i \equiv p_i/p_{i-1} = \frac{\mu x_i - 1}{\mu - x_i} = \left[\mu \frac{N_i}{N_{i-1}} - 1\right] / \left[\mu - \frac{N_i}{N_{i-1}}\right] = (\mu N_i - N_{i-1}) / (\mu N_{i-1} - N_i)$$

This form for y_1, when applied to $\vec{S}_c$, becomes

$$y_c = y_2 = \frac{\mu N(vac, 2) - N(vac, 0)}{\mu N(vac, 0) - N(vac, 2)} = \frac{\mu N_2 - N_0}{\mu N_0 - N_2}$$

For those sequences which included pictures of $\vec{S}_{rc}$, values of $y_{rc} = y_{2'}$ were determined in a similar fashion. The appropriate form here is

$$y_{rc} = y_{2'} = \frac{\mu N_{2'} - N_2}{\mu N_2 - N_{2'}}$$

In the ideal case of normal reflection of a plane shock from a rigid end wall, the relation between y_{rc} and y_c is $y_{rc} = \frac{(\mu + 2) y_c - 1}{\mu + y_c}$

This can be inverted to the form $y_c = \frac{\mu y_{rc} + 1}{\mu + 2 - y_{rc}}$

which was used to determine the "derived" values of y_c from the

measured values of y_{rc}. The experimentally measured values were in general the shifts from the initial 0-state to the (i-1)- and the i-states. By use of the ideal gas law, the value of the shift $N(vac, 0) = N_o$ to the initial state can be written in terms of the experimental conditions, taking the form

$$N_o = \frac{KL}{\lambda}\frac{\rho_o}{\rho_s} = \frac{KL}{\lambda}\frac{p_o}{p_s}\frac{T_s}{T_o}$$

From the International Critical Tables, it was determined that $K = 283 \times 10^{-6}$ for argon at 0^oC and 1 atmosphere, so if L is taken as 2.012" = 5.11 cm, and λ is taken as the center of the magnesium triplet, which is 5170 A^o, then

$$N_o = \frac{p_o(mm\,Hg)}{T_o(^oK)}\;\frac{283 \times 10^{-6} \times 5.11\,cm}{5170 \times 10^{-8}\,cm} = 10.04\,\frac{p_o(mm\,Hg)}{T_o(^oK)}$$

It is to be noted that Kahane displayed the values of the density at the outlet of the convergence as the end result of the reduction of his interferograms. In our case the focus of attention was the effect of the constriction on the shock rather than on the flow field behind it; the parameter used to indicate that effect was the shock strength, i.e. the pressure ratio — even though, by virtue of the nature of the Rankine-Hugoniot relation, the fractional uncertainty for y was greater than for x and increased more rapidly than that for x as y was increased.

In the graphs (Figs. 14, 15 and 16) of the various measured values of y_c for each of the sequences of shots, we have included rough and rather conservative indications of the limits of precision on the various measured values of y. These were intentionally conservative, so that when the gap between a calculated value for y_c and a measured value was substantially larger than the extent of the associated imprecision - flag, it could reasonably be concluded that the discrepancy

was very likely a real one.

CHAPTER IV

CORRELATION OF THE THEORY WITH THE EXPERIMENTAL RESULTS

1. PRECISION OF THE MEASURED VALUES OF SHOCK STRENGTH

The precision with which the values of shock strength could be measured for the waves of interest was a function of the precision with which the interferometric fringe shifts could be measured and the precision with which the gas conditions corresponding to the no-flow reference fringe pattern were known. Attention has already been given in the previous chapter to the uncertainties in the relationship between the 0-region fringe pattern in the no-flow interferograms and the presumably identical 0-region pattern at the instant of the shot; this was contained in the treatment of fringe slippage. In view of the presumed nature of the cause of slippage, it seemed reasonable for us to say that the actual value of N(vac,0) ahead of $\vec{S}_c$ was itself known from the initial values of p_o and T_o, and that the occurrence of slippage, of essentially the same magnitude as the imprecision in the values of the fractional fringe shift, was effectively a second contribution to the imprecision of all the other fringe shifts that were measured by using the no-flow interferogram as a reference.

In our use of the fringe-shift-reading interferogram comparator described previously, it was our experience that careful settings on a condition of optimum fringe opposition were reproducible to about ±1 mil. This precision was, of course, affected by a number of factors: the fringe pattern spacing, its photographic density and contrastiness; the care with which the observer's eye was kept centered with respect to the microscope eyepiece, so as to reduce the effect of parallax; backlash,

and "stiction" looseness of the drive mechanism in the mechanical stage.

The density and contrastiness of the fringe patterns were usually far from optimum. Experiments were conducted to determine the amount of improvement readily available in this area by way of contact-printing the interfercgrams onto extremely contrasty film. We concluded that considerably more work would be needed in order for the improvement in contrastiness not to be offset by the increased influence both of the graininess and the emulsion thickness of the original interferograms on the sharpness of the edges of the dark fringes. Furthermore, it appeared at the time that the added task of reprinting all of the interferograms that were taken in the course of this experiment would be nearly prohibitive. More is said about this matter in the chapter on conclusions and recommendations for further work.

As would be imagined, decreasing the fringe spacing permitted a gain in the incremental precision of settings on conditions of optimum fringe opposition, but these gains were not commensurate with the decrease in the spacing, so not only could the fractional-fringe-shift precision of the settings not be improved, but as, with decreasing fringe spacing, the graininess of the film began to play a more important role, the fractional-fringe-shift imprecision became substantially poorer.

Involved in each determination of a fractional fringe shift were three settings of the comparator, as was noted in the previous chapter. Roughly speaking, one could say that the precision of the three corresponding values of distance were similar, although under certain circumstances of low photographic density, etc., the setting on the location of the superposition of horizontal reference line shadows was somewhat less precise than the other settings. These three uncer-

tainties were each assumed to have an appropriately random, non-systematic character, so that they could be combined by the usual sum-of-the-squares method.[27] It was true, to be sure, that the exact value of the combined uncertainty was dependent on the value of the fractional fringe shift, but the combined value was always nearly $\pm$ 2 mils.

Since the fringe spacing was usually in the range of 20 to 30 mils on the interferograms themselves - sometimes larger, rarely smaller - it was reasonable to use as a rule-of-thumb that values of the fringe shifts were measured to within ε = the fractional-fringe-shift imprecision = (approx.) $\pm$ 0.1 fringe. There was the expectation, then, that the actual value of the imprecision might well be somewhat smaller than this in many cases, but only rarely would it be much larger. By way of comparison, it should be noted here that Ladenburg[28] also spoke of $\varepsilon = \pm$ 0.1 as a "conservative" value for the imprecision in measuring fringe shifts. Werner,[29] however, reported that he used fine - grain films and reprinting techniques to increase markedly the contrastiness of the interferograms. He also used a semi-automated non-visual technique for making the settings on the conditions of optimum opposition of the fringes; by doing this, he was able to achieve reproducibility of fringe shift readings to within $\frac{1}{50}$ fringe.

2. PROPAGATION OF THE PRECISION OF MEASUREMENT

Two approaches were taken with regard to determining the propagated effect of the imprecision of the fringe shift measurements on the derived values of shock strength. Initially, formulae were derived for the fractional imprecisions in the derived values of the shock strengths as

functions of the value of y_o, of the total equivalent fringe value N(vac, i-1) ahead of the shock and of the fractional-fringe-shift imprecision; its derivation can be summarized as follows.

The basic equation for an arbitrary $y_i = y_i(N_i, N_{i-1})$ is

$$y_i = \frac{\mu N_i - N_{i-1}}{\mu N_{i-1} - N_i}$$

The variation-form of this is

$$y_i(1 + \delta_i) = \frac{\mu(N_i + \varepsilon_i) - (N_{i-1} + \varepsilon_{i-1})}{\mu(N_{i-1} + \varepsilon_{i-1}) - (N_i + \varepsilon_i)}$$

where the ε's are the individual additive imprecisions in the various values of the total fringe shifts, and δ_i is the propagated fractional imprecision in the derived value of the shock strength.

From this, one can obtain

$$\delta_i = \frac{1}{\mu N_{i-1} - N_i}\left[\varepsilon_i\left(\frac{\mu}{y_i} + 1\right) - \varepsilon_{i-1}\left(\frac{1}{y_i} + \mu\right)\right]$$

If now $|\varepsilon_{i-1}| \simeq |\varepsilon_i| \equiv \varepsilon$, i.e. if they are Gaussian random uncertainties of essentially equal magnitudes, then they can be combined as the sum of the squares.[27] After some reduction, utilizing the Rankine-Hugoniot equation, the final form is

$$\frac{\delta_i}{\varepsilon} = \frac{\mu + y_i}{(\mu^2 - 1) N_{i-1}}\left[(\mu^2 + 1)\left(\frac{1}{y_i^2} + 1\right) + \frac{4\mu}{y_i}\right]^{1/2}$$

Note that for $y_1 \geq 5$, the coefficient for ε_i can safely be neglected with respect to the coefficient for ε_{i-1}, so for large y_1, we see that the fractional imprecision in y_1 is due almost exclusively to the uncertainty in measuring N_{1-1}.

Now we make use of the earlier discussion of the possible cause for the fringe slippage in the 0 - region: we assert that the gas conditions p_o and T_o did not change but that the cause - whatever it was - for the change in the optical length of the test-section path was external to the working gas in the test section. Thus N(vac, 0) would still be

determined from p_o and T_o to within an imprecision of certainly less than 1%, and the slippage could be treated as another additive uncertainty in the values of all the other fringe shifts that were measured by use of the no-flow fringe pattern. As mentioned before, wherever the o - region was visible in the interferograms, the slippage, if it occurred, was taken into account in determining the values of the succeeding ΔN's; in these cases the imprecision of measuring the slippage was certainly no greater than . On the other hand, when the C-region was no longer visible, the shock to be measured was $\overleftarrow{S}_{rc}$; in this case N_{i-1} was enough larger, especially for large values of y_o, that adding the slippage imprecision to the fractional-fringe-shift imprecision still did not make the fractional imprecision of y_{rc} unusably large.

The procedure was that the fringe slippage imprecision ϵ_s was considered not to apply in the case of $N(vac,C) \equiv N_o$, while in the case of all other fringe shifts, the measurement of which involved use of the no-flow fringe pattern as a reference, ϵ_s was considered to be a separate additive imprecision, to be combined with the other imprecisions by the sum-of-the-squares method. Thus for y_c, the variation-form is

$$\eta_c (1+\delta_c) = \frac{\mu(N_2+\epsilon_2+\epsilon_s) - N_o}{\mu N_o - (N_2+\epsilon_2+\epsilon_s)}$$

If we assume that $|\epsilon_s| = |\epsilon_2| \equiv \epsilon$, this reduces to the form

$$\frac{\delta_c}{\epsilon} = \frac{(\mu+\eta_c)\sqrt{2}}{N_o(\mu^2-1)}\left(\frac{\mu}{\eta_c}+1\right)$$

This is the coefficient for the propagation of imprecision for the channel shock strength y_c. In the case of y_{rc}; the term ϵ_s applies to both of the fringe-shift values that enter the formula for y_{rc}; here the variation form is $\eta_{rc}(1+\delta_{rc}) = \dfrac{\mu(N_2'+\epsilon_2'+\epsilon_s) - \mu(N_2+\epsilon_2+\epsilon_s)}{\mu(N_2+\epsilon_2+\epsilon_s) - (N_2'+\epsilon_2'+\epsilon_s)}$

Again we assume that $|\varepsilon_2| = |\varepsilon_2| + |\varepsilon_3| \equiv \varepsilon$; by straightforward algebraic manipulation, we can obtain the corresponding form for the coefficient for the propagation of imprecision for the channel-reflected shock strength y_{rc}: $$\frac{\delta_{rc}}{\varepsilon} = \frac{2\sqrt{2}}{N_o \mu(\mu-1)} \frac{\gamma_c + \frac{\mu-1}{2}}{\gamma_c + \frac{1}{\mu}} \left[(\mu^2 - \mu + 1)\left(\frac{1}{\gamma_{rc}^2} + 1\right) - (\mu^2 - 4\mu + 1)\frac{1}{\gamma_{rc}} \right]^{\frac{1}{2}}$$

In addition, the relation $y_c = y_c(y_{rc})$, which was introduced in the section on reducing the fringe shift data, can also be written in variation-form, and a value for the ratio of the fractional imprecisions for y_{rc} and for $y_c(y_{rc})$ can be obtained: $$\frac{\delta_{c(rc)}}{\delta_{rc}} = \frac{(\mu + \gamma_c)[(\mu+2)\gamma_c - 1]}{\gamma_c(\mu+1)^2}$$

A direct comparison can now be made of the relative magnitudes of the imprecisions δ_c and $\delta_{c(rc)}$. The values of $\frac{\delta_c}{\varepsilon}$, $\frac{\delta_{rc}}{\varepsilon}$, $\frac{\delta_{c(rc)}}{\delta_{rc}}$ and $\frac{\delta_{c(rc)}}{\varepsilon}$ are displayed in Table 1. The value of y_c that was used for each of the various values of y_o was the one calculated from Laporte's theory for that value of y_o, since it is particularly in the immediate vicinity of the calculated values of y_c that we need to know what degree of precision to ascribe to the experimentally measured values of y_c. From this table it is evident that $y_c(y_{rc})$ is in general a less precise indication than y_c of what the channel shock strength was at the end of the channel, or would have been farther along the constricted channel, had the end of the channel not been there.

It should perhaps be pointed out explicitly that the tabulated values in Table 1 are themselves not the actual fractional imprecisions in the shock strengths, but must be multiplied by the fractional-fringe-shift imprecision, which is nominally 0.1, to yield the actual values of δ .

From this table, it can resonably be inferred that, insofar as the precision of the fringe shift measurements is concerned, the experimental results should be a fair quantitative indication of the actual wave strengths for the weaker incident shocks, but can be expected to give only a very rough indication of the wave strengths for the stronger shocks.

The second approach to determining the propagated effect of the fringe-shift-measuring imprecision was the one used in determining the "imprecision-flags" associated with certain data points in Fig. 14, 15 and 16. In order to provide a conservative indication of the imprecision of the measurements, varied-values were calculated for those values of y_c and of $y_c(y_{rc})$ that were closest to the corresponding theoretical values of y_c for each of the values of y_o that were studied. This was done whether the closest measured values were from locations of $\vec{S}_c$ and $\overleftarrow{S}_{rc}$ that were closest to the end of the channel or not, in order that a better indication could be given of the magnitude of the imprecision of the experimental values in the neighborhood of the calculated values. The varied-value for each such closest measured value of y_c and of $y_c(y_{rc})$ was determined by varying each of the values of the constituent fringe shifts by 0.1 fringe in such a direction that the varied value of y_c or $y_c(y_{rc})$ was displaced toward the calculated value of y_c. This procedure involved, of course, no allowance for the randomness of the constituent imprecisions; the magnitudes of the propagated imprecisions were thus, it is believed, conservatively large.

In cases where some of the experimental values of y_c differ considerably from the calculated value, as was the case for the stronger inci-

dent shocks, it should be realized that the values of the imprecision change considerably with y_c(experimental) for y_o fixed: the fractional imprecisions δ_c and $\delta_{c(rc)}$ both increase with y_c(experimental) and of course the additive, as distinct from the fractional, imprecision for a fixed δ_c or $\delta_{c(rc)}$ increases with y_c(experimental). Thus the significance of experimental values of y_c or $y_c(y_{rc})$ that were much larger than y_c(calculated) was diminished, while for values much less than y_c (calculated) the relative significance of the experimental values was presumably enhanced.

The various values of y_c(experimental) for each value of y_o were plotted in Figs. 14, 15 and 16 and were numbered in sequence down the constricted channel. The numerical values of the measured shock strengths are recorded in Tables 3, 4 and 5, along with the locations x of the shocks $\vec{S}_c$ or $\overleftarrow{S}_{rc}$; these values of x were measured with respect to the center line on the model. The experimental values of y_{rc} for each y_o are separately identified and also identified in sequence by letter, starting from the reflection. Each value $y_c = y_c(y_{rc})$ that was derived from a measured value of y_{rc} is represented as a value of y_c and is identified by the same letter as is the value of y_{rc} from which it was derived.

It is appropriate to consider the degree of precision in y_c and $y_c(y_{rc})$ that could be obtained from the x-t plots by measuring the local velocity of the channel shock. In view of the uncertainties arising from the transients in the opening and closing of the gate circuits, it seems reasonable to take the imprecision of the time coordinate of a typical x-t point as ± 2 μsec., and the imprecision of the distance coordinate (in full-scale test section units, not in terms of distances

on the interferograms) of a shock as $\pm$ 1 mm. Because of the substantial changes in the strength and velocity of $\vec{S}_c$ as it travels down the channel and particularly because of the catching-up of the trailing wave patterns, it is evident that, at most, only a relatively short base line - say, 50 mm - near the end of the constricted channel is available for determining the velocity of $\vec{S}_c$ from the x-t data. For this base line the transit time would be 45 μsec for y_c = 15, 116 μsec for y_c = 2.

When the random imprecisions of the two ends of the base line and of the beginning and end of the time interval are all taken into account in a sum-of-the-squares fashion, the imprecision of the resulting experimental value of shock velocity turns out to be 6% for y_c = 15, 4% for y_c = 2. Since the shock strength varies essentially as the square of the shock velocity, the ultimate imprecision in the value for y_c obtained from the x-t data would be about 12% for y_c = 15, about 9% for y_c = 2. Thus it was concluded that little was to be gained from an extensive program of determining values of y_c by this alternate method. It should be noted, however, that continuous, as distinct from discrete, measurements of x and t for $\vec{S}_c$ could very easily be much more precise; as is noted in the section on conclusions and recommendations for further work, schlieren streak-camera records of the time history of $\vec{S}_c$ in the constricted channel would give values for y_c with much greater precision than would the method just considered above; this would be particularly true for the stronger shocks.

3. THE THEORIES OF LAPORTE AND OF CHISNELL: OUTLINE AND NUMERICAL CALCULATIONS

It was noted in the introductory discussion of Laporte's theory

that his report included some numerical calculations for the "remote" values of the channel shock strength y_c and the tip-reflected strengths y_{rt} in a monatomic gas. Unfortuately the ranges of these calculations did not include all the values of incident shock strength y_o which were deemed suitable for measurement in this experimental program, so a calculating program was set up to extend the range of y_o to include the additional values of interest. It seemed appropriate to combine the description of this calculating program with a review of Laporte's theory and some additional details related to it. By chance it turned out that the particular extensions of his calculations that were needed were all in the regime of unchoked flow, so the principal emphasis in the following discussion is on the procedure for the unchoked regime; the changes in the procedure needed for the choked flow regime, which are chiefly in the line of simplications, are discussed more briefly. The section is concluded with a short discussion of some of the details of the related theory of Chisnell. Some calculated values of y_c, based on this theory, are tabulated and plotted along with the values calculated from Laporte's theory in Table 2 and in Figs. 14, 15 and 16.

By way of a brief review of Laporte's theory, the main features are listed here:

1) the fixing of the attention on the strengths of the main shocks produced by the interaction as being the chief dependent variables in the problem;

2) the concern with the situation "in the large", i.e. after most of the secondary waves generated by the interaction of the shock and the flow with the convergence had either died away or caught up with the main shocks or, in the case of choked flow, amalgamated with the stand-

Values for the channel and tip reflected shock strengths y_c and y_{rt} as calculated from Laporte's theory.

	$\mathcal{R} = 2$		$\mathcal{R} = 5$	
y_o	y_c	y_{rt}	y_c	y_{rt}
2	2.2998*	1.3157*	2.6046*	1.5858*
3	3.5766	1.5942		
4	4.8424	1.8321	5.5905*	2.4011*
5	6.1013	2.0326		
6	7.3549	2.2020	choking starts at $y_o \cong 6$	
	choking starts at $y_o \cong 7$			
6	---	---	8.5410	2.9179
8	9.8560	2.4676		
10	12.360	2.6596	14.439	3.5180
12	14.868	2.8040		
16	19.890	3.0064	23.340	3.9690

* Values calculated for this study; other values from Laporte [1] pp. 14, 22, 23.

Values for the channel shock strength y_c as calculated from Chisnell's theory.

	$\mathcal{R} = 2$	$\mathcal{R} = 5$
y_o	y_c	y_c
2	2.34	3.00
4	5.10	7.24
6	7.84	11.4
8	10.5	15.4
10	13.2	19.5
12	16.1	23.7

Table 2. Values of the strengths y_c and y_{rt} of the channel and tip-reflected shocks, as calculated from the theories of Laporte and Chisnell.

ing rarefaction;

3) the postulation of isentropic flow through the convergence;

4) the introduction of an interface I to allow for the different entropy states of the regions 2 and 3, which have quite separate histories following the arrival of $\vec{S}_1$ or $\vec{S}_c$;

5) for the case that the incident shock strength and the area ratio are such that the outlet flow from the converging section is sonic, the introduction of a rarefaction $\overleftarrow{R}$ anchored to the outlet of the convergence, to complete the transition of the flow to conditions that can be continuous in pressure and flow velocity across the interface;

6) the use of the proper non-isentropic formulae for the changes in the gas parameters across the shock waves.

In the case of choked flow, it is to be noted that the flow can be said to be choked only so long as M_4 is fixed by the sonic condition (i.e. $M = 1$) at the outlet of the convergence. This in turn imposes the condition that there be a reflected shock $\overleftarrow{S}_{rt}$ that moves upstream or at the least is stationary at the inlet to the convergence. This condition on the nature of the wave solution is actually a very weak one for the area ratios that are used here, since by applying Oppenheim's analysis[6] to the case of a monatomic gas such as is used in this experiment, we can determine that the wave solution does indeed include a tip-reflected shock for arbitrarily large values of y_0. To show that this is indeed the case, we can take a more straight-forward approach, that does not directly involve the notion of the regime of ambiguity. For an arbitrarily strong incident shock traveling into gas at rest there is a limiting value of the flow Mach number M_1 behind it: in the

case of monatomic gases, M_1 (limiting) $= \frac{\mu-1}{\sqrt{\mu+1}} = \frac{2}{\sqrt{5}} \simeq 1.34$. When this supersonic flow passes through a converging section, the Mach number is decreased, but by the usual argument, we see that the Mach number cannot be decreased below the value 1 by a monotonic convergence. The area ratio of the convergence that would bring M_1 (limiting) just to the value 1 is, again for a monatomic gas, $\mathcal{R} = 1.073$. For any larger value of area ratio this flow situation would not be an allowable solution, so a tip-reflected shock would neccessarily be formed, and the flow through the convergence would be entirely subsonic.

One of the basic distinctions between the approaches of Laporte and of Kahane et. al. is that, while Kahane achieved a direct graphical solution of the wave strengths by the expedient of approximating the shock waves as isentropic compression waves, Laporte, on the other hand, carrying over many of the features of Kahane's work, went on to treat the shocks as truly nonisentropic and to undertake (within the framework of the solution "in the large") the iterative procedure needed for calculating the values of the main shocks arising from the interaction. Here we shall consider in some detail the more complicated iterative procedure that was needed for the unchoked regime, since it was in that regime that additional values of y_o were needed for our purposes; we shall only briefly describe the changes in these procedures that would be needed for the choked regime.

The basic procedure was as follows: for a given y_o and area ratio $\mathcal{R}$, we made an educated guess of the values of y_{rt} and y_c, we determined the resulting values of u_3 and u_2, and of p_3 and p_2, and then we improved the choices of y_c and y_{rt} by using the magnitude and direction

of the mismatches u_3/u_2 and p_3/p_2. Clearly the number of initial unknowns, i.e. y_c and y_{rt}, was just matched by the number of conditions imposed on them, i.e. $u_3 = u_2$, $p_3 = p_2$. The formulae for the intermediate calculations are given by Laporte for the case of a monatomic gas; the sequence of computations can be schematized as follows:

$$\frac{u_1}{c_0} = \frac{u_1}{c_0}(\mu, y_0)$$

$$\frac{c_1}{c_0} = \frac{c_1}{c_0}(\mu, y_0)$$

$$\frac{u_4 - u_1}{c_1} = \frac{u_4 - u_1}{c_1}(\mu, y_{rx})$$

From these three, we obtained

$$\frac{u_4}{c_0} = \frac{u_4}{c_0}(\mu, y_0, y_{rx}).$$

$$\frac{p_4}{p_0} = y_0\, y_{rx}$$

$$\frac{c_4}{c_1} = \frac{c_4}{c_1}(\mu, y_{rx})$$

$$\frac{c_4}{c_0} = \frac{c_4}{c_0}(\mu, y_0, y_{rx})$$

$$M_4 = \frac{u_4}{a_4} = M_4(\mu, y_0, y_{rx})$$

$$M_3 = M_3(M_4, R, \mu)$$

$$\frac{u_3}{u_4} = \frac{u_3}{u_4}\left(\frac{M_3}{M_4}, R, \mu\right)$$

$$\frac{p_3}{p_4} = \frac{p_3}{p_4}\left(\frac{M_3}{M_4}, R, \mu\right)$$

$$\frac{u_3}{c_0} = \frac{u_3}{u_4}\,\frac{u_4}{c_0}$$

$$\frac{p_3}{p_0} = \frac{p_3}{p_4}\,\frac{p_4}{p_0}$$

$$\frac{u_2}{c_0} = \frac{u_2}{c_0}(\mu, y_c)$$

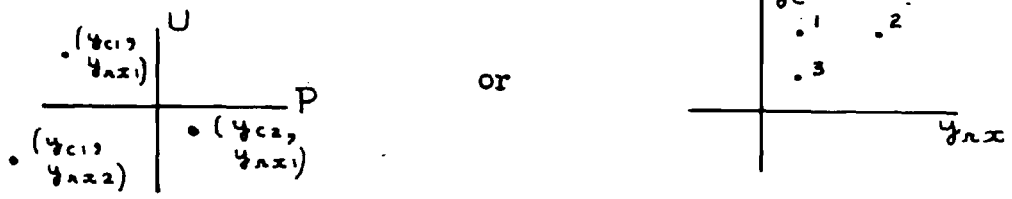
Finally we achieved the two "mismatch" equations

$$U \equiv \frac{u_3}{u_2} = \frac{u_3/c_0}{u_2/c_0}$$

and

$$P \equiv \frac{p_3}{p_2} = \frac{p_3/p_0}{\gamma_c}$$

The procedure used in this present calculation for improving on the original guesses for y_c and y_{rt} was as follows. First we took as trial values three successive pairs of y_c and y_{rt}, involving the use of only two values each for y_c and for y_{rt}: thus we used the pairs y_{c1}, y_{rt1}; y_{c1}, y_{rt2}; y_{c2}, y_{rt1}. The three resulting pairs of mismatch values, (U_1, P_1), (U_2, P_2), (U_3, P_3) were substituted in a bivariate linear interpolation formula appropriate for the imposition of two conditions on the values of the two variables. In graphic form this would have the appearance:



The geometric interpretation of the interpolation process is the finding of the linearly interpolated values of y_c and y_{rt} at the origin of the U-P plane.

In actual practice, it turned out that extrapolation from the values of y_c already tabulated by Laporte made possible very good guesses for the values of y_c that we sought. This was made possible by the fact that $y_c = y_c(y_o)$ is almost exactly a straight line for given values of μ and R; for this unusual dependence no ready explanation could be offered. There is certainly nothing obvious in the

actual formula by which the values of p_3/p_o were calculated for given values of y_o, μ and $\mathcal{R}$ that would indicate that the matching values of p_2/p_o could be very nearly linearly dependent on y_o .

In view of the fact that the extrapolated guesses for y_c were presumably much better than those for y_{rt}, the iterative procedure was altered somewhat in its initial phase for each value of y_o. The initial guess for y_c, which was just the extrapolated value, was held constant while y_{rt} was varied so as to minimize U and P simultaneously. Only then was a very small variation made in y_c in order to provide the third, non-collinear point in (y_c, y_{rt}) space for the bivariate interpolation calculation. In the actual calculations we performed, it was found that convergence of this iterative procedure was quite rapid.

It was our understanding that for each successive cycle of iteration for each value of y_o included in the tables in Laporte's report, each of the various flow and shock functions was calculated from the specifying equations. Much of this tedium was avoided in our calculations by the use of a set of gas tables[30] that proved to be of considerable assistance in this work. This set consisted of a complete collection of both isentropic flow and normal shock functions for a number of values of μ , including $\mu = 4$, in both cases with the incoming flow Mach number as the independent variable. The normal shock tables were, of course, for standing shocks, so for the various shocks of interest, $\frac{\Delta u}{c_o} = M_1 \left(1 - \frac{1}{x_1}\right)$ was the form for the change in flow velocity across the shock, in terms of the sound speed ahead of it; M_1 was the Mach number ahead of the shock, which is equivalent to the

shock Mach number $M_s \left(= \frac{\text{shock velocity}}{\text{sound speed ahead of the shock}}\right)$ for a shock moving into gas at rest.

The principal advantage in using these gas tables, as compared with calculating each value as needed from the specifying relation, was in the computation of $M_3 = M_3(M_4, \mathcal{R})$. The form of this relation can be derived from the expressions for

the conservation of mass $\rho_3 u_3 A_3 = \rho_4 u_4 A_4$

and the conservation of energy $u_3^2 + (\mu - 1)c_3^2 = u_4^2 + (\mu - 1)c_4^2$

across the area change, by eliminating the sound speeds. The form is

$$A_4 M_4 / [M_4^2 + \mu - 1]^{\frac{\mu}{2}} = A_3 M_3 / [M_3^2 + \mu - 1]^{\frac{\mu}{2}} \qquad (1)$$

The direct explicit determination of $M_3 = M_3(M_4, \mathcal{R}, \mu)$ would itself be an iterative procedure for each succesive value of M_4. Alternatively, Rudinger[31] suggested the construction of a large and detailed graph of $M_3 = M_3(M_4)$ for a fixed value of $\mathcal{R}$. The approach used here was much simpler and allowed for much greater precision of calculation: it involved using the table of values of the area-Mach number relation $\frac{A}{A^*} = \frac{1}{M}\left(\frac{M^2 + \mu - 1}{\mu}\right)^{\frac{\mu}{2}}$, which was one of the isentropic flow functions in the gas tables. This relation gave the flow Mach number at an area A in terms of the area A^* at which the flow was sonic, as for example at the throat of a Laval nozzle. Note that $\frac{A}{A^*}$ differed from the form of Equation 1 only by a factor $\mu^{\mu/2}$, which was of no concern here because only the ratios of values of A/A^* were of interest.

Specifically, $\mathcal{R} = \frac{A/A^*(M_4)}{A/A^*(M_3)}$

was the form that Equation 1 took when adapted for use with the gas tables. Since as M approached 0, A/A^* became very large, it was found

convenient, for purposes of precision in interpolating, to use the reciprocals of the values of A/A^* for all values of M less than about 0.5.

In the case of choked flow, $M_3 \equiv 1$, so $M_4 = M_{crit.}$ could either be computed from Equation 1 or could be found from this same tabulation of the area - Mach number relation: the appropriate form was

$$\frac{A}{A^*}(M_{crit}) = \mathcal{R}$$

With y_o and M_{crit} given, y_{rt} could be determined iteratively by a single-variable interpolation scheme. p_3/p_2 and u_3/c_o were then determined by y_{rt}, M_{crit} and $\mathcal{R}$. Separating the now-known region 3 from the known region 0 were two waves, $\vec{S}_c$ and $\overleftarrow{R}$. Solving for y_c was another iterative calculation involving a single-variate interpolation; specifically, one guessed a value for $y_c = p_2/p_o$, and directly obtained the corresponding value of the strength p_3/p_2 of $\overleftarrow{R}$. Then $u_{2'}/c_o = u_3/c_o + \frac{(\text{a function of } p_3/p_2)}{c_o}$; the successive approximations to y_c were determined by interpolation using pairs of values of the mismatch function $u_{2'}/u_2$.

For the initial "guess" for y_c, linear extrapolation proved to be just as suitable in the choked regime as it was in the unchoked case. Alternatively, one could iteratively solve the single implicit relation $y_c = y_c\,(M_{crit}, y_o, y_{rt})$ that is to be found on p. 18 of Laporte's report.

To conclude the discussion of theories and calculating procedures, we shall add here some more of the details concerning the Chisnell theory and especially concerning the calculations based on the theory; these calculated values were plotted in Figs. 14, 15 and 16 along with

the values calculated from Laporte's theory.

As noted in the literature survey, Chisnell derived a differential equation $\frac{dA}{dy} = g(y)$ relating the change in channel area to the change in strength of a shock traversing it. He assumed that for area changes that were not too large the shock would tend to become uniform after it left the varying-area channel and that its strength would approach the area-average value of the strength that it had at the moment it emerged from the area change. He further assumed that the effect of the interaction of any of the other waves, that followed after the main shock, with the shock itself while it was in the converging section, could be neglected. By direct integration of the derivative $\frac{dA}{dy}$, he obtained the expression $A\,f(y) = \text{constant}$,

where

$$f(y) = \frac{y^{1/\gamma}(y-1)}{\sqrt{y+1/\mu}} \left[\frac{1+\sqrt{y/\mu+y}}{1-\sqrt{y/\mu+y}}\right]^{\frac{\sqrt{\mu+1}}{2}} \frac{\sqrt{y/\mu+y} - \frac{1}{\sqrt{\mu+1}}}{\sqrt{y/\mu+y} + \frac{1}{\sqrt{\mu+1}}} \exp\left\{(\mu-1)\tan^{-1}\left[\sqrt{\mu^2-1}\sqrt{\frac{y}{\mu+y}}\right]\right\}$$

He noted the equivalence of his differential equation to one derived by Chester[32], which was of the form

$$\frac{1}{A}\frac{dA}{dy} = -\frac{1}{(\gamma y - 1)K(y)} ;$$

here $K(y)$ was found to vary very slowly with y and so could be treated approximately as a constant. It was not surprising, then, to find that the integral form $Af(y)$ could be approximated by $A(y-1)^{1/K(y)}$.

The numerical values included in Chisnell's paper were for a diatomic gas. When our calculated values for $\mu = 4$ were plotted in the form $\log_{10} f(y)$ vs. $\log_{10}(y-1)$, it was found that the resulting curve was for all practical purposes a straight line, with a slope of about 2.2, which was appropriately close to the expected narrow range of values for $K(y)$. The values of $y_c = y_c(y_o$: Chisnell) that were plotted on Figs. 14, 15 and 16 were determined from the form

$\log f(y_c) = \log f(y_o) + \log \mathcal{A}$. The values $y_c(y_o)$ also formed a straight line, which of course passed through the point (1,1); thus the Chisnell curves are not quite straight lines on the log-log graphs.

It is particularly interesting to note that for the values $y_c(y_o)$ from both the Laporte and the Chisnell theories, at least for the case of $\mu = 4$, fall on very nearly straight lines which, of course, intersect at ($y_o = 1$, $y_c = 1$). For neither theory is it at all clear why this should be the case.

Finally, it would have been interesting to compare the experimental values of $y_c(y_o)$ and the calculated values from the two theories with the values that could be derived from Kahane's isentropic theory: however, Kahane's, like Chisnell's, work dealt only with the case $\mu = 6$, and the recalculation of Kahane's superposed array of curves for $\mu = 4$ would have taken too long.

4. DISCUSSION OF THE RESULTS OF THE EXPERIMENT

The results of the interferometric measurements of the strengths y_c of the channel shocks in the various sequences of shots are shown in Figs. 14, 15 and 16. These measured values were also recorded in Tables 3, 4, and 5. The results for each model were graphed with y_o as the independent variable; superposed on each of these were the corresponding curves of $y_c = y_c(y_o)$, that were calculated from the theories of Laporte and of Chisnell. The numerical values for these theoretical curves are shown in Table 2. In addition, the straight lines $y_c = y_o$ were drawn in order to make it easier to evaluate the degree of increase of the strength y_c over the initial strength y_o.

As will be recalled from the discussion on the precision of the

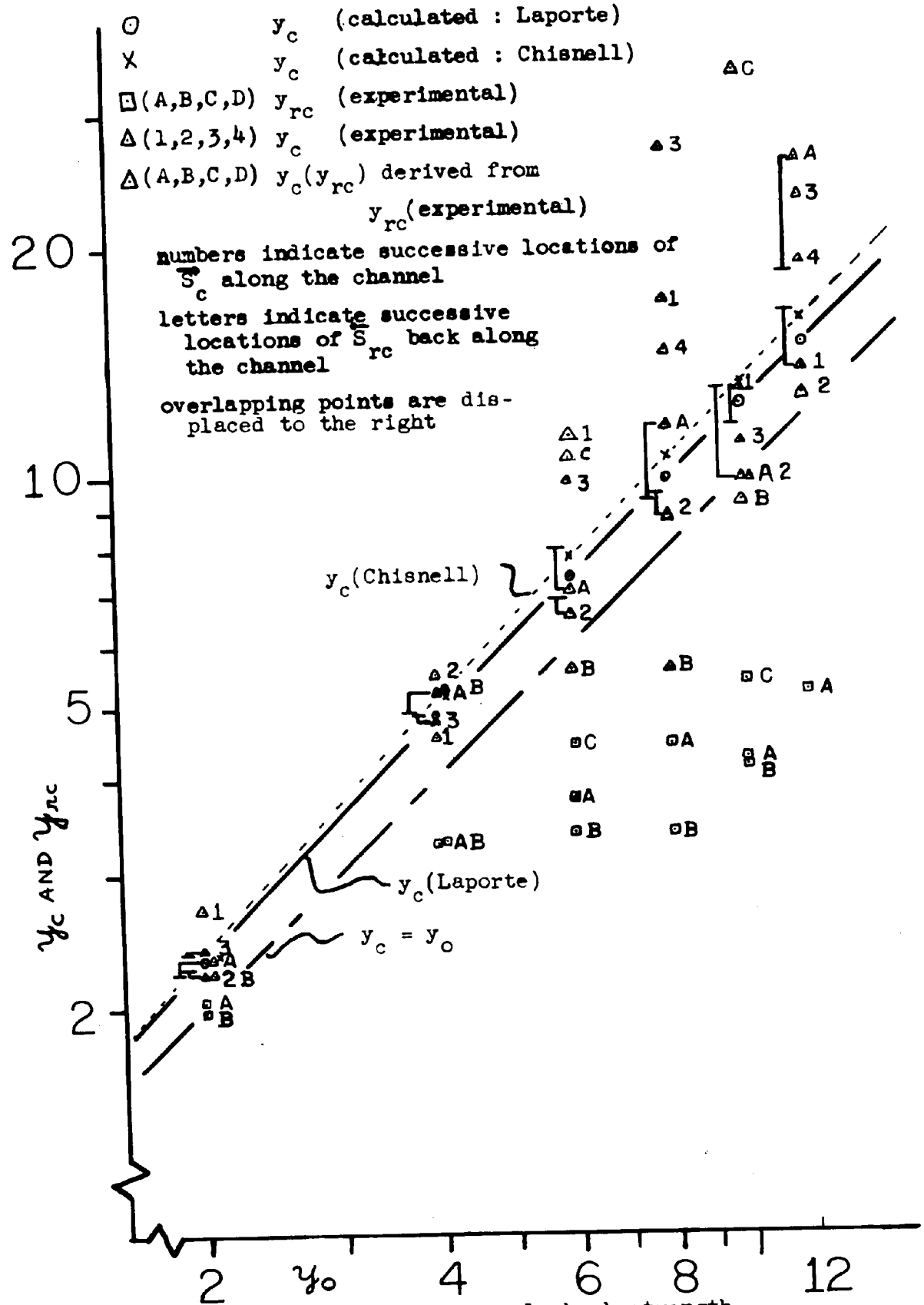


Figure 14. Graph of channel shock strength measurements for the 2-unit 2:1 model.

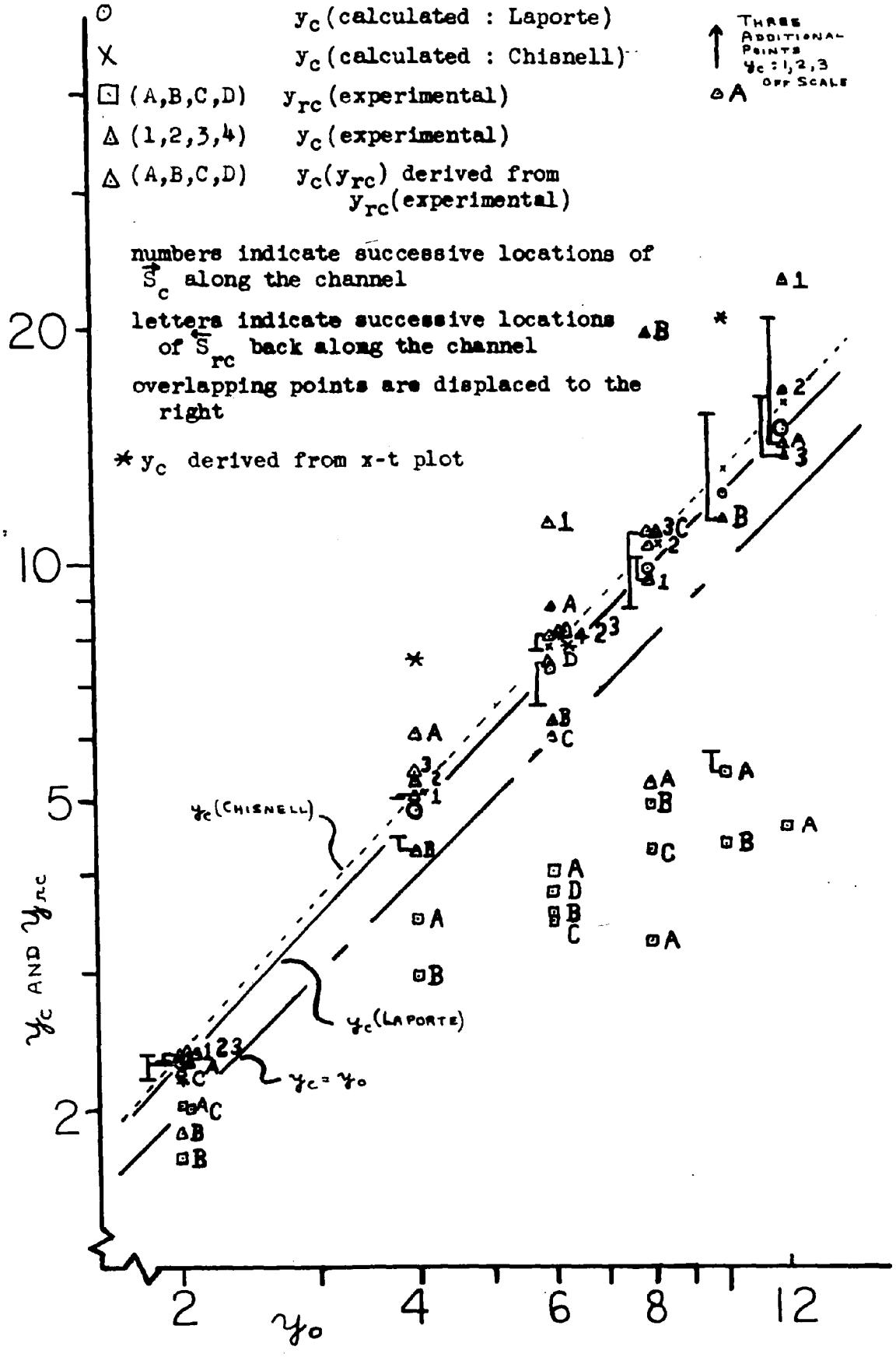


Figure 15. Graph of channel shock strength measurements for the 5-unit 2:1 model.

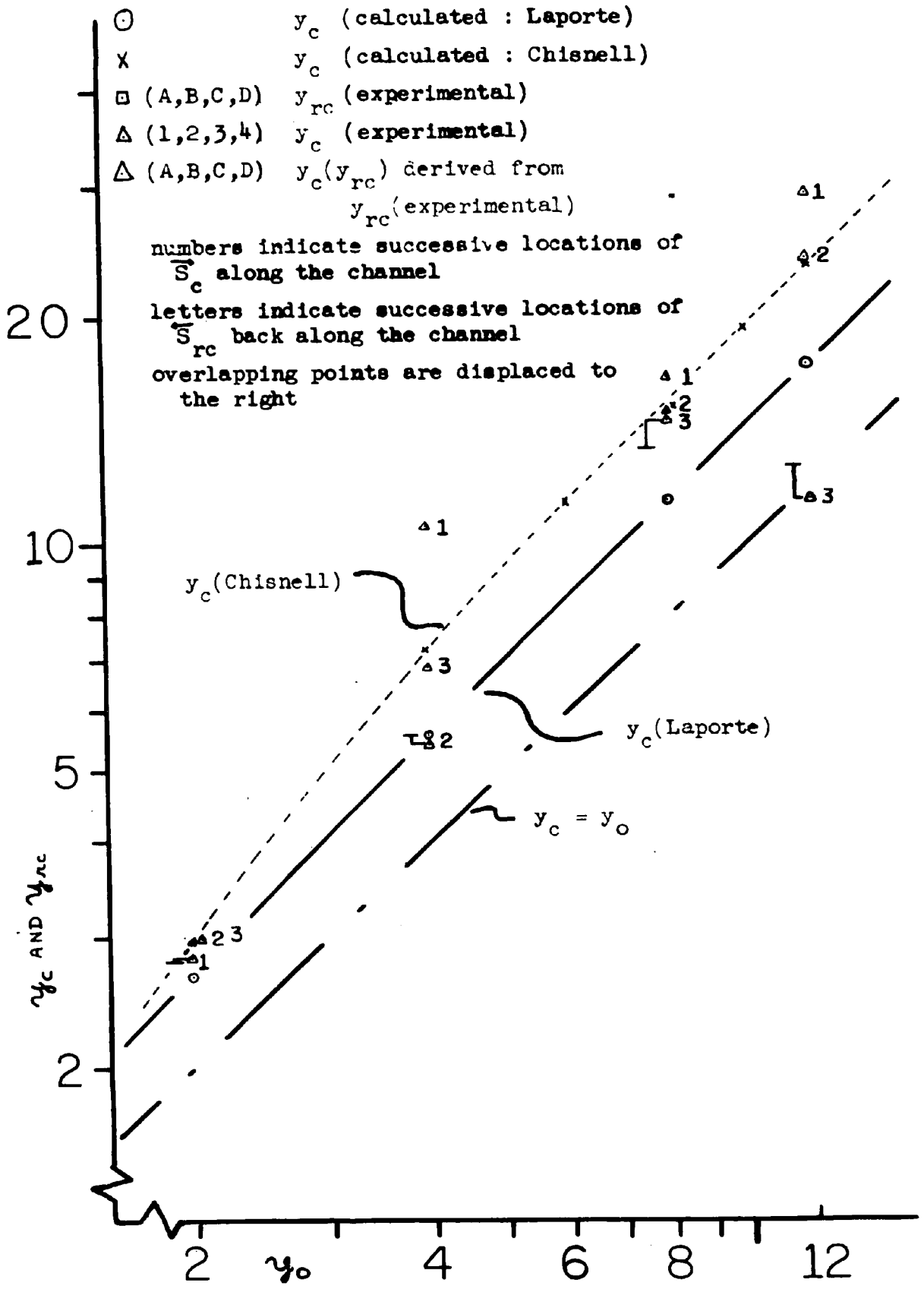


Figure 16. Graph of channel shock strength measurements for the 5-unit 5:1 model.

2-unit 2:1 Model: ℄ 183 mm from end of channel

y_o	y_c	$y_c(y_{rc})$	y_{rc}	x (location of shock with respect to ℄ on model)
2	2.69			+33 mm
	2.21			+75
	2.39			+171
		2.31	2.04	+157
		2.22	1.98	+72
4	4.51			+74
	5.46			+144
	4.74			+167
		5.12	3.26	+162
		5.23	3.29	+67
6	11.3			+36
	6.58			+66
	9.80			+163
		7.06	3.74	+166
		5.54	3.38	+75
		11.72	4.41	+30
8	17.00			+41
	8.80			+80
	26.88			+165
	14.62			+178
		11.63	4.40	+164
		5.54	3.38	+25
10	12.96			-3
	9.93			+84
	11.00			+156
		9.89	4.20	+171
		9.23	4.11	+68
		33.88	5.34	+60
12	13.81			-4
	12.76			+82
	23.27			+133
	19.09			+163
		26.12	5.17	+148

Table 3. Measured values of the shock strengths y_c, y_{rc}, $y_c(y_{rc})$ for the 2-unit 2:1 model at the various constricted-channel locations x.

5-unit 2:1 Model: ℄ 127 mm from end of channel

y_o	y_c	$y_c(y_{rc})$	y_{rc}	y_c (from x-t data)	x (location of shock with respect to ℄ on model)
2	2.35				+28 mm
	2.39				+71
	3.38				+118
		2.30	2.03		+66
		1.87	1.74		+44
		2.25	2.00		+40
				2.22	
4	5.08				-10
	5.28				+72
	5.40				+111
		6.08	3.52		+106 to +103
		4.29	2.98		+84 to +49
				7.53	
6	11.3				+32
	8.19				+37
	8.19				+75
	8.14				+110
		8.89	4.06		+114 to +113
		6.30	3.58		+113
		6.04	3.51		+37 to +41
		7.42	3.81		+41
				8.12	
8	9.54				-21
	10.59				+33
	11.00				+39
		5.26	3.30		+115
		19.81	4.95		+26 to +25
		10.97	4.33		+25
10	53.00				-20
	138.50				+51
	67.30				+120
		39.86	5.43		+104
		11.43	4.38		-36
				20.75	
12	23.00				+6
	16.77				+76
	13.81				+104
		14.25	4.63		+64

Table 4. Measured values of the shock strengths y_c, y_{rc}, $y_c(y_{rc})$ for the 5-unit 2:1 model at the various constricted-channel locations x.

5-unit 5:1 Model: ℄ 127 mm from end of channel

y_o	y_c	x (location of shock with respect to ℄ on model)
2	2.81	+12 mm
	2.96	+67
	2.98	+112
4	10.67	+5
	5.45	+65
	6.89	+113
8	17.71	+26
	13.37	+52
	12.94	+92
12	29.50	+20
	24.20	+62
	11.53	+109

Table 5. Measured values of the shock strength y_c for the 5-unit 5:1 model at the various constricted-channel locations x.

measurements, for that data point in each y_o- set that was closest to the corresponding value of y_c (calculated: Laporte), tne fringe-reduction calculation was repeated with each of the component fringe-shift values varied by 0.1 fringe in such a direction as to displace the value of y_c toward the calculated value. The magnitudes of these resulting displacements are indicated by the imprecision flags attached to these points. This varied-value procedure was also applied to that one of the values of $y_c(y_{rc})$ in each y_o - set that was closest to the calculated value, so each y_o - set has separate precision flags for y_c and for $y_c(y_{rc})$.

The most striking aspect of these graphs of results is that there are several sets of experimental values of y_c for which the data points are far more widely scattered than could be accounted for at all by the lengths of the imprecision flags. In other cases, the relative amounts of scatter are much less; so the good grouping of these sets of data points appears to imply that the approximate agreement of the values of y_c indicated by the locations of these sets with the corresponding calculated values for y_c is indeed significant. In the ensuing discussion we shall note some of the regularities in the relative amounts of scatter of the sets of data points and shall indicate possible causes of the difficulties.

Consider the sets of data points for $y_o = 2$ and 4 on the 2-unit and the 5-unit 2:1 graphs and also the set for $y_o = 2$ on the 5-unit 5:1 graph. In these cases the data points are all fairly well grouped near the corresponding calculated values. It is within reason to suppose that much of the scatter that is evident here was caused by the imprecision of the fringe - shift measuring process. The

scatter of the values of $y_c(y_{rc})$ in the set $y_o = 2$ on the 5-unit 2:1 graph is, to be sure, a separate matter.

Next we note that in the sets of points for $y_o = 6$ for the 2-unit and the 5-unit 2:1 models, the scatter is from somewhat to very much worse: the very much worse case is associated with the 2-unit model that has the blunter wedge tips (20^o wedge half-angle, as against 10^o). On the 5-unit 2:1 model, we note again for $y_o = 8$, much as for $y_o = 2$, that the data points for $\overrightarrow{S}_c$ are well grouped, and it is only for $\overleftarrow{S}_{rc}$, which occurs later in the channel flow, that the associated values $y_c(y_{rc})$ appear to deviate widely. For the same value of y_o on the blunter-tipped 2-unit model, we again see that the scatter is much worse, especially for the data points for y_c. The sets for $y_o = 10$, however, show just the opposite behavior: the blunter-tipped model yields a fairly close grouping, if one disregards the point Δ C, which occurred quite long after reflection, while for the model with the smaller wedge angle the data points are scattered so wide of the mark that all of the experimental values of y_c fell beyond the limits of the graph. For $y_o = 12$, both the 20^o and the 10^o half-angle wedge models with 2:1 area ratio show a moderately large amount of scatter within the sets of data points, although in both cases, the indicated magnitudes of the fringe-shift imprecision seem capable of accounting for much of the scatter.

The graph for the 5-unit 5:1 model data is quite striking, in that the scatter for $y_o = 4$ is already much worse than for $y_o = 2$, while for $y_o = 8$, the points are well within the domain of the associated imprecision flag. For $y_o = 12$, the scatter is again very great.

Thus for all three curves we notice first that for low values of y_o there is quite a fair grouping of the points; second, that for the higher values of y_o, there is a rough sort of fluctuation in the amount of scatter of the groups of data points as y_o is increased. This can be seen more readily in Table 6:

Table 6

Qualitative Indication of the Relative Amount of Scatter in the Sets of Data Points

y_o	Model 2-unit 2:1	5-unit 2:1	5-unit 5:1
2	well grouped	very well grouped (except for $\overleftarrow{S}_{rc}$)	well grouped
4	well grouped	fairly well grouped (except for $\overleftarrow{S}_{rc}$)	scattered
6	scattered	somewhat scattered	
8	badly scattered	well grouped (except for $\overleftarrow{S}_{rc}$)	well grouped
10	slightly scattered	very badly scattered	
12	somewhat scattered	slightly scattered	scattered

Note that the indicated amounts of scatter are relative to the lengths of the imprecision flags for the various sets of data points.

This somewhat systematic nature of the relative amount of scatter would seem to give some weight, at least tentatively, to the notion that most if not all of the wide scatter of the data points could be attributed to the interaction of trains of strong trailing waves with $\vec{S}_c$ and with $\overleftarrow{S}_{rc}$. In the case of choked flow, the simplified wave diagram shows a standing rarefaction wave; in reality the role of the rarefaction was filled by a pair of expansion waves that originated at or near the wedge-tip shoulders and sloped downstream. These inclined waves reflected and re-reflected from the top and bottom of

the constricted channel and formed a part of the trailing wave pattern; the other part consisted of the multiple-reflected relatively weak compression waves arising from the tip-reflected wavelets.

Thus our tentative explanation for the somewhat systematic variation in the relative amount of scatter is that for certain combinations of incident shock strength, wedge tip angle, area ratio and constricted channel height, the composite trailing wave trains constituted a very strong perturbation in the region behind $\vec{S}_c$. In addition, we suggest that these wave trains were generated at such times after the passage of $\vec{S}_i$ that the amalgamation of successive portions of these trains with $\vec{S}_c$ occurred during the time interval during which $\vec{S}_c$ was being observed at various locations along the constricted channel, so that at its successive points of measurement, the measured strength of $\vec{S}_c$ would be found to deviate widely from its steady-state value. It would also appear that in these cases the wave trains were not predominantly either compressive or rarefactive, so that as successive portions of the train amalgamated with $\vec{S}_c$, the measured strength would deviate first one way then the other.

On the other hand, for values of y_o not far removed from these certain values, the strengths of the trailing waves, or the relative times of their formation, were such that the values of $\vec{S}_c$ (and possibly even of $\vec{S}_{rc}$) were not substantially affected by them. This fluctuation of the strength of the trailing wave trains as the value of y_o was increased seems to be somewhat analogous to the fluctuations in the value for the wave drag in a Busemann biplane[33] in supersonic flow as the inlet flow Mach number is increased. These latter fluctuations

are caused by the phenomenon of oblique wave cancellation: in the related case of a configuration such as this,



it is true for certain values of the inlet flow Mach number that the oblique bow waves are cancelled when they are reflected at the shoulders of the opposite wedges, while for neighboring values of Mach number, such cancellation does not occur. Even though wavelets reflected from the wedge tips eventually detach and amalgamate to form a tip-reflected shock, it has been observed that portions of these wavelets are multiply reflected in the converging section and do contribute to the trailing wave train, so the possibility of the occurrence first of wave cancellation, then of no cancellation as the shock strength is increased, may indeed have a bearing on the fluctuations in the amount of data-point scatter and deviation as a function of y_o. It should be noted, however, that in the Busemann case, the flow is steady and entirely supersonic, while in our case the flow in the converging section is always subsonic, so the wave cancellation could occur only for the portions of the transient tip-reflected wavelets that are swept downstream through the convergence. We should also point out that in our case the question of the time of formation of the perturbing wave trains is important, since especially in the case of the 5-unit 2:1 model, for $y_o = 2$ and 8, and to some lesser extent for $y_o = 4$, the grouping of the points for $\vec{S}_c$ is fairly close, while for $\overleftarrow{S}_{rc}$-points there is considerable scatter.

If the major cause of the wide scatter of the data points for some values of y_o is indeed the interaction of the trailing wave pattern

with $\vec{S}_c$, then conversely, the occurrence of good grouping for a set of data points would seem to indicate the absence of trailing wave interaction. The argument we offer for this is that it appears quite unlikely that the locations of the four to six points of measurement for $\vec{S}_c$ and $\overleftarrow{S}_{rc}$ could accidentally be coupled with a strong trailing wave interaction in such a way that the measured values of y_c could be well grouped and still all be strongly perturbed by the interaction. Thus it seems reasonable to say that for those values of y_o, even in the case of choked flow, for which the data points are well grouped, substantial significance can be attached to the experimental values of y_c indicated by the location of the grouped sets of data points.

Furthermore, it appears that this conclusion should hold true even if, for a set of data points, only the values of y_c, as distinct from the values of $y_{c(rc)}$, are well grouped. Thus, for example, for the subset of y_c values in the case of $y_o = 10$ for the 5-unit 2:1 model and more particularly in the case of $y_o = 8$ for the 5-unit 5:1 model (for which there were no measured values for $y_{c(rc)}$), it is felt that the close grouping of the subset of y_c values alone confers a degree of significance onto the average of the y_c values. In the latter case only, this would point to better agreement of the experimental data with the Chisnell value than with the Laporte value, but it would be presumptuous to judge between the two theories on the basis of this one instance.

In the case of the 2:1 area ratio, the differences between Laporte's and Chisnell's values are not great enough to permit reasonable experimental discrimination between the two theories. Hence it is

unfortunate that there were not more values of y_o examined for the 5:1 area ratio, on the chance that there might have been some other values of y_o for which the trailing waves would not have caused excessive scatter of the data points.

CHAPTER V

CONCLUSIONS AND RECOMMENDATIONS

1. CONCLUSIONS FROM THE RESULTS

By restricting our attention now to those relatively few sets of measured values of y_c that were free of excessive scatter and for which the precision of fringe-shift measurement was adequate, we can reasonably conclude that the grouping of these sets near the corresponding calculated values of y_c gives a degree of experimental confirmation to Laporte's or Chisnell's analysis for a range of values of y_o well beyond that which was studied by Kahane. In the absence of the extension of Kahane's isentropic calculations to the present experimental conditions, we cannot say to what extent, if any, our useful sets of data would make possible a significant experimental confirmation of the real-shock as opposed to the isentropic-wave approach in the strong-shock regime. Likewise, lacking a value of y_c calculated from Laporte's theory for the experimental conditions of Bird's work, we cannot say with certainty whether the fact that Bird's measured value for y_c was off by 10% from the corresponding Chisnell value would mean that this measured value would be closer to the value calculated from Laporte's theory. However, by observing the change, as $\mathcal{R}$ was changed from 2 to 5, in the width of the gap between the curve for y_c (calculated: Laporte) for large y_o and the curve for y_c (calculated: Chisnell) for large y_o, we can roughly estimate that Bird's value would still be somewhat closer to Chisnell's value.

For the 5:1 area ratio the difference between Laporte's and

Chisnell's values was large enough that an experimental confirmation of one theory or the other could have been achieved within the limitations of the precision of our measurements. However, it turned out there simply were not enough well-grouped sets of data points for this area ratio to allow us to discriminate between them. On the other hand, it can be said with considerable assurance that there is a real increase in the shock strength y_c over the initial strength y_o and that the data-point sets that were found to be usable indicated that a reasonable degree of precision of measurement, that the magnitude of that increase approximately agreed with the predictions of Laporte's theory.

2. RECOMMENDATIONS FOR FURTHER WORK IN THIS AND RELATED AREAS

Our recommendations and suggestions for additional work include some that are concerned with doing essentially the same kind of experiment in a more precise and reliable fashion, and also some that deal with extension of the range of the measurements to interesting and important regimes of values not touched upon in this work.

There are several changes in the experimental conditions and procedures that could be suggested as possibly helping to make additional measurement programs of this type more precise and more productive. Some of these suggested changes are directed toward decreasing the fractional imprecision of the interferometrically measured shock strengths. These would include the following. The compression chamber should be substantially reinforced or replaced so that the value of p_o and thus of N(vac, 0) could be increased for each value of y_o. A better interferogram-recording medium should be found: the available

emulsions should be studied more intensively in an effort to find one with much finer grain, with better contrast, and with higher speed or at least less reciprocity failure. The practicality of reprinting the interferograms to increase their photographic density and their contrastiness should be looked into much more thoroughly. Some system of standardizing the fringe spacing should be worked out, so that the process of "working around" the occurrence of a unit of roll over, which up to now has been rather a makeshift process, could be systematized; white-light interferograms at close intervals of fringe shift could be prepared for the various fringe spacings that would be used; a system could be worked out to make possible direct juxtaposition of these calibrated interferograms with the white-light fringe patterns in the regions of interest, most likely by some optical-projection system. The possibility should be examined of mechanizing the process of locating the optimum opposition of the fringe patterns either on the same physical scale as the original negative interferograms or more likely by use of a technique involving optical projection. The question of the "fringe slippage" should be studied intensively by use of a chrono-interferometer[34] (a device for producing an extended time record of the motions of a fringe pattern with respect to a fixed point in the test section) to determine if, say, the motion of the fringes in the O-region in the flow interferograms is indeed due to vibration of the test section windows; if this is the case, some form of vibration damping of the windows should be tried. Along this same line, a region of no-flow reference fringes should be provided directly on the flow interferograms by making holes through the models in the

direction of the interferometer beam and connecting these holes to the back end of the model so that the density that the interferometer beam "sees" at these holes is just the ρ_o of the initial state.

The suggestions we would offer with regard to some of the other aspects of this same type of measurement program would include the following. Further studies of the interaction of a shock with a constriction of the channel area should make use of a single-unit model; multi-purpose models and experiments of the sort essayed here should be avoided as being unduly restrictive. The wedge tip shoulders should be rounded, as in the case of Bird's 15^{o} rounded nozzle blocks.

Once the single-unit model is adopted, the length of the constricted channel should be made much longer; then the trailing wave patterns could be studied in much greater detail, so that for example the question of possible fluctuations in their strengths as y_o is increased could be settled; it would also be possible to determine, for those values of y_o for which the trailing wave pattern proved to be a strong perturbation, whether the pattern does indeed catch up with the shock sufficiently to fulfill the conditions for the solution "in the large" before the shock has travelled so far along the constricted channel that the ordinary processes of shock attenuation would have significantly changed its strength.

Furthermore, a study should be made of the relative merits of schlieren wave speed recording and of interferometry as techniques for determining significant values of shock strengths in the presence of various kinds of trailing wave perturbations. Thus, in view of the fact that values of wave velocity taken from wave speed records are time-averaged values and that a continuous record of wave velocity shows

graphically if there is any tendency toward a stabilized value of wave speed, it should be considered whether using both wave speed recording and interferometry, the one for an initial survey of the stabilization process, the other for more exact strength measurements at selected locations, would give more significant results. In addition, the possible advantages of using piezoelectric transducers in the direct measurement of shock strengths should be considered, and especially the possibly greater precision that could be obtained by their use in the regime of strong shocks and low values of p_o.

As has been noted already, the values of area ratio and shock strength used in this research were far removed from Oppenheim's regime of ambiguity. It would be urged that an effort be made to study this regime, whether by interferometry or by some of the other techniques mentioned here. In particular, the detailed study that Kahane made of the development of the wave and flow configurations in the converging section should be extended to values of area ratio and incident shock strength in the regime of ambiguity. It would be of particular interest to examine the formation processes for the tip-reflected shock for values of y_o and $\mathcal{R}$ that are very near to the curve we referred to as the lower bound for the absence of $\overleftarrow{S}_{rt}$. The purpose here would be to attempt to confirm Rudinger's conclusions about the non-accessibility of the $\overleftarrow{S}_{rt}$ solution in the ambiguous regime.

It should be noted that for ordinary values of μ, i.e. 4 and 6, the range of values of y_o and $\mathcal{R}$ for the regime of ambiguity are such that it is not easy to study this regime experimentally. As Oppenheim noted and as can be seen from the sketch of the regime of ambiguity in the $(\mathcal{R}, y_o)$ plane, both the lower and the upper bounds approach asymp-

totic values of $\mathcal{R}$ as $y_o \to \infty$. The values of these asymptotes provide a very rough indication of the range of area ratios with which one would be concerned when working in this area.

The forms for these limits are as follows.

$$\lim_{y_o \to \infty} \mathcal{R} \text{ (upper bound)} = \frac{1}{\sqrt{\gamma-1}} \left[\frac{2}{\gamma(3-\gamma)} \right]^{\frac{1}{\gamma-1}}$$

$$\lim_{y_o \to} \mathcal{R} \text{ (lower bound)} = \sqrt{\gamma-1} \left(\frac{2}{\gamma} \right)^{\frac{1}{\gamma-1}}$$

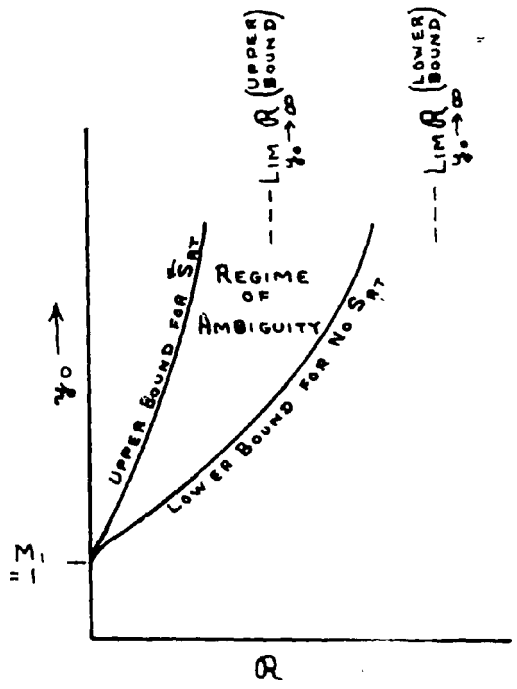


Figure 17. Sketch of the regime of ambiguity in the $\mathcal{R}$, y_o plane

For μ =		4	6
lim	(upper bound)	1.046	1.193
lim	(lower bound)	1.073	1.543

Actually it appears that lim $\mathcal{R}$ (upper bound) is a fair indication of the value of area ratio that would be needed for even fairly strong shocks in order to reach the lower-bound curve.

Thus it can be seen that the detailed study we recommended of the formation processes for $\overleftarrow{S}_{rt}$ in the vicinity of the lower-bound curve would involve very shallow convergences, accompanied, it is presumed, by very long times of stabilization for $\vec{S}_c$ and of formation for $\overleftarrow{S}_{rt}$. One possible way out can be seen by noting that both asymptotic values for $\mathcal{R}$ increase very sharply as μ increases. Thus in the case of sulfur hexafluoride SF_6, for which $\mu = 22$,

lim $\mathcal{R}$ (lower bound) = 1.72; lim $\mathcal{R}$ (upper bound) = 3.11

(These values are based on the assumption that μ is a constant.)

Thus we would strongly urge consideration of the feasibility of studying the regime of ambiguity by use of SF_6, which would involve more ordinary values of area ratio and, probably, shorter times of shock formation and stabilization. One of the principal difficulties in the use of SF_6 is the fact that the value of μ for this gas is strongly dependent on temperature even for relatively moderate temperature ranges. For this reason the calculations of y_c and y_{rt} based on Laporte's theory would have to take this real-gas behavior for SF_6 into account, and consequently would probably become a much larger computational program.

It was noted earlier that while there was no particular reason to doubt the experimental validity of the relationship $y_{rc} = y_{rc}(y_c)$, there has been,on the other hand, no definitive experimental verification of this relationship, so far as direct measurements of y_{rc} are concerned, especially in the ranges of low to intermediate shock strengths. We suggest a detailed study of the strength of $\overleftarrow{S}_{rc}$ in the simple case of normal reflection from a rigid end wall. The particular area of interest here should be the effect that the steadily thickening wall boundary layer in the 2 - region has on the measured strength of $\overleftarrow{S}_{rc}$, and also its effect on the validity of the assumption of ideal theory that in the 2' - region behind $\overleftarrow{S}_{rc}$ the gas is completely at rest. To be sure, some work has been done in this area for other ranges of shock strengths and values of p_o, especially in connection with recent efforts to study in detail the conditions in the 2' - region insofar as these affect the usefulness of this region as a high temperature heat bath for spectroscopic studies;[35,36] but the attention here was focused on the conditions

in the 2' - region, rather than on the strength of $\overleftarrow{S}_{rc}$.

It would seem appropriate to conclude this set of recommendations for additional research by suggesting that a close study be made of the theoretical significance of the following curious numerical relationships:

1) y_c(calculated:Laporte) is for all practical purposes a straight-line function of y_o, at least in the range of y_o from 2 to 50 for $\mu = 4$;

2) in the Chisnell calculations, $1/K(y)$ is very nearly a constant over a very broad range of values of y_o for $\mu = 4$ and is fairly constant over a similarly broad range for $\mu = 6$;

3) on the graphs of $\log y_c$ vs. $\log y_o$ for fixed values of $\mathcal{R}$, both the Laporte and the Chisnell curves rapidly approach asymptotic straight lines that are parallel to the line $y_c = y_o$.

A preliminary part of this study should be the calculation of the Laporte and the Chisnell curves for a variety of values of μ and for a much broader range of values for $\mathcal{R}$.

As we noted earlier, there is, for example, nothing at all obvious in the nature of the sequence of calculations involved in determining p_3/p_o in Laporte's calculating scheme that would lead one to suspect that the value of p_2/p_o that was matched to it across the interface would, for a fixed value of $\mathcal{R}$, have a straight line dependence on $p_1/p_o = y_o$. It is similarly not clear why this sort of relationship should continue unchanged across the transition from unchoked to choked flow in the convergence. Even in the case of the Chisnell theory, there is apparently no ready explanation for the fact that the function $f(y)$,

which is not at all simply dependent on y, should be such that log f(y) is a straight line function of log (y-1). It seems reasonable to infer from these peculiarities that there may be some underlying and as yet unperceived relationship between y_o and y_c -- perhaps some unsuspected similarity parameter -- that would account for the unexpectedly simple results of our numerical calculations; it is because of this possibility that this area is particularly recommended for study.

REFERENCES

1. Laporte, O., "On the interaction of a shock with a constriction," Los Alamos Scientific Laboratory Report LA-1740 (Aug. 1954).

2. Dosanjh, Darshan S., "Interaction of traveling shock waves with grids," Part II of Ph.D. dissertation, Johns Hopkins University (1953); also see, by the same author, "Some comments on 'A theoretical and experimental study of shock tube flows,'" Jour. Aero. Sciences, 22, 797(1955), and also "Interaction of grids with traveling shock waves," N.A.C.A. TN3680 (1956).

3. Kahane, A., Warren, W. R., Griffith, W. C., and Marino, A. A., "A theoretical and experimental study of finite amplitude wave interactions with channels of varying area," Jour. Aero. Sciences, 21, 505 (1954).

4. Chisnell, R. F., "The motion of a shock wave in a channel, with applications to cylindrical and spherical shock waves," Jour. Fluid Mech., 2, 286 (1957).

5. Bird, G. A., "The effect of wall shape on the degree of reinforcement of a shock wave moving into a converging channel," Jour. Fluid Mech., 5, 60 (1959).

6. Oppenheim, A. K., Urtiew, P. A., and Stern, R. A., "Peculiarity of shock impingement on an area convergence," Phys. Flu., 2, 427 (1959).

7. Prigogine, I., Introduction to Thermodynamics of Irreversible Processes, Charles C. Thomas, Springfield, Illinois (1955).

8. Rudinger, G., "Passage of shock waves through ducts of variable cross section," Phys. Flu., 3, 449 (1960).

9. Kantrowitz, A. "The formation and stability of normal shock waves in channel flow," N.A.C.A. TN 1225 (1947).

10. Geiger, F. W., and Mautz, C. W., "The shock tube as an instrument for the production of transonic and supersonic flow patterns," Engineering Research Institute, University of Michigan (1949).

11. Rudinger, G., Wave Diagrams for Nonsteady Flow in Ducts, D. Van Nostrand Co., Inc., New York (1955), p. 161.

12. Turner, E. B., "The production of very high temperatures in the shock tube with an application to the study of spectral line broadening," Engineering Research Institute, University of Michigan (1956), p. 51.

13. Cole, A. L., Hunting, A. C., and Upham, D. L., "Electrical breaking

of shock tube diaphragms," University of Michigan Research Institute (1958), p. 3.

14. Cole et. al., ibid.

15. Millman, J., and Taub, H., Pulse and Digital Circuits, McGraw-Hill Book Co., New York (1956), p. 221.

16. See, for example, Forgacs, R. L., "A fractional microsecond light source of high intensity," Inst. Radio. Eng. Nat. Conv. Record, Pt. 5, 114 (1957), or Devaux, P., "Flash generators with built-in chronometry," in Collins, R. B., ed., Proc. 3rd Int. Cong. on High-Speed Photography, Butterworths, London (1957).

17. Ladenburg, R., and Bershader, D., "Interferometry", p. 59, in Taylor, H., ed., Physical Measurements in Gas Dynamics and Combustion, Princeton University Press (1954).

18. Lamla, E., "Ueber die Justiering des Mach-Zehnderschen Interferometer," Z. Instrumentenkunde, 62, 337 (1942).

19. Wood, G. P., "Interferometer Methods," Part II of Nelson, W. C., ed., "Optical methods for examining the flow in high-speed wind tunnels," AGARDograph No. 23, N.A.T.O. Advisory Group for Aero. Res. and Dev., Paris (1956).

20. See, for example, Courant, R., and Friedrichs, K. O., Supersonic Flow and Shock Waves, Interscience Publishers, Inc., New York (1948), p. 351, or Liepmann, H. W., and Roshko, A., Elements of Gasdynamics, Wiley and Sons, New York (1957), p. 51.

21. See, for example, Courant and Friedrichs, op. cit., p. 87.

22. Liepmann and Roshko, op. cit., p. 64.

23. Ref. 22, p. 127, or Prandtl, L., Essentials of Fluids Dynamics, Hafner Pub. Co., New York (1952).

24. Curtis, C. W., "Use of white light in the measurement of gas density by optical interferometry," Institute of Research, Lehigh University, Tech. Rep. 9 (1958).

25. Candler, A. C., Modern Interferometers, Hilger and Watts, London (1951), p. 480.

26. Adams, L. H., "The use of the interferometer for the analysis of solutions," Jour. Amer. Chem. Soc., 37, 1181 (1915).

27. See, for example, Wilson, E. B., Jr., Introduction to Scientific Research, McGraw-Hill Book Co., New York (1952), pp. 272-274.

28. Ref. 17, p. 64.

29. Werner, F. D., and Leadon, B. M., "Very accurate measurement of fringe shift in an optical interferometer study of gas flow," Rev. Sci. Inst., 24, 121 (1954).

30. "Compressible flow tables and graphs," Vol. 2 of Handbook of Supersonic Aerodynamics, Navord Report 1488 (Vol. 2), U.S. Govt. Print. Off. (1950).

31. Ref. 11, p. 96-98.

32. Chester, W., "The quasi-cylindrical shock tube," Phil. Mag., (7), 45, 1293 (1954).

33. Liepmann and Roshko, op. cit., p. 115.

34. Mack, J. E., "Density measurements in the shock tube with the chrono-interferometer," Institute of Research, Lehigh University, Tech. Rep. 4 (1954).

35. Doherty, L. R., "The measurement of absolute spectral line strengths with the shock tube," Univ. of Michigan Sponsored Research Report (to be published).

36. Wilkerson, T. D., "The use of the shock tube as a spectroscopic source with an application to the measurement of gf-values for lines of neutral and singly ionized chromium," Univ. of Michigan Sponsored Research Report No. 02822-3-T (1961).

37. Schaefer, H. J., "Physical optic analysis of image quality in schlieren photography," Jour. Soc. Motion Picture Eng., 53, 524 (1949), p. 540; also ref. 17, article A2 on "Shadow and schlieren methods", p. 31.